



Reinhard Schmid, BSc

# Investigation of the interlaminar interfaces in a lithium ion pouch cell

Master thesis for obtaining the degree Master of Science in the field of studies  
Mechanical Engineering and Economic Sciences - Production Science and Management

Realized at the Vehicle Safety Institute,  
Faculty of Mechanical Engineering and Economic Sciences,  
Graz University of Technology

Chair: Univ.-Prof. Dipl.-Ing. Dr.techn. Hermann Steffan

Supervisor: Dipl.-Ing. Dr. techn. Florian Feist

Graz, January 2014



This page intentionally left blank

## I. Statutory declaration

### STATUTORY DECLARATION

I declare that I have authored this thesis independently, that I have not used other than the declared sources/ resources, and that I have explicitly marked all material which has been quoted, either literally or by content from the used sources.

Graz, 15 December 2013

Date

.....

Signature (Reinhard Schmid)

## II. Abstract

Increasing oil prices as well as the awareness of our environmental responsibility make people turn to battery electric vehicles. Depending on the source of energy used for charging batteries, probably less fossil fuels are burnt and less CO<sub>2</sub> is emitted. Batteries featuring a high energy density, like lithium ion batteries, are crucial for the breakthrough of electric vehicles. In case of abuse a safety threat is inherent to lithium ion batteries. Therefore lithium ion batteries have to be researched in terms of crash safety.

To understand failure mechanisms due to mechanical loads a very detailed modelling of the cell is necessary. At the so-called microscopic model approach every layer of the cell (separator, electrodes with collector and active media and pouch) is modelled separately.

The lithium ion pouch cell under study is made up of very thin layers, interacting at their surfaces. Previous research had indicated that the structural behaviour at deformation is sensitive to the interlaminar friction interactions.

A test stand for interlaminar effects was developed for the investigation of the frictional behaviour and governing parameters. These tests were performed by pulling out the specimen (i.e. the anode, the cathode, or the pouch), which was clamped between an anvil and a plate, both covered with the separator material. The tests were performed with various surface pressures and at different velocities. The specimens were entirely submerged in a substitute electrolyte. Using electron microscopy the specimen's surface was investigated before and after testing. In future the derived interaction model shall be implemented into a numerical battery model of a lithium ion battery cell for mechanic load cases.

It was found that interlaminar interactions in the cell under study depend on surface pairing, normal force and shear velocity. The surface pairings anode with separator, cathode with separator and pouch with separator were investigated. Relevant values for the interaction model could be determined.

Tests series considering further parameters like temperature and state-of-charge are necessary to refine the interlaminar model.

### III. Kurzfassung

Steigende Ölpreise und das Verantwortungsbewusstsein gegenüber der Umwelt führen zu einer Wende in Richtung Elektroautos. Abhängig von der Energiequelle, die für das Laden von Batterien verwendet wird, werden möglicherweise weniger fossile Brennstoffe verbrannt und weniger CO<sub>2</sub> ausgestoßen. Batterien mit hohen Energiedichten, wie etwa Lithium Ionen Batterien, sind wesentlich für den Durchbruch von Elektroautos. Im Falle einer Fehlanwendung geht von Lithium Ionen Batterien eine Gefährdung der Sicherheit aus. Deshalb müssen Lithium Ionen Batterien in Hinblick auf Unfall-Sicherheit erforscht werden.

Um den Mechanismus des Versagens aufgrund von mechanischer Beanspruchung zu verstehen, ist eine detaillierte Nachbildung der Zelle notwendig. Beim sogenannten mikroskopischen Modellansatz wird jede Schicht der Zelle (Separator, Elektrode mit dem Stromleiter und dem Aktivmaterial und die Hülle) getrennt nachgebildet.

Die betrachtete Lithium Ionen Beutel-Zelle besteht aus sehr dünnen Schichten, welche an ihren Oberflächen aufeinander wirken. Eine vorangegangene Forschungsarbeit hat gezeigt, dass das Strukturverhalten bei Verformungen sensitiv auf die Wechselwirkungen aufgrund von Reibung zwischen den Schichten reagiert.

Zur Untersuchung der Effekte zwischen den Schichten wurde ein Prüfstand entwickelt, um das Reibungsverhalten und die Einflussgrößen zu untersuchen. Bei den Untersuchungen wurde die zwischen zwei Platten eingeklemmte Probe (Anode, Kathode oder Hülle) herausgezogen. Die Platten waren mit Separator-Material überzogen. Die Untersuchungen wurden mit unterschiedlichem Oberflächendruck und verschiedenen Geschwindigkeiten durchgeführt. Die Proben waren dabei in einem Ersatzelektrolyt eingetaucht. Mit Hilfe von Elektronenmikroskopie wurde die Oberfläche der Probe vor und nach dem Test untersucht. Im Weiteren soll das abgeleitete Kontaktmodell in ein numerisches Batteriemodell einer Lithium Ionen Batterie Zelle für mechanische Beanspruchung eingesetzt werden.

Die Untersuchung hat gezeigt, dass Wechselwirkungen zwischen den Schichten der untersuchten Zelle von der Materialpaarung, sowie der Normalkraft und den Schergeschwindigkeiten abhängen. Die Oberflächenpaarungen Anode mit Separator, Kathode mit Separator und Hülle mit Separator wurden untersucht. Relevante Werte für das Wechselwirkungsmodell konnten bestimmt werden.

Für die Verfeinerung des Wechselwirkungsmodells der Zwischenschichten sind Untersuchungsreihen mit weiteren Parametern wie Temperatur und Ladezustand notwendig.

## IV. Table of contents

I.	Statutory declaration .....	II
II.	Abstract .....	III
III.	Kurzfassung .....	IV
IV.	Table of contents.....	VI
V.	Acknowledgements.....	IX
1	Introduction.....	1
1.1	Electro mobility.....	3
1.2	Vehicle safety.....	9
1.3	Batteries.....	10
1.4	Investigated Battery .....	13
1.4.1	Battery testing.....	16
1.4.2	Mechanical abuse tests .....	17
1.5	Physical effects in interfaces .....	21
1.5.1	Adhesion.....	22
1.5.2	Van der Waals forces.....	23
1.5.3	Electro static force.....	23
1.5.4	External forces.....	23
1.5.5	Capillary forces .....	24
1.5.6	Friction.....	26
2	Motivation .....	30
2.1	Current battery model.....	31
2.2	Fields of improvement of current model .....	31

3	Hypothesis and objective .....	32
3.1	Hypothesis .....	32
3.2	Objective.....	32
4	Methods .....	33
4.1	Test station development.....	34
4.2	Preparation of Specimens .....	35
4.3	Boundary Conditions for Test stand .....	36
4.4	Test stand design .....	37
4.4.1	Test stand validation .....	43
4.5	Test Matrix.....	47
4.7	Microscopy .....	50
5	Results .....	52
5.1	Strip draw test .....	52
5.1.1	Pre-Test electrodes combined with aluminium.....	52
5.1.2	Pre-Tests electrodes combined with polyethylene .....	53
5.1.3	Recovery properties .....	55
5.1.4	Final tests.....	58
5.2	Microscopy results.....	61
5.2.1	Anode .....	62
5.2.2	Cathode .....	65
5.2.3	Separator.....	68



6	Discussions .....	71
6.1	Discussion of the test station development.....	71
6.2	Discussions of the strip draw tests .....	71
6.3	Discussions of the microscopy results.....	73
6.3.1	Anode .....	73
6.3.2	Cathode .....	73
6.3.3	Separator.....	74
7	Conclusion .....	75
8	Outlook.....	82
9	Bibliography.....	83
10	List of Figures.....	89
11	List of Tables.....	93
12	List of Equations .....	94
13	List of symbols.....	95
13.1	SI base units .....	95
13.2	Units .....	95
13.3	Constants .....	96
13.4	Used Symbols.....	96
14	List of Abbreviations.....	98
15	Appendix.....	102
15.1	Curriculum Vitae .....	102

## V. Acknowledgements

This thesis was written based on the findings gained while working at the Vehicle Safety Institute at the Graz University of Technology.

Numerous people helped and supported me during that time and so I want to start by expressing my special thanks to a lot of very important people.

First of all I want to thank Univ.-Prof. Dipl.Ing. Dr.techn. Hermann Steffan, the head of the institute, who aroused my interest in vehicle safety in his fascinating lectures.

Dipl.-Ing. Dr.techn. Florian Feist, my supervisor, was of great help and always had a sympathetic ear for all my questions. Therefore I want to thank him a lot.

I also want to express my special thanks to Dipl.-Ing. Dr.techn. Wolfgang Sinz for his support.

Dipl.-Ing. Christoph Breitfuß supported me during the whole thesis. I really appreciate his help a lot.

Further I am grateful to all my colleagues at the institute for their help and for creating a uniquely cooperative atmosphere.

Finally I want to thank my family as well as my partner Iris who have supported me during my studies in many different respects. Above all I want to thank my parents who made my studies possible and have always promoted me.

All the support I was given was invariably excellent and I am looking forward to new challenges!

Graz, 15 December 2013

Reinhard Schmid

## 1 Introduction

*'There is no safety, just different degrees of uncertainty'*<sup>1</sup> this quote by Anton Neuhäusler, a German philosophy professor, perfectly illustrates that absolute safety cannot be gained.

The research field of vehicle safety has the target to increase the degree of safety on the one hand and make safety, as well as the effects resulting from the absence of absolute safety, better calculable and predictable. This is important for setting action to further enhance safety by making technical improvements or implementing new regulations and laws.

Both, mobility and safety are elemental requirements for the well-being of people. According to the model of Maslow illustrating the hierarchy of human needs, as shown in Figure 1, there are different levels. A fundamental need is people's wish to feel safe and out of danger. Safety in general and also vehicle safety in particular, can be found at this stage. Also mobility can be classified into a stage of the hierarchy model. In many cases social mobility is a key factor for satisfying one's own needs. (1)

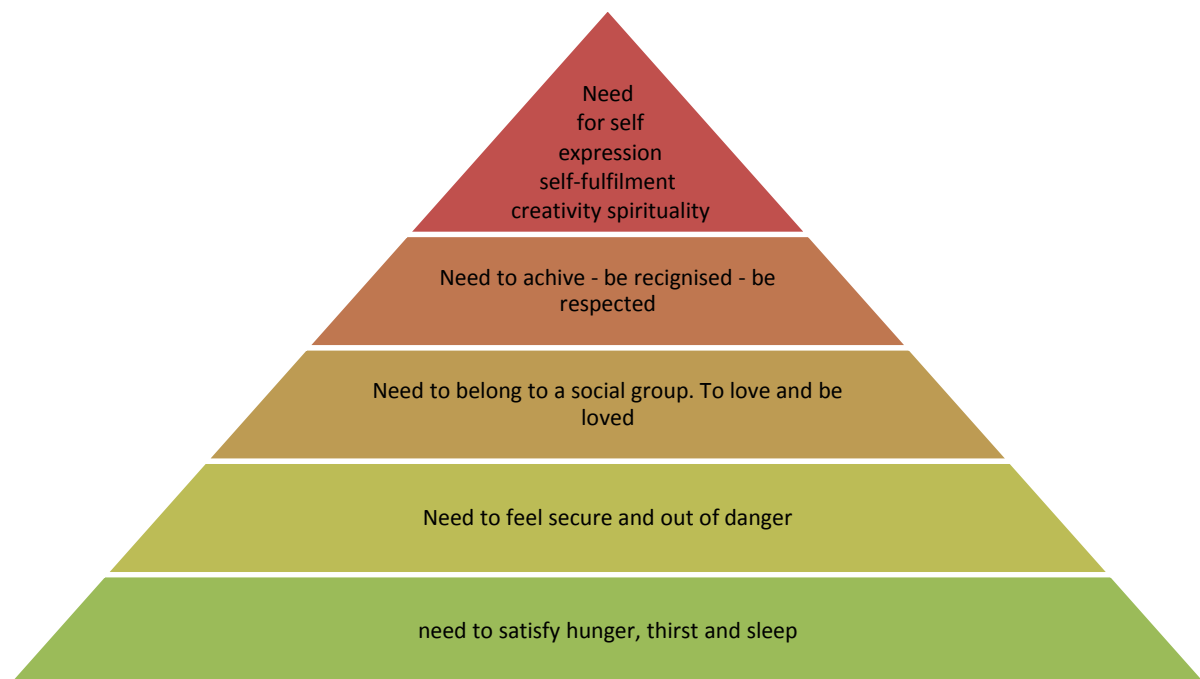


Figure 1: Maslow's Hierarchy (1)

<sup>1</sup>Translated original Quote by Anton Neuhäusler (20.02.1919 - 15.01.1995) *'Es gibt keine Sicherheit, nur verschiedene Grade der Unsicherheit'*

It is hard to imagine life without mobility and traffic. This is evident in the high number of registered vehicles exceeding 1.5 billion cars worldwide in 2013, according to a study of the WHO (World Health Organization), and which is still increasing (2). The density of cars (registered cars per inhabitant) depends on the country under study. For the EU27 states 473 personal cars per 1,000 inhabitants were estimated by Eurostat (3). Figure 2 illustrates the forecast numbers of newly registered vehicles which will even exceed those of the year 2012. These figures show that the newly registered passenger cars increase by approximately 5.4% p.a. (4).

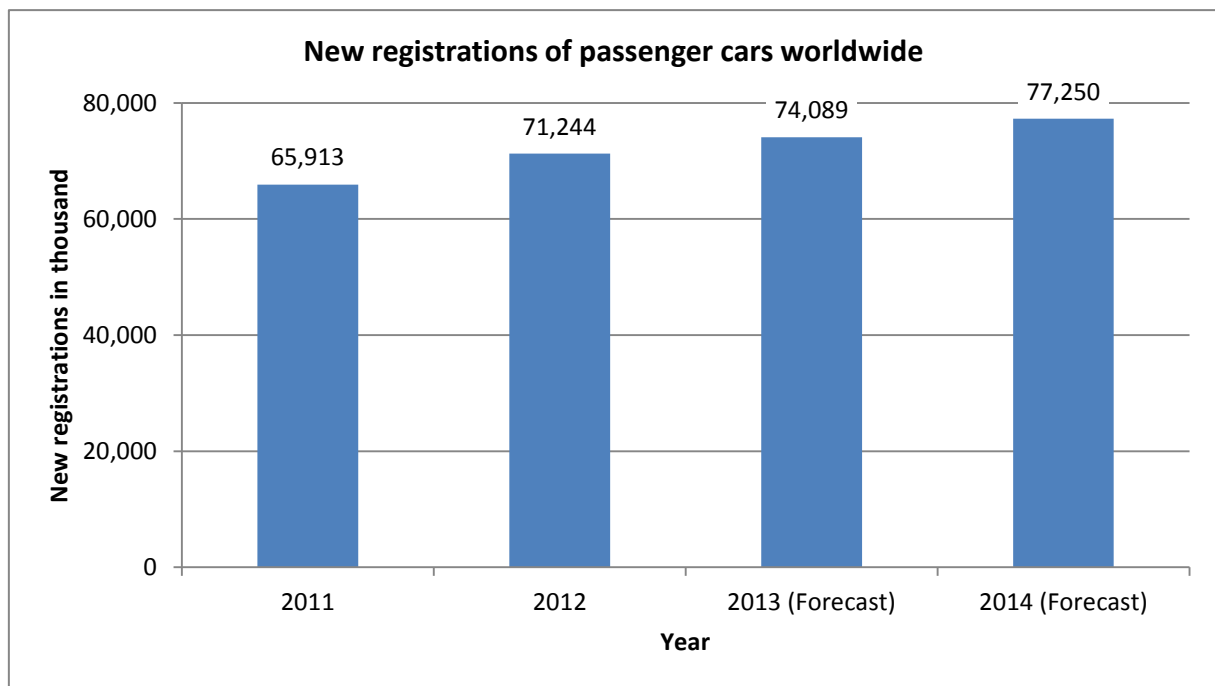


Figure 2: New registrations of passenger cars worldwide (4)

The increase in passenger-related road traffic as well as the requirement for a safer mobility shows the tremendous importance of vehicle safety. Especially new technologies which enter the market are challenging for vehicle safety.

With respect to the huge numbers of newly registered cars there is an endeavour for developing new propulsion concepts, like electro mobility, in order to make mobility more sustainable.

## 1.1 Electro mobility

Electric vehicles are on everyone's lips these days and a lot of research work is currently being done in this field. There are two clearly distinguishable motives for the rise of electric vehicles. One of them is that the resources of fossil fuels are limited. The other one is the emission of CO<sub>2</sub> caused by the combustion of fuel containing carbon in vehicles. The latter motive is environmentally relevant because of the climatic change, which is at least partly caused by the rise of the CO<sub>2</sub> content in the atmosphere. Considering the level of CO<sub>2</sub> it is not just important if a vehicle is electrically driven but also which kind of power plant the required energy is transformed in. If the electric power is generated for example in a caloric power plant where fossil coal is burnt, the CO<sub>2</sub> emission is even doubled. But there are also very promising concepts of power plants which cause little or no CO<sub>2</sub> exhausts at all when generating electrical energy. (5)

When talking about energy consumption and CO<sub>2</sub> exhausts it is important to have a broad view and not just focus on the driving or operating phase. To compare vehicles with different technologies the LCA (Life Cycle Assessment) phase reaches from the production process to the recycling process. In terms of energy consumption for propulsion, the term WtW (Well to Wheel) is often used, which describes the energy consumption and the CO<sub>2</sub> exhausts starting with the exploitation or generation of the energy and ending with the amount of energy which actually propels the vehicle. Because of production, transportation, storage and efficiency losses it can be that a huge amount of CO<sub>2</sub> was produced before, and only some energy can be used for the propulsion of the vehicle. The different phases can be seen in Figure 3. This figure illustrates the challenge when talking about CO<sub>2</sub> exhausts and energy consumption for an electric vehicle. Even when no CO<sub>2</sub> is produced in the TtW (Tank to Wheel) phase by using electric vehicles, CO<sub>2</sub> emissions can occur in other phases, like the WtT (Well to Tank) phase. The amount of these emissions strongly depends on the power source. (6)

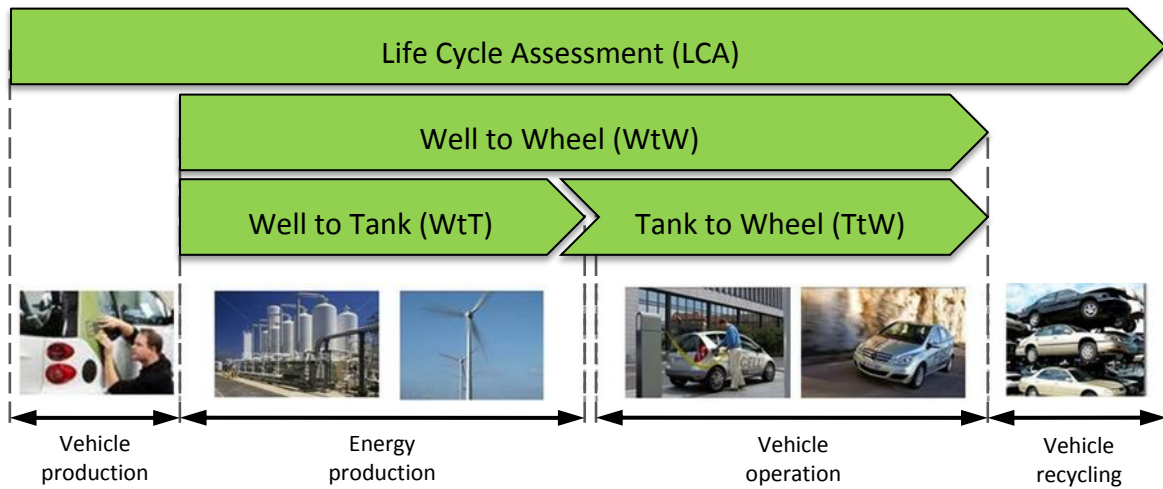


Figure 3: Life cycle assessment (7)

Applying this approach some comparison can be made. According to a calculation program by Daimler three different scenarios are shown in Figure 4 (8).



Figure 4: Energy and CO<sub>2</sub> scenarios (8)

The orange bar represents the gasoline equivalent in litre per 100 km and the green bar represents the CO<sub>2</sub> equivalent in gram per km. The white vertical lines mark the values of the reference vehicle which is a gasoline car.

The first row shows the WtW values for a diesel car, the second and third rows for a battery electric vehicle, whereby the electrical energy is transformed from an average energy mix in the second row and just from the sun in the third row. The amount of CO<sub>2</sub> can be halved when introducing electric vehicles without changing the energy generation, but the decrease

of gasoline equivalent will be minor. When the propulsion energy is solely generated in solar power plants, though, a considerable reduction in gasoline equivalent can be achieved. CO<sub>2</sub> emissions can even be reduced to zero in the WtW phase.

The availability of fossil oil leads to further challenges. Due to the limitation and the increasingly complex extraction of oil in hardly accessible deposits all over the world the prices for fuels are rising and becoming an economic driver for the development of electric vehicles. Figure 5 illustrates the trend of the diesel price in Euro Cent per litre from the years 1970 to 2013. Also the political instability as well as the energy-political independence is a driver to find transportation concepts which are not related to fossil oil. (9)

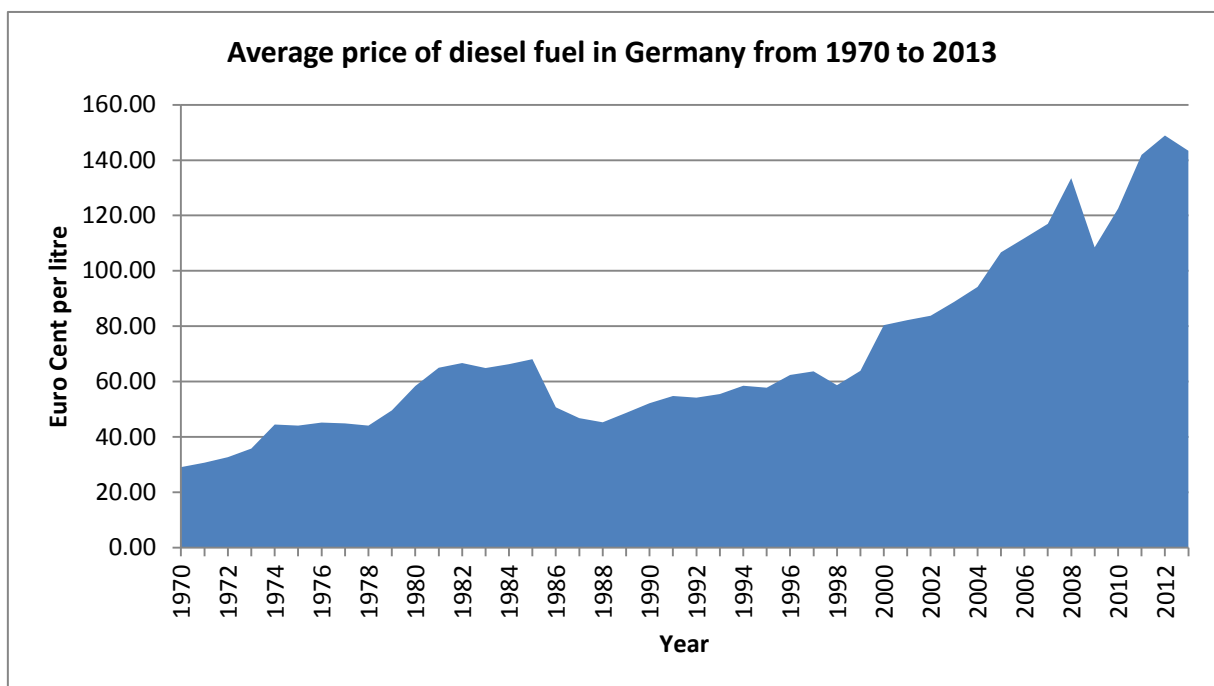


Figure 5: Average price of diesel fuel in Germany (10)

It can be concluded that there is a huge economic and environmental potential in the development and use of electric vehicles, provided there are well developed alternatives to produce the energy which is needed for electric vehicles.

Apart from these two arguments in favour of electric vehicles compared to fossil oil driven ones they are in particular advantageous in city traffic conditions characterised by stop-and-go traffic. Generally, in big cities the average velocity is low and the driven distances are short. These circumstances perfectly suit the strength of electric vehicles. Because there are no exhausts these vehicles could even be used to drive inside buildings. Electric vehicles also

emit significantly less noise, which is a tremendous advantage, especially with regard to further increasing traffic. (11)

Figure 6 shows the forecast of the worldwide numbers of HEV (hybrid electric vehicles) and BEV (battery electric vehicles) for the years 2009 to 2020 in million vehicles. According to these estimates there will be a steady increase in hybrid and electro vehicles.

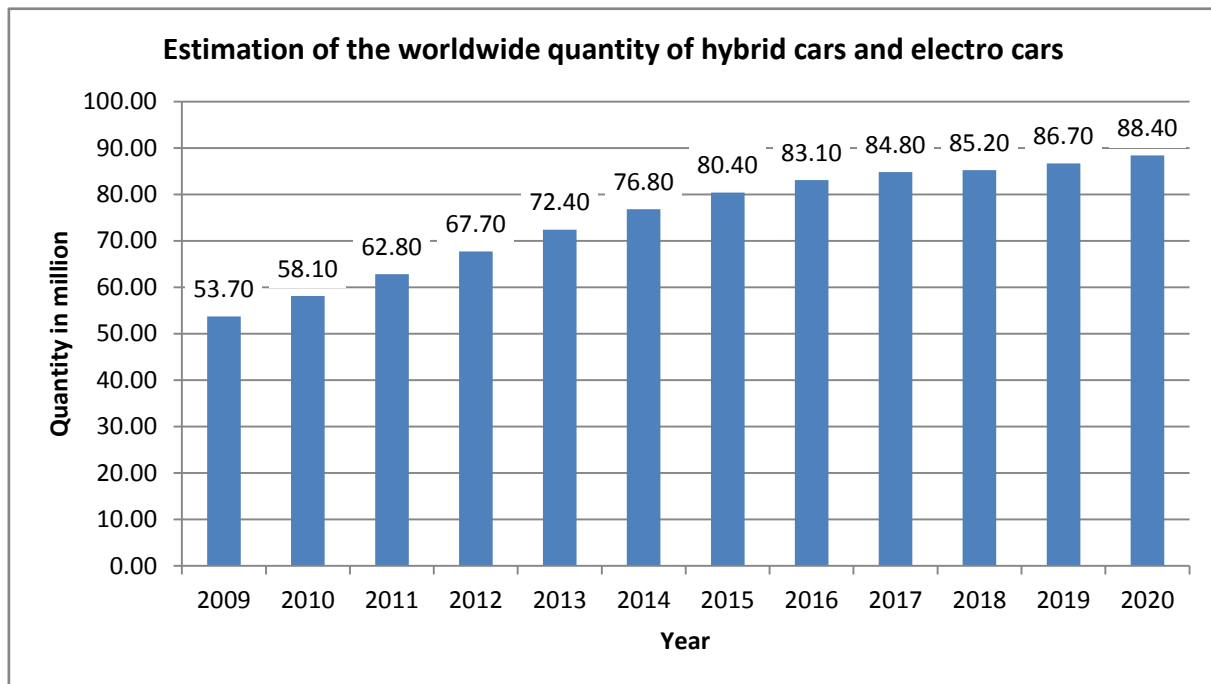


Figure 6: Estimation of the worldwide quantity of hybrid cars and electro cars (12)

A study carried out by Brokate et al. (13) illustrates the development of the new car fleet in Germany till 2040 which can be seen in Figure 7. In 2010 almost the whole new fleet consisted of vehicles driven by petrol or diesel. By 2040 these two segments will amount to just about one quarter.



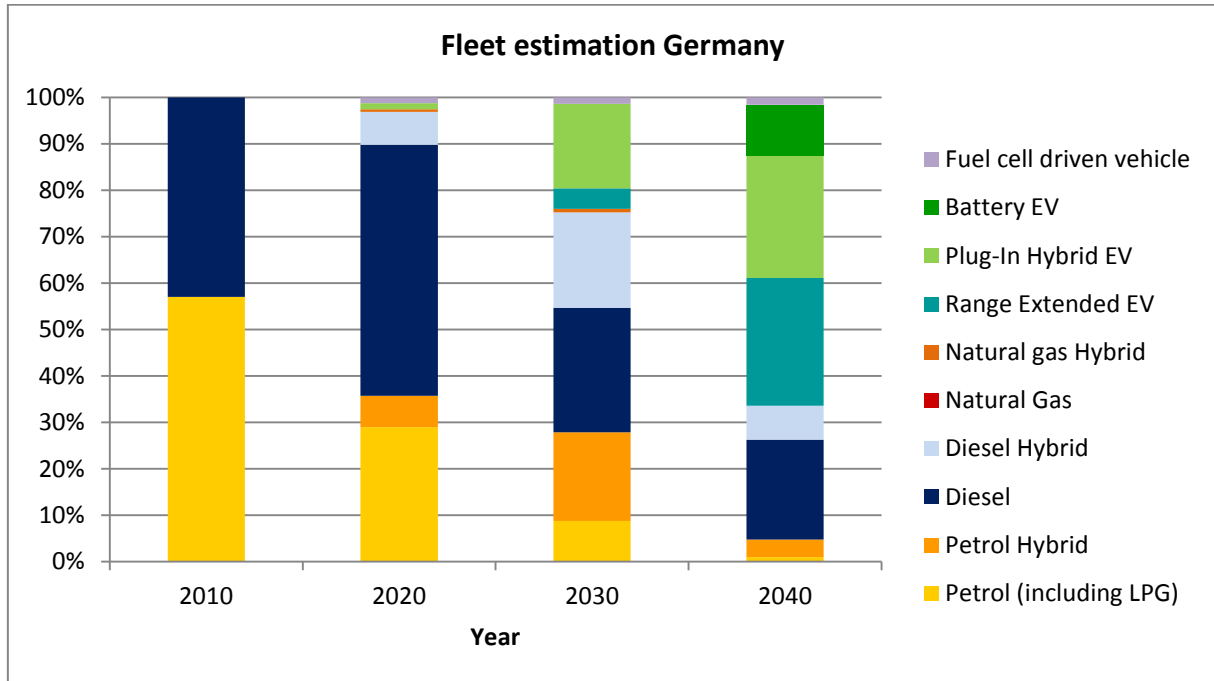


Figure 7: Fleet estimation Germany (13)

In HEV as well as in BEV propulsion energy needs to be stored and therefore an adequate electric energy storage system, short EESS is required.

There are a lot of different principles of EESS. According to a study of the International Electro technical Commission (IEC) the storage systems can be classified according to the form how the energy is stored, which can be seen in Figure 8. This is a comprehensive analysis of electrical energy storage systems and not all of them are suitable for mobile applications. According to this study lithium batteries suit both, hybrid electric vehicles and electric vehicles. Metal air batteries are also in the focus of this study for mobile applications. Especially lithium air batteries have a theoretical specific energy which is even greater than that of petrol, but this battery type poses a high safety risk because of the high reactivity. (14)

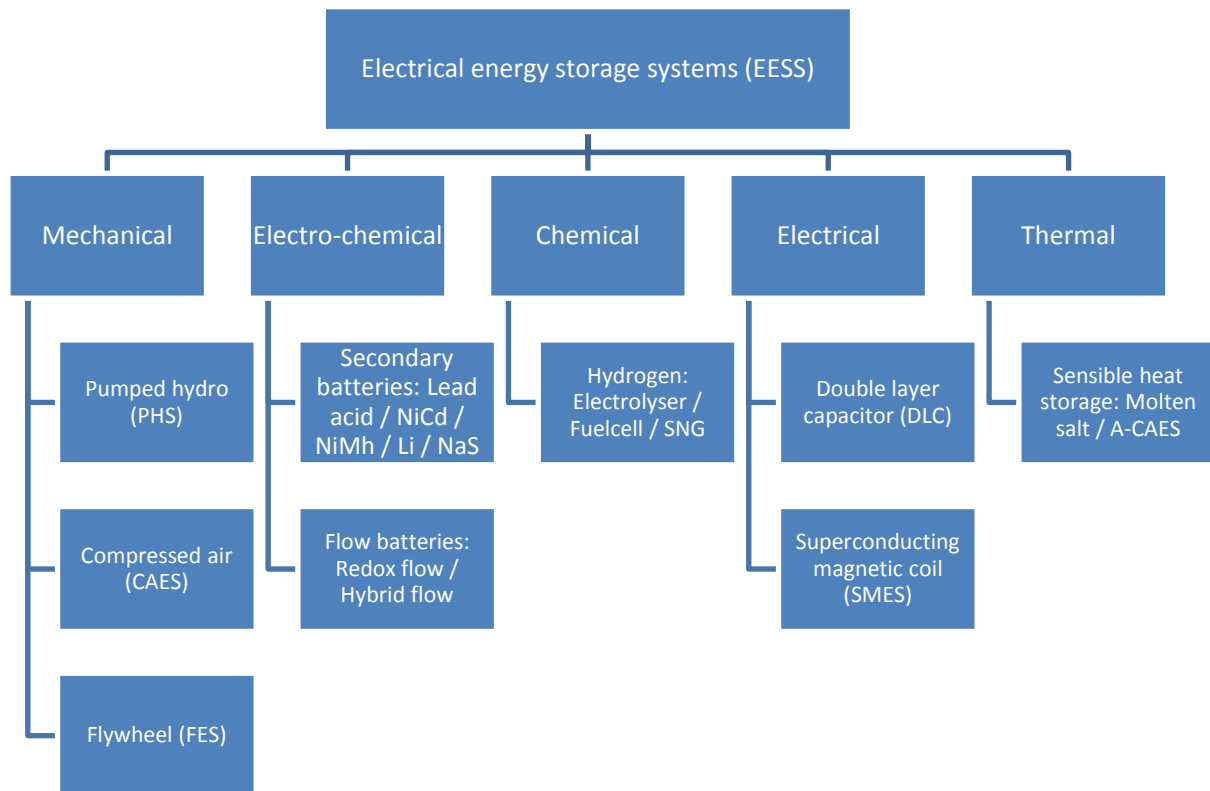


Figure 8: Classification of EESS according to the energy form (14)

The IEC study leads to the conclusion that a great number of lithium ion batteries will be needed in the near future for being applied in battery electric vehicles and hybrid electric vehicles. (14)

As there will be a great number of lithium ion batteries on the roads in the future this technology needs to be researched with respect to vehicle safety.

## 1.2 Vehicle safety

Vehicle safety is a subdomain of traffic safety. It can be divided into active safety and passive safety. All measures that contribute to the avoidance of accidents can be allocated to the active safety segment. Passive safety includes measures which reduce the severity of accidents. The border between active and passive safety is blurred for some safety measures. (15)

Because of these interferences the strict segmentation is counteracted by using the general term of integrated safety when thinking about the chain of concurrent safety measures (16).

Considering the safety of the EESS a passive safety approach is eminent. The positioning of the EESS plays a major role for the safety of a vehicle. Zones with different deformation probability were defined by Justen et al. These results are illustrated in Figure 9. (17)

The different colours visualise the probability for a certain intrusion depth in real world accidents. The dotted line is used for marking the intrusions resulting from performed crash tests.

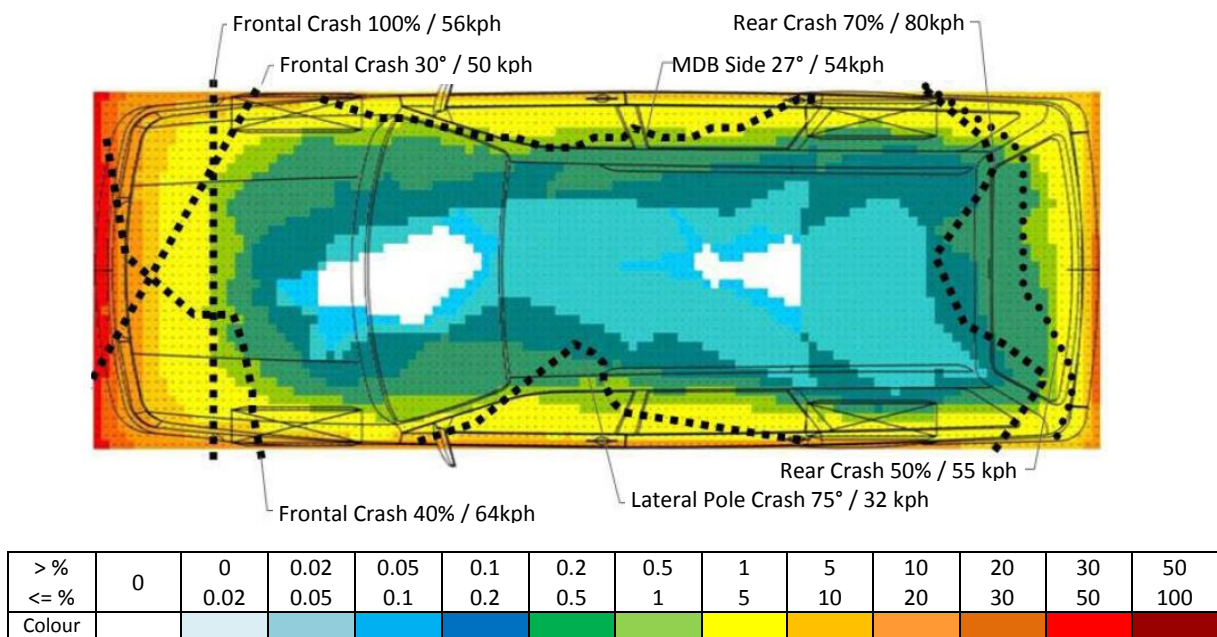


Figure 9: Accident deformations (17)

With respect to these results suitable locations for the positioning of EESS can be determined. As presumed the area in the middle is the best. This investigation was carried out assuming ordinary cars. When talking about electric cars, also new and especially light weight designs may enter the market. For these cars the safety zones may look different.

The zones with a very low probability of deformations are small and total certainty of no deformation at all cannot be guaranteed. Therefore the EESS can be exposed to deformations and must withstand a certain extent of deformation without causing serious danger.

### 1.3 Batteries

A battery is a device which consists of at least one electro-chemical cell in which energy is stored chemically. This energy can be tapped as electrical energy.

Because of this distinction secondary batteries are of interest for being applied in vehicles.

Batteries can further be subdivided into primary batteries, which are not rechargeable, and secondary batteries, which can be recharged (18).

An electro-chemical cell consists of two different electrodes inside the same electrolyte. In order to prevent an internal short circuit a separator is placed between the electrodes. The separator is a membrane which is permeable for ions with a preferably low resistance for ions, which carry charge. There is also the need for a separator with a low net weight and high mechanical and chemical stability. (19)

The two different electrodes are named anode and cathode. The anode, which is the negative electrode, is the donating electrode when the battery is discharged.

Some batteries have solid electrolytes (20). The battery under study has a liquid electrolyte.

As Figure 10 shows there are three major battery cell designs, namely cylindrical cells, prismatic cells and pouch cells for being applied in vehicles. Depending on the design the electrodes are arranged in coils, wraps or stacks. While cylindrical and prismatic cells are rather stiff, pouch cells are flexible. Pouch cells are also called coffee pack cells because a flexible foil is encasing the inner components. (21)

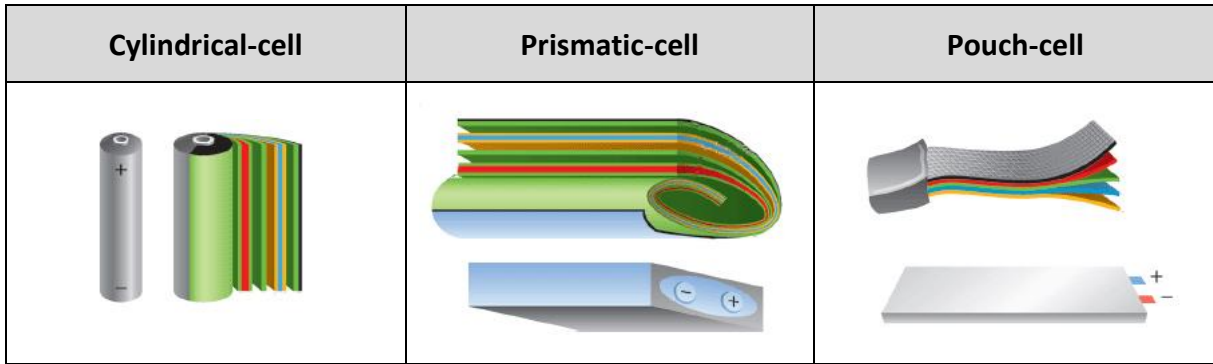


Figure 10: Battery concepts (21)

Figure 11 illustrates different battery types by comparing energy density with power density. The red sector represents the lithium ion battery cell range. Lithium ion batteries have a big advantage when optimized for energy and power. According to a study of the International Energy Agency the specific power ranges from 7 to 9,000 W/kg and the specific energy ranges from 42 to 180 Wh/kg is realizable for these battery cells. (22)

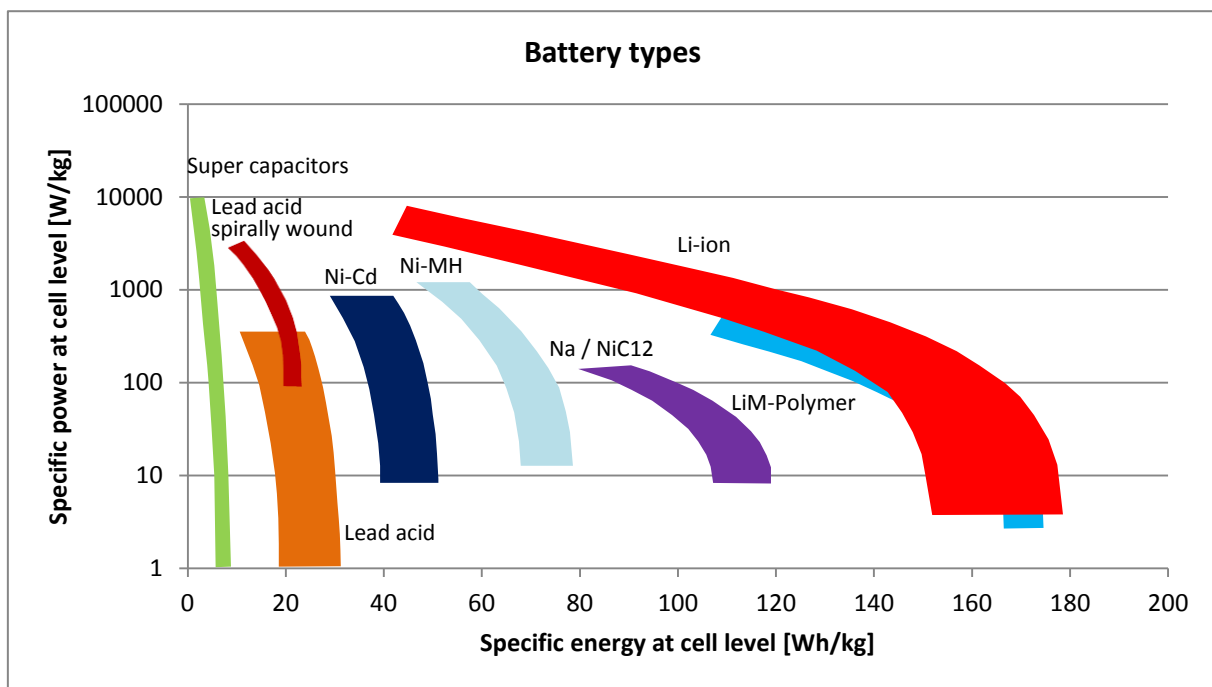


Figure 11: Battery types (22)

There is no optimal battery type for all applications. Whereas electric vehicles have the demand for batteries with a high energy density, hybrid electric vehicles need a high power density. There are also other important criteria for the selection of the suitable battery. The number of charge cycles, which specifies a battery's expected life, is crucial because high energy and power densities are worthless when there are high capacity losses after multiple charging cycles. The number of charge cycles for lithium ion batteries until they show a

capacity loss of ten percent amounts to approximately 2,500 (23). The different battery principles also react differently to temperature conditions and some show a drop in performance when exposed to low temperatures. Due to the increasing importance of batteries for many applications new developments of materials and procedures are continually made. (18)

*'Lithium-ion battery technology provides the highest available energy density of any long-cycling rechargeable battery.'* is declared by Branett et al. in the book Batteries for Sustainability page 286 (18).

Therefore this thesis exclusively deals with lithium ion batteries, although the basic findings also play a role for other battery types as they concern the fundamental makeup of batteries.

In Figure 12 the principle makeup of a lithium ion battery cell is shown.

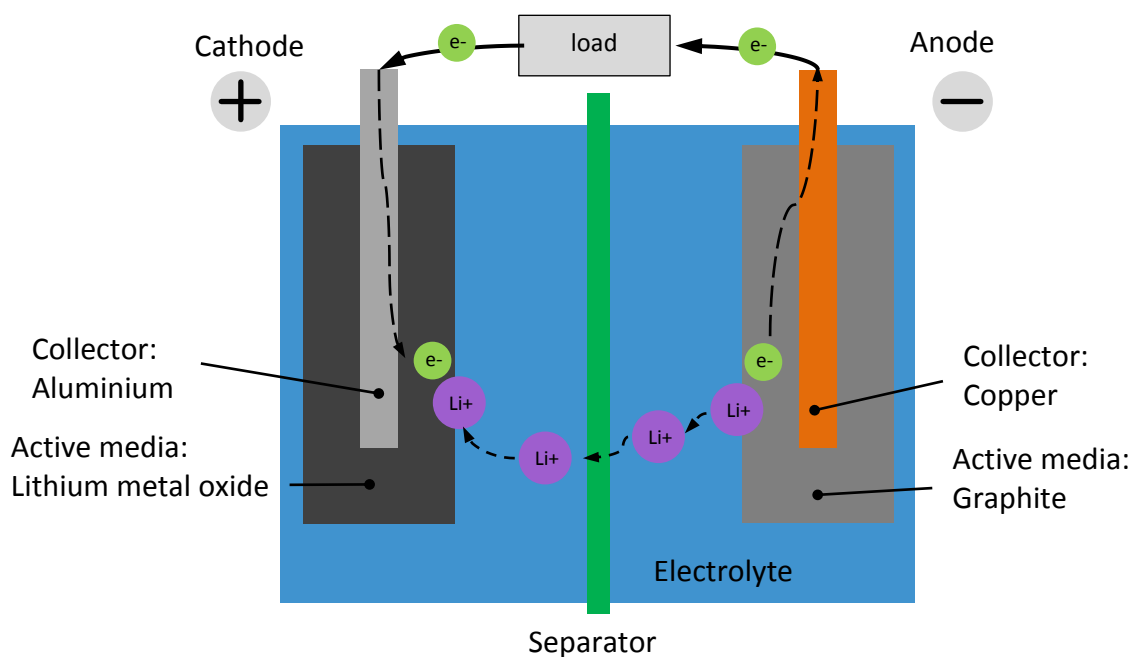


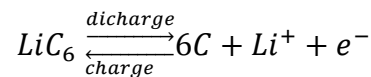
Figure 12: Battery principle (based upon) (9)

The anode consists of a copper collector coated with graphite as active media. Active media is the material which is directly responsible for incorporation processes of ions. During the first initial charging the SEI (solid electrolyte interface) layer is built by reductive decomposition around the anode. With its chemical makeup and its thickness this layer is strongly defines the electro-chemical behaviour of the cell. As the SEI layer is on the surface of the anode it can also be relevant for interlaminar interaction processes. (24)

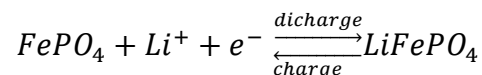
The cathode has an aluminium collector which is coated with lithium ion phosphate.

Because lithium heavily reacts with water the electrolyte is a solvent for ions not containing any water. The electrolyte is a liquid which can evaporate and burn at a certain temperature when ignited starting at 130 °C (25). (24)

The chemical equations for both, the anode and the cathode are given in Equation 1 and Equation 2. The standard chemical potential of a lithium ion cell is in the range of 3.3 to 3.6 V and depends on the chemical composition of the electrodes. (26)



Equation 1: Anode reaction during discharge (26)



Equation 2: Cathode reaction during discharge (26)

This chemical principle is also important when talking about interlaminar interactions of lithium ion batteries because the chemical processes change the active media which could further affect those interactions.

## 1.4 Investigated Battery

This thesis exclusively deals with a lithium ion battery manufactured by the company A123. The investigated battery is a so-called pouch or coffee pack cell and is shown in Figure 13. The battery has a length of 227 mm, a width of 160 mm, is 7.25 mm high and weighs about 496 g. The battery has a nominal voltage of 3.3 V and a nominal energy content of 65 Wh. (23)



Figure 13: A123 AMP20 (23)

The battery is made up by 25 anodes and 24 cathodes with a separator wrapped around the electrodes in an s-shape. The schematic makeup can be seen in Figure 14. Also the different material combinations which there are inside the pouch cell are highlighted.

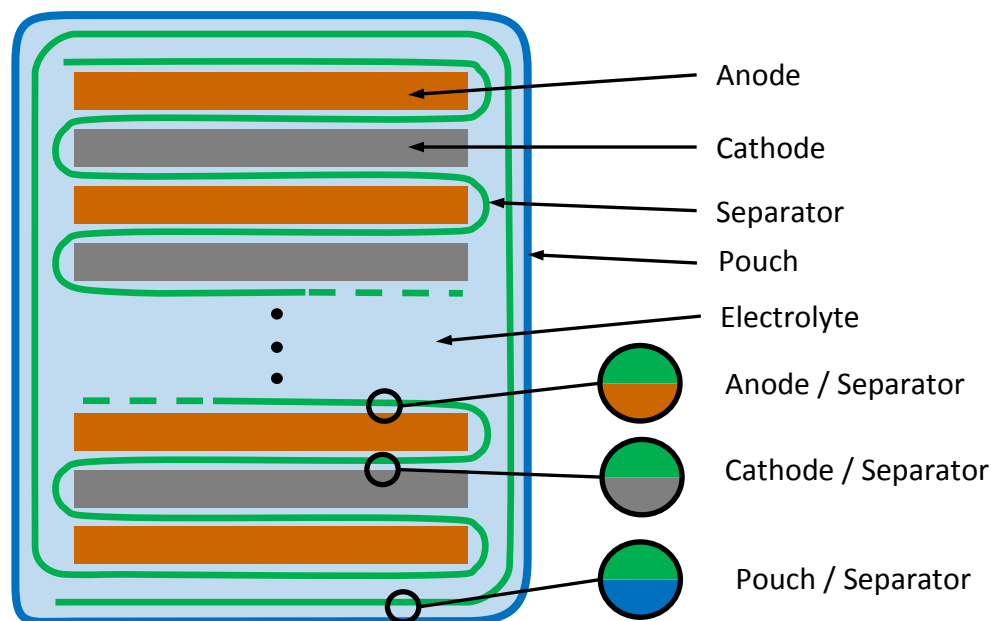


Figure 14: Schematic makeup of the pouch cell

Important for the interactions are the materials of the single components which make-up the battery.

The pouch of this particular battery cell is made up by six layers with an aluminium core layer covered by plastic layers. The anode consists of a collector of copper with a width of about  $10\ \mu\text{m}$  and graphite as the active media used for the coating with a thickness of about  $40$  to  $45\ \mu\text{m}$ . In total the cathode is about  $100\ \mu\text{m}$  thick. The cathode is also a compound of



collector and an active media. The collector is an about 20  $\mu\text{m}$  thick aluminium foil. A phosphate of lithium and iron, exactly  $\text{LiFePO}_4$ , is the active media the cathode is coated with. The thickness of the coating is about 60  $\mu\text{m}$ , which leads to a total thickness of the cathode of about 140  $\mu\text{m}$ . The separator is about 23  $\mu\text{m}$  thin and the material is not clearly identified yet. It is either PP or PE, or a mixture of both. (27)

The structure is important for the behaviour and can either be created with chemical processes or by mechanical methods. Single-layer as well as multi-layer separators are used in battery cells. (28)

The electrolyte is a mixture of ethylene carbonate and diethyl carbonate and contains lithium salts like  $\text{LiPF}_6$ . (24)

### 1.4.1 Battery testing

As the implementation of lithium ion batteries for the purpose of storing energy, which is needed for the propulsion of the vehicle, is a relatively new topic, there is the need for investigation in order to guarantee an impeccable functionality.

In other fields of applications and industries lithium ion batteries have already been introduced in different application fields and safety standards have been developed. These standards can serve as a basis for battery testing standards related to electric vehicles. (29)

The UL1642, an Underwriter (UL)-Standard, was developed for lithium ion batteries in the customer electronics industry and determines electrical and mechanical tests. Tests, like pre-tests, intended use simulation tests, reasonably foreseeable misuse tests and design consideration tests for rechargeable batteries irrespective of the chemical makeup are given by the ANSI C18.2. Abuse tests (mechanical, electrical and environmental) are defined by the UN transportation requirements. IEEE standards, which have been developed for mobile phones or portable computers, provide safety and quality requirements. (29)

According to Cunningham a classification of battery tests can be made into performance tests and abuse tests (30). Performance tests ensure the proper work of the battery when used the way it was designed for. On the other hand there are abuse tests which have the purpose to test how the battery reacts under not normal conditions or environments. Abuse tests are further subdivided into mechanical abuse tests, thermal abuse tests and electrical abuse tests. (31)

The level of assembly is also used for classification and there are tests for units, modules and packs of batteries. (31)

Testing can be divided into component tests and full vehicle tests, which is a further differentiation into sub-domains. Component tests are important because the testing is done under defined conditions with specified loads and in this way detailed conclusions exactly referring to the influence values can be made. One weakness of component testing is, however, that there is no possibility to make statements regarding the performance of the entire system in the case of a crash. As far as costs and effort are concerned component testing has its strengths. It can be done at an early stage of the development of a new electric vehicle when there is still the possibility to modify the construction, which is not so easy when full vehicle tests require modifications. Component tests are also used for the

validation of numerical models. Full vehicle tests show the performance with respect to the integration of batteries. (32)

Battery testing can also be divided into normative and legislative testing, which has to be performed, and additional recommended tests, which consider real world accidents that are not sufficiently covered by normative tests. Generally, there is a big increase in normative tests carried out and a lot are still under review. (31).

#### 1.4.2 Mechanical abuse tests

The sense of mechanical abuse testing is to investigate the behaviour of batteries in special conditions. So the effects caused by mechanic loads can be observed.

There are different groups of mechanical abuse tests whereby the basic test principle is similar, but detailed regulations, as for example the detailed force or orientation of the cell, differ. (33)

In a crush test the specimen is crushed by two surfaces which are approaching each other. The minimum approaching velocity as well as the form of the surfaces is predefined whereby a flat, a curved or a textured surface is pressed against a flat one. Also the crush rate or the crush force is defined. The force can be given as an absolute value or in relation to the mass of the specimen. This test is performed to show the specimen ability to withstand a crush force. (32)

Shock tests were made by accelerating the specimen at different levels in different directions. Each cell has to withstand a specific number of tests at an average acceleration and peak acceleration (31).

A specifically harmonic motion at certain amplitude and specific frequency is applied to the specimen in order to make vibration tests. Impact tests are made for determining the specimen's ability to withstand a specified impact. From a specific height a weight is dropped onto a cylindrical test body which is positioned on top of the specimen. (31)

Also drop tests are part of different mechanical abuse safety standards. In these tests the cell or module is dropped from a certain height onto a barrier-surface. Some standards define the specimen's corner which has to hit the surface first. The barrier surface is either planar or cylindrical. In SAE J2464, for example, the drop-height is 2 m and the diameter of the cylinder is 300 mm. (34)

Penetration tests can be found in various test standards whereby a conductive penetrator like a steel rod with certain dimensions penetrates the specimen at a given velocity. (35)

There are also other tests which attempt to simulate real crash scenarios or which are used for the validation of numerical models. Sinz et al. recommend several tests for this validation process which can be seen in Table 1. (32)

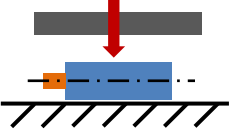
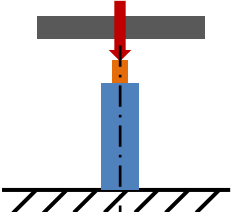
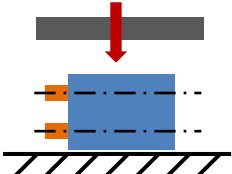
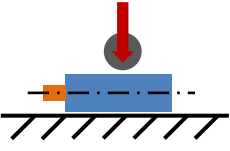
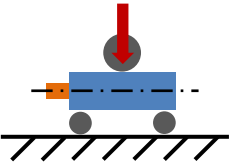
	Thickness	Height	Width
<b>Crush</b>			
<b>Indentation Test</b>		X	X
<b>3 Point Bending</b>		X	X

Table 1: Test recommendations (32)

For evaluating the mechanical abuse tests seven hazard levels have been introduced by EUCAR, the European council for automotive R&D (31). These hazard levels and detailed classification criteria are shown in Table 2.

Hazard Level	Description	Classification Criteria and Effect
0	No effect	No effect. No loss of functionality.
1	Passive protection activated	No defect; no leakage; no venting, fire, or flame; no rupture; no explosion; no exothermic reaction or thermal runaway. Cell reversibly damaged. Repair of protection device needed.
2	Defect/Damage	No leakage; no venting, fire, or flame; no rupture; no explosion; no exothermic reaction or thermal runaway. Cell irreversibly damaged. Repair needed.
3	Leakage $\Delta_{\text{mass}} < 50\%$	No venting, fire, or flame; no rupture; no explosion. Weight loss $< 50\%$ of electrolyte weight (electrolyte = solvent + salt).
4	Venting $\Delta_{\text{mass}} \geq 50\%$	No fire or flame; no rupture; no explosion. Weight loss $\geq 50\%$ of electrolyte weight (electrolyte = solvent + salt).
5	Fire or Flame	No rupture; no explosion (i.e., no flying parts).
6	Rupture	No explosion, but flying parts of the active mass.
7	Explosion	Explosion (i.e., disintegration of the cell).

Table 2: EUCAR hazard levels (31)

These classification criteria were used in different testing standards like in FreedomCAR (31) or modified in SAE\_J2464 (34).

Apart from these rather quantitative classification criteria also quantitative measurements of temperature, current or resistance are suggested by FreedomCAR (31).

The drop test according to FreedomCAR (page 19) serves as basis for the investigations of the interlaminar shear velocity (31). In the test a battery pack is dropped in free fall from a height not exceeding 10 m onto a steel pole with 300 mm diameter (see Figure 15). As the height should be determined according to abuse conditions and the test is proposed for battery packs, the height given in the SAE\_J2464 drop test with 2 m is taken for the calculations (34). The battery shall impact the cylinder with its lateral surface. Instead of a drop a horizontal test with the same configurations (speed and pole orientation) is acceptable. (31)

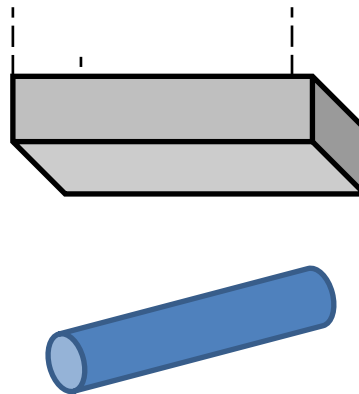


Figure 15: Drop test impact (31)

Suggested measurements include acceleration and high speed videos during the test. Before and after the test a measuring temperature, voltage, resistance between the electrodes and photographs is recommended. Additionally a chemical analysis of vented gas and smoke, their flammability, the deformation and the temperature of the battery as a function of time should be made after the test.

The battery tests dealt with in this chapter also do not depict all loads which can occur in vehicle crashes. Therefore dynamic loads with very high force peaks have to be tested. (32)

## 1.5 Physical effects in interfaces

For the implementation of the interactions into a numerical model it is important to know the sum of all the effects contributing to the interfacial behaviour. Nevertheless, it is very important to know about possible contributing effects to understand the control variables for the impact of the interactions.

An interface separates two phases (36). Numerous physical effects determine the behaviour of interfaces. Particularly when talking about batteries in the mechanical sense, a battery can be seen as a kind of laminate because of its makeup. Due to the word lamina for a sheet of a composite the term interlaminar interface is used to denote the relationship between the laminates (37).

The focus of this thesis is laid on the interface between the inner solid parts of a battery. These interactions exist between the different layers of batteries formed by the alternated arrangement of electrodes on the one hand and separator on the other hand.

There are also interfacial areas in batteries which are not discussed here because in the first stage of research they play a minor role. For example there is an interfacial area inside the electrodes between the collector material, aluminium for the cathode and copper for the anode, and the active media. But these phases are strongly bound together and compared to the shear possibilities between the electrodes as a whole and the separator, the interface inside the electrode can be unattended. According to the definition other interfaces can be found between the solid components and the electrolyte, as these are also different phases. In this thesis the electrolyte is considered as a lubricant and is not investigated as a separate phase.

Especially for systems with a characteristic length scale  $\lambda_c$  within the range of nm to  $\mu\text{m}$  the interface interactions are important compared to gravitation and inertia. Butt and Kappl suggest using the ratio of the total volume and the interfacial area as the characteristic length scale (see Equation 3). (38)

$$\lambda_c = \frac{V}{A}$$

Equation 3: Characteristic length scale

For the investigated battery model a characteristic length scale of about 32  $\mu\text{m}$  can be calculated. With respect to the indication of nm to  $\mu\text{m}$  values the calculated value lead to the conclusion that interfacial forces can be relevant for the whole system.

Figure 16 illustrates a schematic deformation of a battery in the cross section, showing interlaminar shear. The orange and the grey bars represent the different electrodes and the green bar represents the separator. The casing of the battery is not illustrated in this principle. When bending the battery around an obstacle like a pole, which is illustrated as a blue circle, the different layers deform independently, except for the effect caused by the interactions between the layers, and a relative shear, which is illustrated as a red arrow on the right side of the figure, occurs.

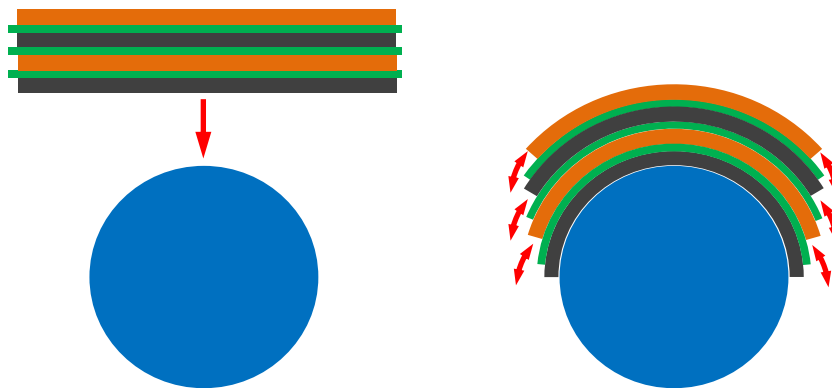


Figure 16: Interlaminar shear

The interlaminar shear occurs because the interlaminar interface, especially in combination with the presence of the electrolyte as a lubricant, acts as a sliding plane. The magnitude of the sliding resistance is of interest and is investigated in this thesis. This is crucial for the deformation behaviour, inner damage mechanisms, deformation work and also as a crucial input for the numerical simulation.

### 1.5.1 Adhesion

Adhesion forces are interacting surface forces between different phases, which strongly decline with distance and are dependent on the contact area and the strength of the attracting interaction. Adhesion is important if the surfaces are very smooth or one body consists of a soft material or if the system is considered as a microscopic system, where volume forces play a subordinate role in general. Contamination particles and humidity strongly affect adhesion.

The adhesion force is the sum of various forces like van der Waals forces, electrostatic forces, chemical bonding force, hydrogen bonding forces, capillary forces and others, as given in Equation 4. (38)



$$F_{adh} = F_{vdW} + F_{el} + F_{chem} + F_H + F_{cap} + \dots$$

Equation 4: Adhesion force (38)

The energy which is stored because of elastic deformations when two rough surfaces are in contact with each other, acts against adhesion and lowers the attracting strength. Because of this adhesion almost disappears for solids having a high surface roughness and Young's modulus. (39).

### 1.5.2 Van der Waals forces

Van der Waals forces are interactions between neutral molecules due to dipolar interactions. Because they exist between any combinations of molecules and surfaces they are important. For a macroscopic view they play a minor role because they have a complex dependence on the distance, which is already resulting from the surface roughness. (38)

### 1.5.3 Electro static force

The surface force due to the charged layers can be calculated with Equation 5.

$$F = \frac{1}{2} * \epsilon_0 * \epsilon_r * \frac{A}{d} * U^2$$

Equation 5: Capacitor force (based upon) (38)

When comparing this force of about 0.005 N, with the force due to the cell's evacuation pressure, the former can be neglected.

### 1.5.4 External forces

The battery cell can be considered as a closed container filled with electrolyte. The pressure inside this container depends on the gas pressure of the electrolyte. The ambient pressure was assumed to be 1 bar. The difference between the pressure inside the cell and the ambient pressure outside is responsible for the compression of the battery layers. Measuring the inner pressure was not possible at the institute. The inner pressure of the battery cell can be assumed to amount to 0.3 bar (27). The force which compresses the battery cell can be calculated by multiplying the differential pressure by the area which is given by Equation 6.

$$F = p * A$$

Equation 6: Force relating to pressure

The maximum specimen size amounts to 200 by 150 mm. In order to extract multiple specimens per layer and in order to have enough surface protruding beyond the clamps, a specimen size of 50 by 150 mm was eventually selected. Hence the required clamp force amounts to approximately 520 N.

### 1.5.5 Capillary forces

Assuming two round glass plates with a liquid film in between the capillary force to separate them is calculated by means of Equation 7 using the surface energy density  $\gamma$ . (40)

$$F = A * \Delta p = A * \gamma * \left( \frac{1}{r} - \frac{1}{R} \right)$$

Equation 7: Separation force round plates (40)

A sketch of the separation principle is shown in Figure 17.

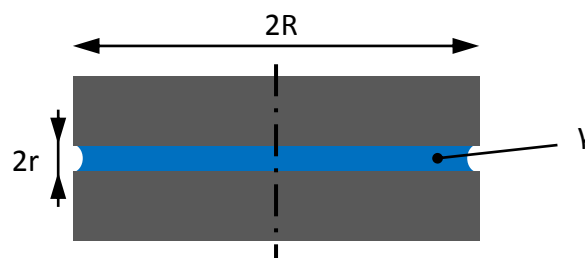


Figure 17: Schematic separation round plates (based upon) (40)

As the radius of the glass plates is distinctly bigger than the radius built by the liquid it is neglected for the calculation of the force. Therefore the force can be calculated by Equation 8.

$$F \approx L * W * \gamma * \frac{1}{r}$$

Equation 8: Separation force electrodes

A sketch of the separation principle is shown in Figure 17.

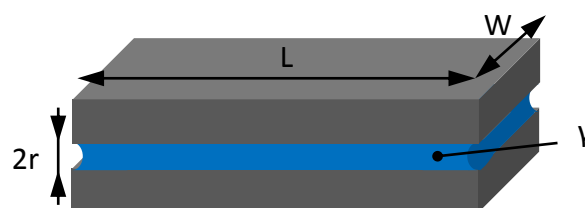


Figure 18: Schematic separation electrodes

Considering the battery the calculation is made with the assumption that the two plates are the electrodes and the separator is seen as the fluid gap as it is fully soaked with electrolyte. For the electrolyte no surface tension was found in literature, but similar substances show a range from 20 to 50 mN/m (41). These values led to a force of about 90 N which has to be overcome to separate two electrodes. This force also acts between the layers when the pouch is removed.

The function of the force according to the percentage of the separator thickness is shown in Figure 19.

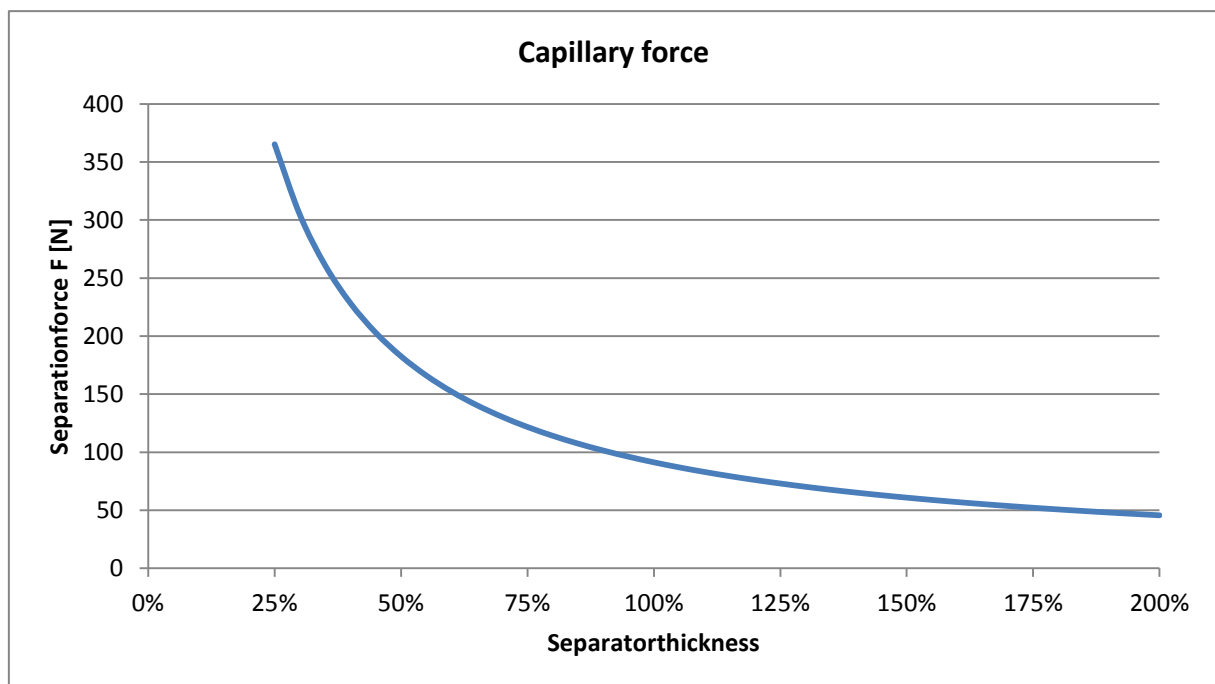


Figure 19: Capillary force

### 1.5.6 Friction

Friction is the term which describes the force that resists a relative movement of two interacting surfaces or even hinders movement at all (38).

If wear and lubrication, which are closely linked to friction, are also dealt with, the word tribology is often used. In tribology processes surfaces of the materials are modified (42).

*'In spite of the importance of this field, there is no general macroscopic theory of friction that would allow us to predict the frictional force between two given bodies, and our understanding is still rudimentary. This results from the complexity of these topics'* (Butt and Kappl 2013, Page 251 (38))

Because there is a significant interaction between friction and relative velocity a differentiation in relation to this relative velocity is crucial. So there is dynamic friction and static friction. Static friction is the resistance against movement while there is no movement yet. (36)

Also with respect to lubrication a differentiation is made.

Coulomb friction, which is the general term for dry friction, occurs when there is no contamination between the two solid surfaces at all. In reality there is nearly always something in between.

Dry friction is described by the Amontons' law, which says that the friction force does not depend on the contact area and is proportional to the load (38).

It can be described with Equation 9 where  $\mu$  is the coefficient of friction.

$$F_F = \mu * F_N$$

Equation 9: Dry friction

Apart from dry friction there is also lubricated friction.

Lubrication is used to reduce friction and wear. The thickness of the lubrication film is crucial for the type of lubricated friction. This can be shown with the Stribeck diagram in Figure 20 where the friction coefficient is illustrated with respect to the sliding velocity. The Stribeck diagram can be divided into three segments. For low sliding velocities the segment is called boundary lubrication. In the third section, the so-called hydrodynamic lubrication, the velocity of the relative movement is responsible for the creation of a lubricant film which

reduces the friction significantly but with higher velocities the friction coefficient rises again due to viscosity resistance inside the lubricant film. The segment in the middle is determined by the coexistence of friction caused by the contact of the solid surfaces and the lubrication friction. This segment is called mixed lubrication. (38)

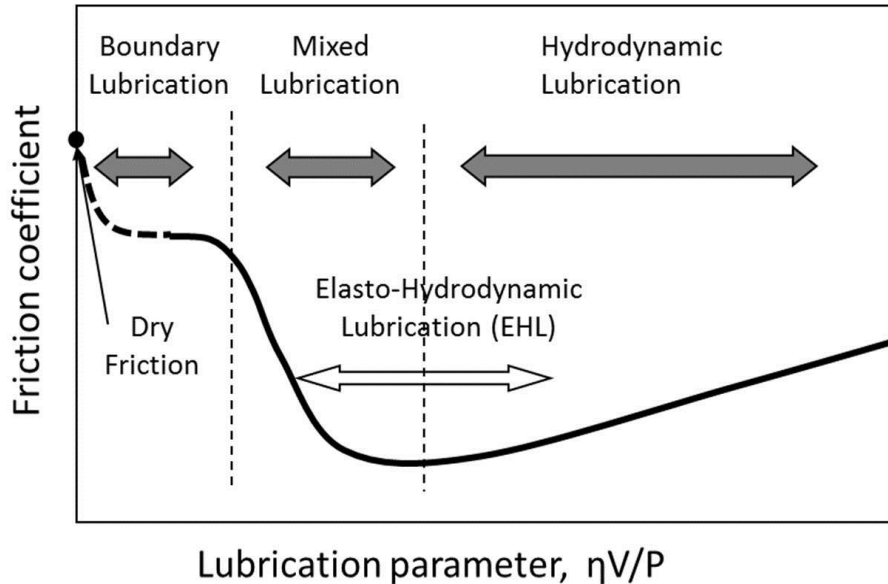


Figure 20: Stribeck curve (43)

Because of the low sliding velocity in combination with the high normal force the lubricant is squeezed out of the sliding plane and boundary lubrication occurs. For some materials it was shown that the number of micro contacts is not changed by the presence of a lubricant. As long as a little lubricant is absorbed, friction is significantly reduced in comparison to dry friction, which in fact does not exist in ambient conditions, but just occurs in ultra high vacuum conditions. As this dry friction is a more theoretical approach, all friction measurements which were done under ambient conditions represent boundary lubrication instead of dry friction. (38)

A schematic illustration of boundary lubrication is shown in Figure 21. The micro contacts between the sliding partners (light and dark grey) as well as the lubricant (yellow) between them are shown.

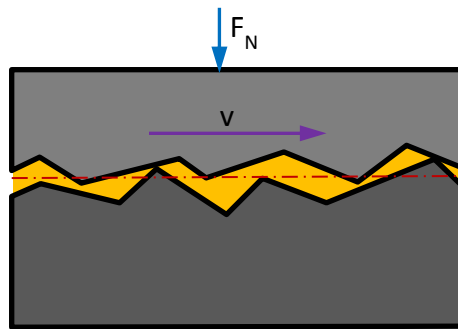


Figure 21: Boundary lubrication (44)

Mixed lubrication is an intermediate state between boundary lubrication and hydrodynamic lubrication. There is a lubricant layer between the surfaces but this layer does not separate the surfaces completely. Because of the surface roughness there are still some contacts but by far fewer. (45)

Figure 22 shows the mixed lubrication. In the figure no contact is visualised, but when one sliding partner moves into a direction the other sliding partner is contacted.

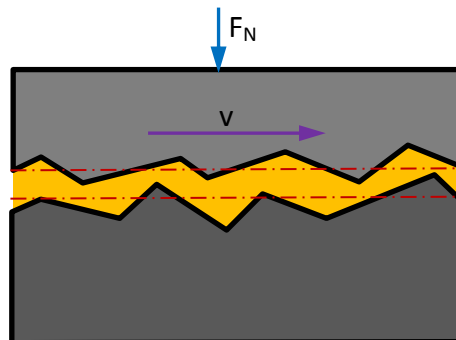


Figure 22: Mixed lubrication (44)

Hydrodynamic lubrication is present when the lubrication film is thick enough to totally separate the sliding partners and no direct contact between them exists. This principle is illustrated in Figure 23 and the shear force can be calculated with Equation 10, which was originally found in the course of experiments. The force  $F$  divided by the area  $A$  of the sliding partners equals the viscosity  $\eta$  multiplied by the relative velocity  $\Delta v$  and divided by the distance of the sliding partners'  $\Delta z$ . (38)

$$\frac{F}{A} = \eta * \frac{\Delta v}{\Delta z}$$

Equation 10: Hydrodynamic force (38)

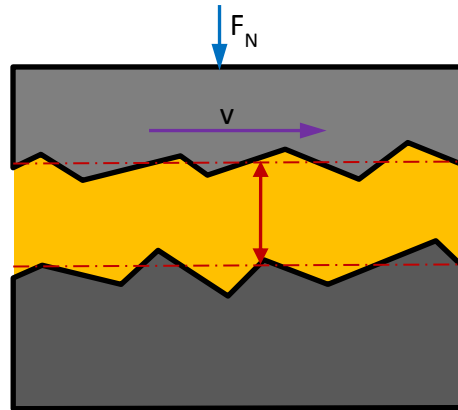


Figure 23: Hydrodynamic lubrication (44)

In this case the dynamic viscosity of the lubricant is an important parameter.

## 2 Motivation

My motivation to do research and write this thesis was to contribute to the safety of electric vehicles which are equipped with or powered by secondary lithium ion batteries.

In previous research work at the VSI (Vehicle Safety Institute) a numerical microscopic battery model was developed (27) (46) (47) (48). Microscopic means that every single battery component and layer is modelled. The model consists of the pouch or casing of the battery, the alternating electrodes and the separator in between.

In order to develop this model various experiment tests were performed. To investigate the structural behaviour two-point and three-point bending tests, among others, were performed with single components as well as with laminates of several layers. The whole battery cell was placed on two poles and the sag due to the own weight was measured. Then the pouch was sliced open and removed. Without the pouch there is no longer a pressure difference between the outside and the inside. Hence, no force resulting from this pressure difference compresses the layers and does not change the sag of the battery cell much. Finally the layers were detached and reattached again and the two-point bending test was performed again. A significant change in the sag was identified as the stiffness of the battery decreased evidently. The question arose what the reason for this behaviour is. Theories about a break up of mechanical connections or the evaporation of the electrolyte and therefore a change in the interface were discussed and the need for detailed investigation of the effects between the layers was identified. The bending tests are sketched in Figure 24.

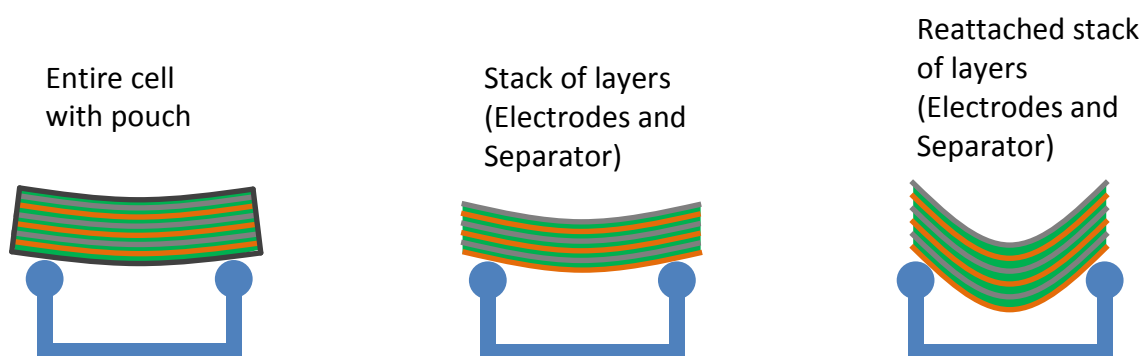


Figure 24: Two-point bending tests



## 2.1 Current battery model

All components are modelled as shell elements (see Figure 25) with material properties derived in tensile tests. The contact between the components has been realised by a simple friction model. The friction coefficient was selected without any prior research work. Just a constant friction coefficient was considered, disregarding dynamic effects. In previous models a tied-contact with failure was used in order to simulate the behaviour observed in two-point bending tests (as described before). (27) (47) (48)

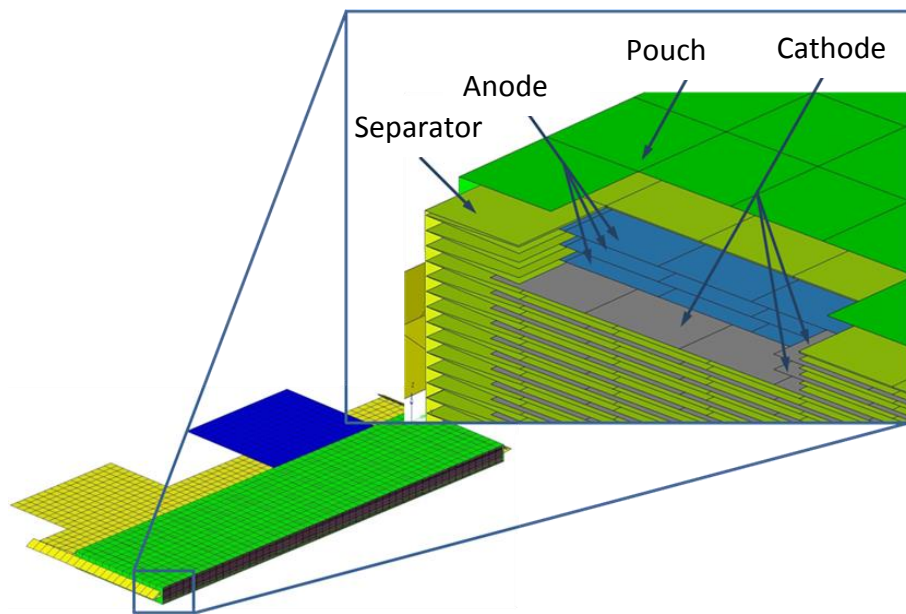


Figure 25: Current battery model (27)

## 2.2 Fields of improvement of current model

Weaknesses of the already existing model are bending tests. For bending deformation the interlaminar shear plays an important role and so there is some room for improvement.

A detailed investigation of the interlaminar interactions can be made in order to find some improvement. The friction coefficient between anode and separator as well as the friction coefficient between cathode and separator shall be investigated separately. Furthermore, not only the interlaminar interactions between the electrodes and the separator, but also the interactions between the pouch and the separator may further improve model-performance and should be investigated as well.

Investigations in dynamic load cases are also a field of improvement for the already existing model.

### 3 Hypothesis and objective

The main objective of this thesis is to explain mechanical interactions inside a battery in order to enhance the performance of the numerical battery model when being bent.

#### 3.1 Hypothesis

Interlaminar interactions in lithium ion batteries may play an important role for the overall deformation behaviour, especially for dynamic loads. The interface is characterised by:

- Large contact surface areas compared to small cross-sections of laminate layers.
- A wide range of material properties in terms of Young's modulus, ranging from 2 to 70 GPa (27).
- Contact partners soaked with electrolyte.
- Pressure difference due to encasing.

#### 3.2 Objective

The objectives of this thesis are:

- Develop methods and tools to characterise the interlaminar interfaces in a lithium ion battery cell.
- Outline an adequate interlaminar interface model, which can be implemented in an existing numerical model of a lithium ion battery.
- Derive input parameters for this interface model, i.e. coefficient of friction, break-away force.
- Identify parameters to which the interfacial behaviour is sensitive, i.e. velocity, pressure.
- Find explanation for behaviour in two-point bending tests observed in previous research.

## 4 Methods

There are different directions and mechanism which can cause different types of loads – see Figure 26. If the load is linear and the acting direction is normal to the interface surface, it is called tension or compression, depending on the direction of the load. A load which tears the surfaces open is named cleave load. Further, the relative movement could occur in the mode of a peel load, where one surface is pulled and rotated simultaneously and the second one performs no movement at all. The last type of an interfacial load is the shear load, where the load is induced in the plane of the surfaces and the direction of the load is also in the plane of the surface.

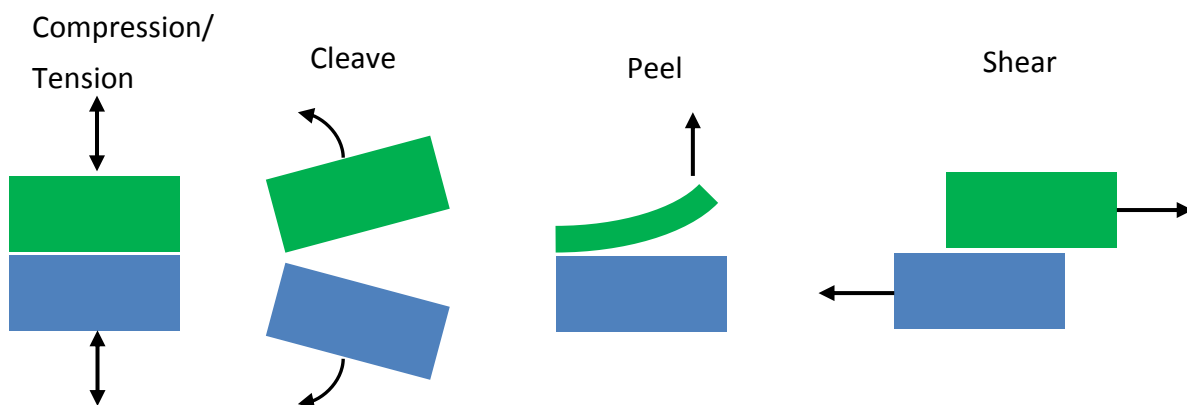


Figure 26: Types of interfacial loads (49)

This thesis will mainly focus on shear. In case of a bending deformation there are interfacial shear loads. Because of the weaker shear resistance in the interface plane relative movements occurs there.

## 4.1 Test station development

Two principles must be fulfilled in order to investigate interlaminar interactions. First, the surfaces of the contact partners have to be aligned and pushed against each other with a pre-defined force. Second, the shear movement has to be ensured and interactions have to be measured in terms of shear-force and shear-displacement.

For providing the movement two variants could have been implemented. The first was a linear movement and the second a rotation movement. The rotation movement has the big advantage that always the same surfaces are in contact, and no new contacting surfaces with newly defined contacts influence the measuring. A disadvantage is that there is a velocity difference because of the rotation movement. While there is the full velocity at the circumference, there is hardly any movement in the centre. To counteract this interfering fact the rotation of two annuluses was discussed. This had the advantage of using the same surfaces combined with negligible gradient in movement and velocity. The disadvantage was that the outer diameter of the annulus was limited by the width of the electrode and the length difference of the circumference of the inner diameter compared to the circumference of the outer diameter should be negligible compared to the length of the average circumference. Otherwise the gradient could play an important role in the measurements. This would lead to the fact that the area of the annulus would be very small and inaccuracies in measurement could play a significant role. A further disadvantage is that influences of the orientation of the materials cannot be observed as they change due to the rotating process.

The second variant of movement is the linear one. For this variant the relative displacement and velocity are almost constant for the entire interacting surfaces. But there is a disadvantage. The interacting surfaces are moved on and are not the same all the time. So there is steadily a new contact between surfaces which have not been in contact before, and changes due to the relative movement have not occurred to at least one of these surfaces.

When considering the pros and cons of the two possibilities, the linear variant surpasses the rotation variant and therefore served as principle for the test station development. As principle the linear relative movement was taken. The force which is needed to make the movement of the clamped specimen possible and which is caused by the interactions is the aim of the measuring.

Table 3 illustrates the principles and lists advantages and disadvantages of the different principles.

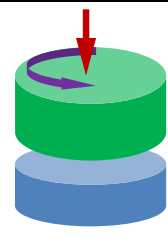
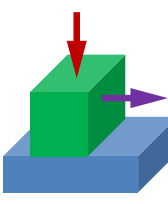
Principles	Sketch	Advantages	Disadvantages
Rotation	 Rotation Moment as function of the normal force Fixed Part	Same interacting surface	Velocity gradient Orientation changing
Linear	 Linear Force as function of the normal force Fixed Part	Same velocity over the whole acting surface	Changing interacting surfaces Elasticity

Table 3: Test principles

## 4.2 Preparation of Specimens

To get specimens for testing the battery cell had to be disassembled. Due to the danger resulting from electric energy inside the battery, potentially leading to fire or explosion caused by a short circuit during disassembly, the battery cells had to be fully discharged. Batteries were discharged with a battery charger and further to this with a resistor connected to the terminals. Gases, fumes and liquids which leak during disassembly are hazardous to health. During disassembly protective equipment, i.e. goggles, gloves, and respiratory protection was worn.

The active material reacts when exposed to humid air. Therefore specimens had to be extracted, stored and even tested in an electrolyte bath.

The electrolyte had to be replaced by a substitute. The original electrolyte contains special salts to make conductivity possible by providing ions. These salts are dangerous because they build hydrofluoric acid when exposed to water or humidity. To simulate the conditions inside the battery a substitute electrolyte was taken. The substitute electrolyte is made up by seven weight parts of Diethyl carbonate and three weight parts of Ethylene carbonate (50). The substitute electrolyte does not contain these dangerous salts.

Accordingly, the disassembly of the battery, as well as all other work with the electrodes, was performed in a substitute electrolyte bath. Also the storage of the specimens for later usage in the test stand or for microscopy had to be done in closed containers filled with substitute electrolyte.

The separator, which is not chemically affected by water, was taken out, put into a water bath, washed and dried for further use. The washing and drying was necessary for attaching the separator to test bodies, which is described in the test station design. Without sufficient washing the electrolyte leftovers in combination with the water chemically attack the separator and the specimens could not be used any more.

### 4.3 Boundary Conditions for Test stand

The maximum size of the specimens used in the test stand was limited to the dimensions of the components of the cell. There was no possibility to get specimens in other dimensions than those used in the battery under study.

The separator is folded around the electrodes in an S-shape. The total dimension of the separator is about 7,800 by 200 mm. Also the maximum size of separator specimen is limited to the size of the electrode, i.e. 150 by 200 mm, because wrinkles had developed due to folding.

One objective is the investigation of the sensitivity to shear velocity. The velocity range was estimated by using the battery drop test described in the paper by Doughty as reference (34).

An Excel spreadsheet was created to calculate the shear velocity. Shear velocity is estimated by assuming a loose stack of layers. The stack is made up of electrode and separator layers. Layers are 0.1 mm and 0.025 mm respectively thick. The entire stack is assumed to be 7.25 mm thick. This stack is hitting a pole with a diameter of 300 mm with an impact velocity of 6.3 m/s, which corresponds to a drop height of 2 m due to the drop test procedure. No interlaminar shear forces are assumed. Hence it was assumed that the stack is fully wrapping around the pole.

The radius  $r_m$  of the stack's middle layer when fully wrapped around the pole amounts to 153.63 mm. The adjacent outer layer's radius amounts to approx. 153.69 mm, assuming an average layer thickness of 0.0625 mm. The arc-length of the middle layer was assumed to be 200 mm, which is the length of the cell. The aperture angle  $\alpha$  therefore amounts to 75 deg. Hence, the shear-displacement between the middle layer and the adjacent layer measured at the outermost edges amounts to 81  $\mu\text{m}$ . It was assumed that the outermost edges are decelerated at a constant rate within the circle-segment height (assuming  $r_m$  and  $\alpha$ )

$h=12$  mm. Maintaining that the shear velocity at the outermost edges amounts to 620 mm/min and is zero in the middle, the average shear velocity is 310 mm/min.

Therefore, the test stand should supply shear velocities up to 600 mm/min.

Next the required contact forces were estimated. There are different causes which influence the normal surface force which the test stand has to recreate. With the findings of chapter 'Physical effects' the force due to the pressure difference is the dominant force and so a maximum normal force of 520 N has to be reached for the test stand construction.

As will be shown in the results, the clamp force had to be reduced, because the separator ripped several times when tests were performed even by starting with a clamp force of about 200 N.

All tests were performed at room temperature. The temperature may play a role, especially for viscosity effects of the electrolyte and also for the substitute electrolyte. Effects resulting from higher or lower temperature were not considered.

The test stand was designed in a way that a temperature control can be implemented by heating the electrolyte bath.

#### 4.4 Test stand design

Due to the consideration of the advantages and disadvantages of the different investigation principles the most suitable principle was the strip draw test, shown in Figure 27. The electrode, either the anode or the cathode, which is illustrated as an orange line, is fixed with a gripper. The load cell between the gripper and the draw arm can measure the resisting forces. The movement and the measuring of the displacement are performed by the draw arm. The electrode is put between an anvil and a guided compression plate and then pulled out. The guided compression plate applies a normal force onto the contact surface. Compression forces can be adjusted by adding weights on top of the compression plate. The clamp-surfaces (i.e. the top of the anvil and the bottom of the compression plate) were covered with separator material.

This principle is simple and robust and therefore suitable for testing under chemically aggressive conditions. The entire setup is submerged in substitute electrolyte filled into a glass tub. The glass tub is additionally filled with glass beads in order to cut costs for electrolyte.

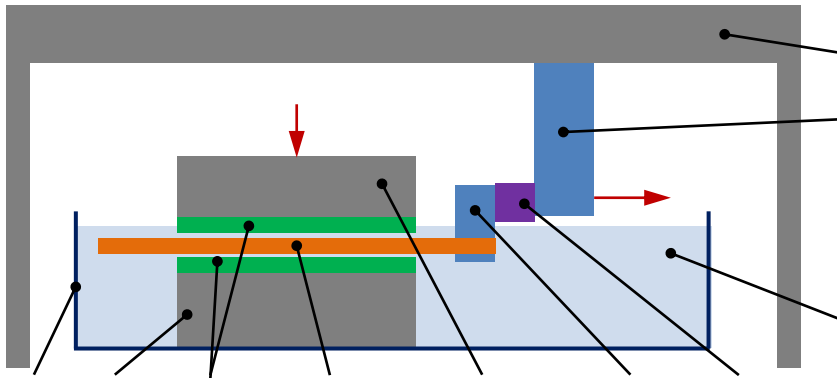


Figure 27: Schematic strip draw principle

Having agreed upon the principle the individual parts were designed in detail.

It was planned to develop a coefficient, similar to the friction coefficient for dry friction, in order to calculate occurring shear forces in the case of deformation with respect to influencing factors like the displacement velocity and the normal force.

Because of the principle that the electrode is clamped between two surfaces the calculation of friction coefficients has to be aligned to this principle.

The principle and the free body diagram of the friction model for a block on a flat surface can be seen in Figure 28.

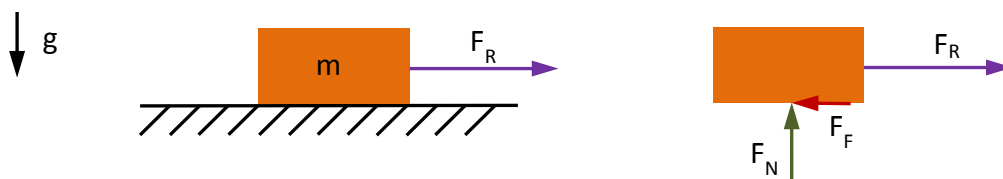


Figure 28: Conventional friction model

Because of the construction of the test stand the friction model for calculating the coefficients is different. An illustration of this model as well as the free body diagram can be seen in Figure 29.



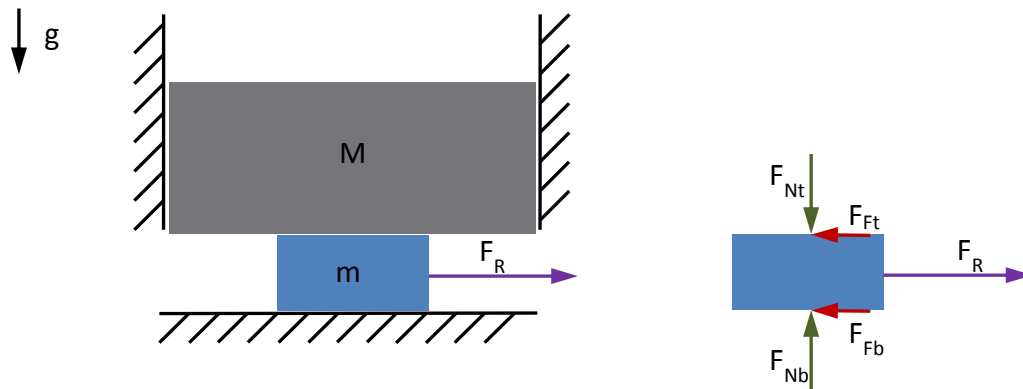


Figure 29: Test stand friction model

The model serves as simplification for the calculation of the coefficients. The lateral guidance of the mass  $M$  is seen as perfect guidance without any friction. The resulting force can be calculated according to Equation 11.

$$F_R = F_{Fb} + F_{Ft} = \mu * F_{Nb} + \mu * F_{Nt}$$

Equation 11: Relative force test stand

The mass  $m$  of the drawn electrode can be neglected as it is many times lower than the mass  $M$  of the clamping plate's weight. So the bottom and the top normal forces  $F_N$  as well as the friction forces  $F_F$  are equal. The developed coefficient can be calculated by using the Equation 12.

$$\mu = \frac{F_R}{2 * F_N}$$

Equation 12: Coefficient calculation

As the specimen is submerged in substitute electrolyte and also a bit of the covering plate is immersed in substitute electrolyte buoyancy occurs which can be calculated with the Equation 13.

$$F_B = \rho * g * V$$

Equation 13: Buoyancy force

The density of the substitute electrolyte is approximately  $1.1 \text{ g/cm}^3$  and as the displacement of substitute electrolyte is only about  $1 \text{ cm}^3$  the buoyancy force is negligible as it is just about  $0.01 \text{ N}$ .

A core element is the drive and the measurement of the displacement. To guarantee the proper functioning of these features a tensile test machine was taken and modified to our needs. A Z3-X500 from Testmatic, which is shown in Figure 30, was selected for its features and because it already existed at the Vehicle Safety Institute.



Figure 30: Z3-X500 (51)

Draw forces were measured with load cell TCTN-9110-100N (see Figure 31) with a measuring range of 0 to 100 N (52). The load cell cannot be immersed in the electrolyte. The selected load cell therefore had to be insensitive to torques induced by the offset between specimen and load-cell.

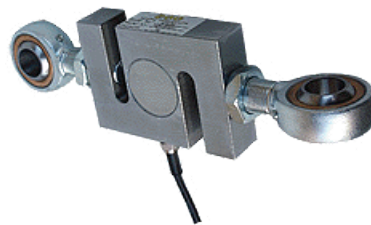


Figure 31: Load-cell (53)

The wet electrodes were clamped in a grip. The grip was designed for a quick and simple exchange of specimens with a notch to provide the precise positioning of the specimen.

The separator was attached to the anvil's and the compression plate's free surface. The separator is a thin foil with a thickness of 23  $\mu\text{m}$ . Achieving an even contact surface without wrinkles was difficult. Vacuum attachment could be excluded, because the separator is not airtight and suction channels would have prevented a smooth contact surface. Next, gluing was considered. Because of the boundary conditions gluing was challenging, too. The glue had to withstand the aggressive electrolyte or substitute electrolyte on the one hand and had to bond the separator made of a PE (polyethylene) or PP (polypropylene) to the metal anvil and compression plate on the other hand. Numerous glue tests failed. Eventually, the company Loctite-Henkl was asked for support. The laboratory at Loctite-Henkel tried some special treatments like a corona treatment of the plastic surface and the use of special primers and activators. A strong bond was gained but the thin and flexible separator could not be applied wrinkle-free to anvil or compression plate, which can be seen in Figure 32.



Figure 32: Bound with wrinkles

Then using adhesive tape was considered as a practicable alternative. The bond was found to be strong enough because only minor forces occur during the test. A double sided adhesive tape which withstands the electrolyte without major degradation was found.

So the separator material was fixed with a double sided adhesive tape to the anvil and the compression plate. For the pre-tests the double sided adhesive was applied to the whole area. During the pre-tests it was found that there were influences probably caused by effects of the adhesive tape in combination with the substitute electrolyte. It was assumed that the substitute electrolyte, which the separator is soaked with, solves some glue of the adhesive tape and this glue influences the interface. Because of that another fixation method was applied in the final tests by just gluing the separator laterally to the anvil and compression plate. The different fixation methods are sketched in Figure 33.

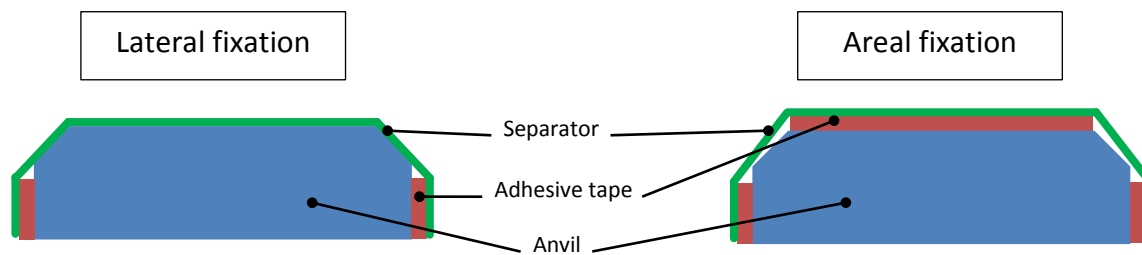


Figure 33: Separator fixation methods

The entire test stand was made of aluminium, which withstands the substitute electrolyte.

As the substitute electrolyte destroys several plastics like PVC and PMMA the tub was made of glass to ensure the chemical resistance. Finding a possibility to join the glass plates in a way that the tub is tight and the joining material is resistant to the electrolyte proved to be challenging. Numerous tests with different glues, like cyanoacrylate or silicone, were conducted to find an appropriate bonding technique. The two-component epoxy glue DP 490 Scotch-Weld by 3M met the requirements and was applied.

For filling the tub up to the required height so that the test specimens are fully submerged a considerable amount of the substitute electrolyte is needed. As the substitute electrolyte is expensive and the containing chemicals are dangerous, the tub, in which the specimens were immersed during testing, had to feature a small volume. This was achieved by filling the tub with glass beads and plates which can be seen in Figure 34. Glass is supposed not to react with the substitute electrolyte or other cell components.



Figure 34: Glass beads and plates

A three-dimensional sketch of the developed test stand can be seen in Figure 35.

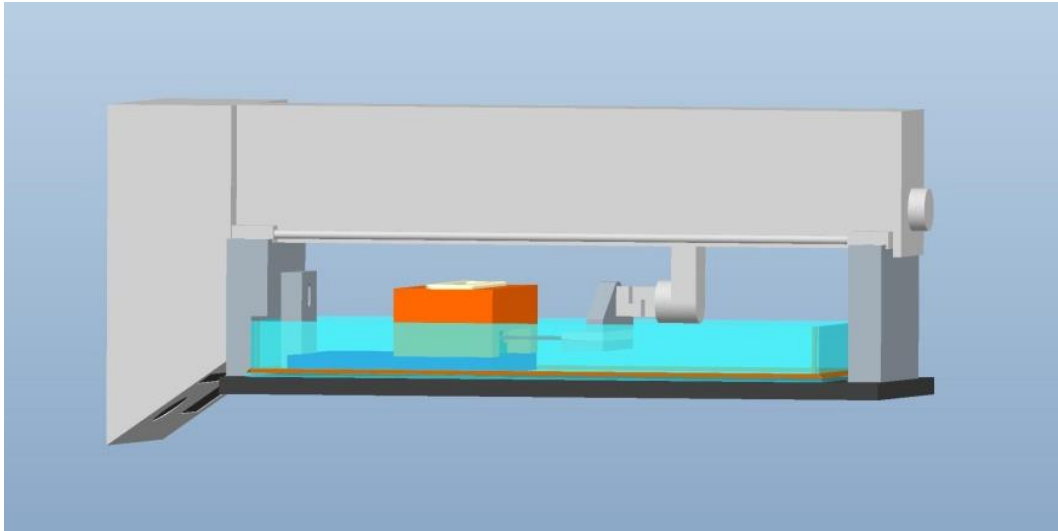


Figure 35: Test stand 3D

Figure 36 shows the assembled test stand without the glass tub for the electrolyte.

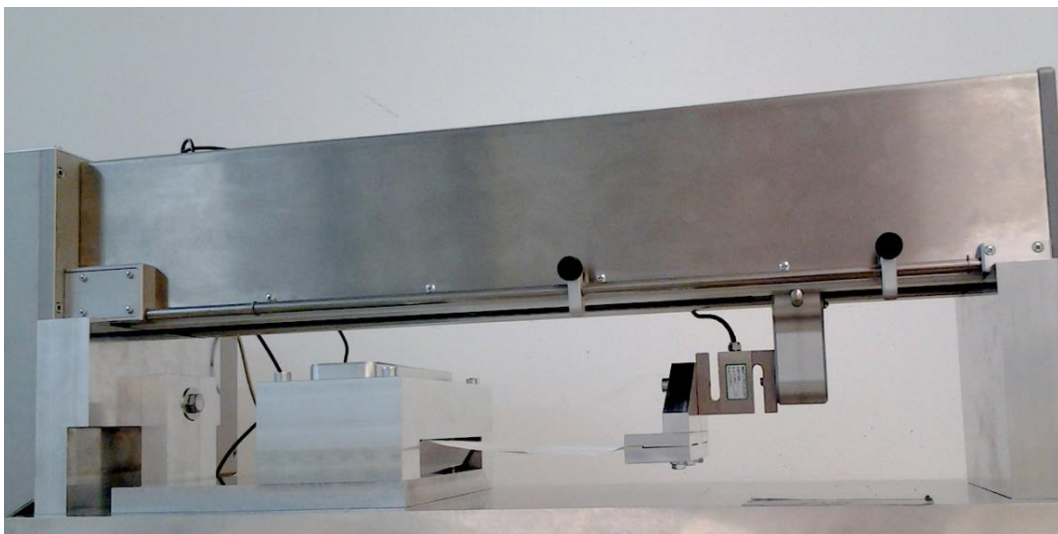


Figure 36: Test stand

#### 4.4.1 Test stand validation

Before tests of the interlaminar interactions were conducted, the proper function of the test stand was validated.

First, the validation was made by performing draw tests with the tests stand of materials, where values for these materials were found in specialist literature. This validation procedure has the following weaknesses: The test stand was constructed for measuring thin

and flexible membrane-like foils. A precise levelling between the anvil and the grip was not necessarily required. Validation tests with inflexible specimen induced additional loads biasing the results. Another problem for a validation based on values published in specialist literature is that the measured force strongly depends on specimen properties. Inconsistent surface treatment, coating and/or surface roughness might bias results. Most of the data found in specialist literature contain no additional information about specific properties to rule out such inconsistencies.

One source of values was taken where at least more detailed information concerning the material was provided. The part which was drawn was zinc coated, 1 mm thick steel sheet metal. As contact partner-surfaces the same zinc coated sheet metal was used. The values for the friction coefficient of the zinc coated friction counterparts are shown in Table 4.

Friction partner 1	Friction partner 2	max	min
Zn 3	Zn 5	0.40	0.20
Zn 7	Zn 5	0.45	0.15
Zn 14	Zn 5	0.34	0.14

Table 4: Friction as provided in specialist literature (54)

Validation tests were conducted at various velocities and by applying various normal pressures. The values were calculated by taking the maximum friction values out of several tests for each configuration and calculating their average. The results are summarized in Table 5. It can be seen that the values range from 0.23 to 0.45, but all of them were within the range provided in specialist literature.

Test velocity [mm/min]	1	10	100
2 kPa pressure	0.426	0.448	0.390
4 kPa pressure	0.229	0.393	

Table 5: Validation results

Friction values published in specialist literature generally indicate a wide range. To narrow down the values and to provide a second reliable validation, another approach was selected. A specimen is put on an inclined plane (see Figure 38). The pitch angle is slowly increased until the specimen starts to slide. In this case the specimen is not clamped between two

surfaces and therefore the validating test with the developed test stand was also done without clamping. In that way the friction angle (compare Equation 14) for the material pairing was established.

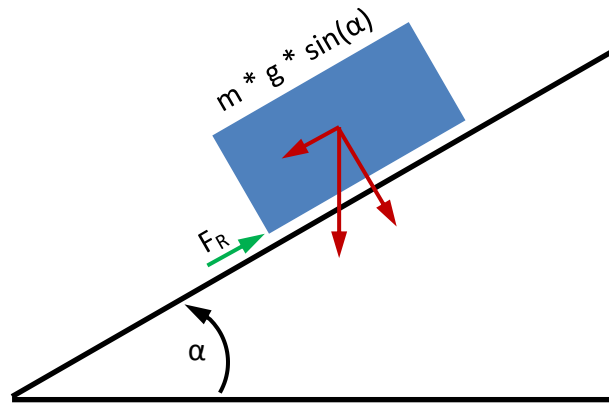


Figure 37: Principle inclined plane

Figure 38 illustrates the test procedure with the measuring device of the angle.



Figure 38: Inclined plane

The principle of determining the friction coefficient is shown in Equation 14.

$$\mu = \frac{F_R}{F_N} \stackrel{\text{def}}{=} \frac{m * g * \sin(\alpha)}{m * g * \cos(\alpha)} = \frac{\sin(\alpha)}{\cos(\alpha)}$$

Equation 14: Static friction coefficient inclined plane

Several tests with the same material pairings were made and a mean value for the angle was calculated with which the friction coefficient was calculated later on.

Then the same specimen was placed at the same surface which served as inclined plane before and was pushed with the gripper. The test stand measured the force and with the weight of the specimen the friction coefficient was calculated. The tests were performed with a velocity of 1 mm/min. The first peak is of interest as this is the value when static friction turns into dynamic friction. Because of the low operating velocity a stick slip effect occurred and several peaks representing the static friction can be determined.

The validation test for the pairing of an aluminium sample on top of a PTFE inclined plane can be seen in Figure 39. The blue graph shows the measured force. The green graph represents the value of the average friction coefficient gained with the inclined plane angel measurement method.

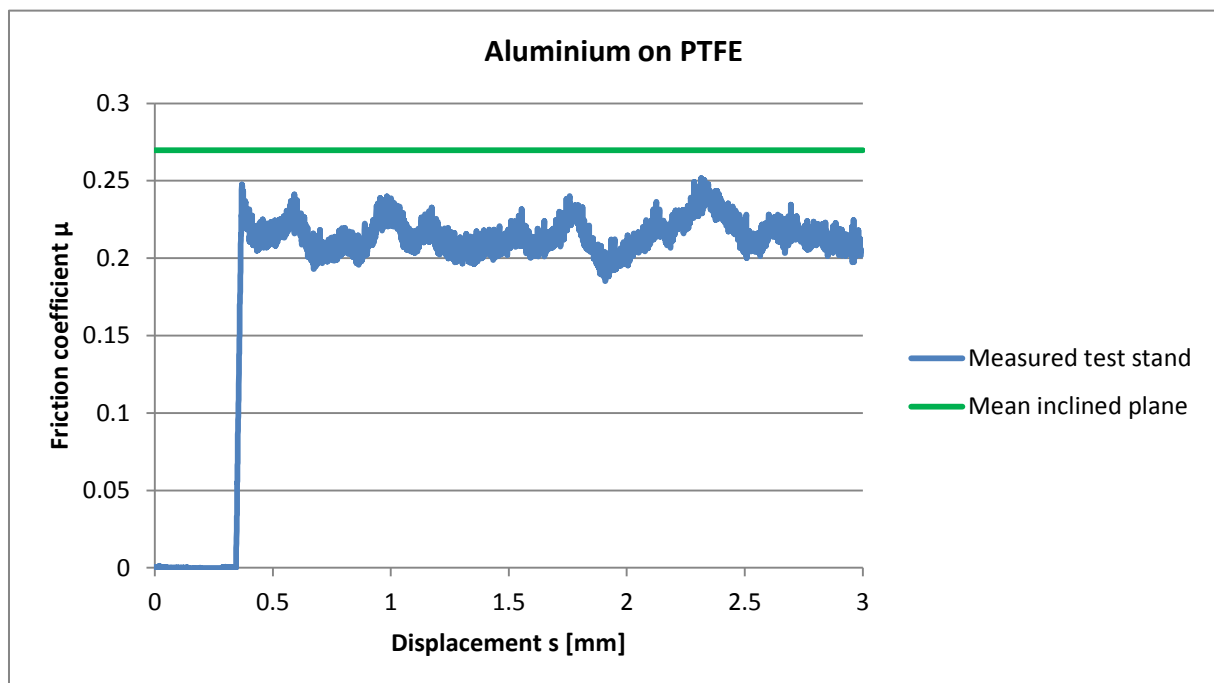


Figure 39: Inclined plane aluminium PTFE

This second validation test showed that the tests stand provides similar values. In this specific test a deviation of about 6 % was identified. Normal force decreases with increasing pitch angel compared to horizontal normal force in test station tests. As the friction angle in the aluminium PTFE material combination was 15.1 deg the normal force was just 3.5 % smaller than in initial position. The deviation can be caused by measuring errors of the load cell and of the angle measurement device. The jolt when the measuring starts can be an influencing factor for the measured values.



#### 4.5 Test Matrix

The focus of the investigations was to examine the different material combinations which can be found inside a battery. Due to the make-up of the cell under study there are three material combinations. By far the largest contact surface area is between electrodes and the separator. That is why the main focus in the test matrix was put on the pairings anode-separator and cathode-separator. Upper and lower electrodes are covered by an additional layer of separator. This whole stack is surrounded by the pouch. Hence, the third investigated material combination is separator and inner side of the pouch.

Apart from the material pairings, the main parameters were the normal force and the draw velocity. In order to draw conclusions various fixed values from within the range of interest were picked.

In addition to this some other parameters were investigated for the final test in advance. Also some special treatments like a pre-drawing of samples to sufficiently tighten them were found out in the pre-tests and were considered after the determination of these effects.

In the first pre-tests, the anvil and compression plates were not covered with any material. The coefficient of friction for the material pairings anode-aluminium and cathode-aluminium respectively were determined to see if there is a difference. Also the repeatability was checked in these tests (see Table 6).

Drawn component	Counterpart	Velocity	Normal Force	Remarks
Anode	Aluminium	50 mm/min	29 N	3#
Cathode	Aluminium	50 mm/min	29 N	3#

Table 6: Tests: electrodes - aluminium

In a second pre-test anvil and compression plate were covered with polyethylene (see Table 7).

Drawn component	Counterpart	Velocity	Normal Force	Remarks
Anode	Polyethylene	50 mm/min	29 N	3#
Cathode	Polyethylene	50 mm/min	29 N	3#

Table 7: Tests: electrodes - PE

Another investigation was designed to find out if the repetition of the same tests using the identical specimens would lead to a significantly different outcome for drawing conclusions if effects like wear or abrasion occurred. In this third pre-test the influence of test-interruptions, i.e. stopping the drawing, was investigated, to find out whether there are break-free properties and whether the stop time has an influence on these properties. The test matrix for these investigations is illustrated in Table 8.

Drawn component	Counterpart	Velocity	Normal Force	Remarks
Anode	Separator	50 mm/min	15 N	Stops
Cathode	Separator	50 mm/min	15 N	Stops

Table 8: Tests: electrodes – separator with stops

The experiments for determining the frictional properties of the material pairings cathode-separator and anode-separator were designed consistently. The compression force was 15, 29 and 42 N and the test velocities amounted to 50, 100 and 200 mm/min, see Table 9 and Table 10.

The cell background colours serve as code for the interpretation of the graphs found in the results chapter.

In order to eliminate the differences caused by the clamping of the electrodes between the plates all test set-ups were pre-tensioned, but not totally pre-drawn. This is crucial, because the first draw test always showed a peak which is of great interest. To achieve a constant starting tension, without changing the surfaces too much, the tensioning was performed with the smallest force, which is 15 N, and the specimen was just drawn for 5 mm at the very slow velocity of 5 mm/min.

The purpose of these final tests was the investigation of the sensitivity to velocity and normal force.

For the final tests always new specimens were used. This was done because when using the battery there are usually no pre-deformations.

Anode Final				
Drawn Specimen	Surfaces Clamping	Normal force [N]		
Anode	Separator lateral fixed	15	29	42
Relative velocity [mm/min]	50	#1	#4	#7
	100	#2	#5	#8
	200	#3	#6	#9

Table 9: Final tests anode

Cathode Final				
Drawn Specimen	Surfaces Clamping	Normal force [N]		
Cathode	Separator lateral fixed	15	29	42
Relative velocity [mm/min]	50	#1	#4	#7
	100	#2	#5	#8
	200	#3	#6	#9

Table 10: Final tests cathode

The pouch has an unsymmetrical make-up, outer and inner surface are not alike. In order to investigate the inner side, which is in contact with the separator, the pouch was folded in a way that the former inside is on both sides of the specimen and in contact with the separator.

For the material pairing separator-pouch a reduced test matrix applies (compare Table 11).

Pouch Final			
Drawn Specimen	Surfaces Clamping	Normal force [N]	
Pouch folded	Separator lateral fixed	15	29
Relative velocity [mm/min]	50	#1	#4
	100	#2	X

Table 11: Final tests pouch

#### 4.7 Microscopy

So far all the described methods have been quantitative methods. To understand the effects better and to find explanations for some of them qualitative methods are of utmost importance. That's why microscopy investigations were made.

The microscopy of specimens was conducted at the Institute of Paper-, Pulp- and Fibre Technology, which can be seen in Figure 40. Specimens of the disassembled battery were compared to specimens after the test procedure to gain further information. The magnification range of the used light microscope was not sufficient to identify any major changes to the surface.



Figure 40: Microscopy

For this reason specimens were investigated with the help of an electron-microscope at the FELMI-ZFE, which is the 'Austrian centre for Electron Microscopy and Nanoanalysis', in order to make a more detailed investigation.

Two sets of specimens consisting of an anode, a cathode and a separator were analysed. One set of specimens was tested before with the strip draw test and the other one was not, which provided reference for later comparison.

All specimens were kept in containers with substitute electrolyte all the time. For getting the undrawn specimens a battery cell was disassembled on the same day when the specimens were taken to the investigation institute. The drawn specimens had been disassembled one week before the microscopy investigations because the strip draw tests were performed during that week. So the drawn specimens were outside the battery longer than the others. Also for performing the tests the specimens had to be taken out of the substitute electrolyte two times. Once for inserting them into the test stand and once for putting them back into the storage container. So apart from the impact caused by the drawing, also an influence caused by the handling and the being outside the battery longer could have been responsible for possible changes of the specimens.

Also the orientation of the specimens is of importance and was marked. The specimens were cut of the components in that way that the longer side of the trapezium was a parallel line to the longer side of the component, which can be seen in Figure 41. On the one hand the structure of the component is not the same for different directions and on the other hand the drawing of the specimen is performed in the direction of the longer side. Anisotropic changes can be investigated with this measure.



Figure 41: Microscopic specimen orientation

The special shape of the specimens can also be seen in the chapter 'Microscopy results'.

## 5 Results

In this chapter the results are exhibited and described.

### 5.1 Strip draw test

The tests were performed with the developed strip draw test station. All specimens that were tested were submerged in a substitute electrolyte during the whole test.

#### 5.1.1 Pre-Test electrodes combined with aluminium

The first tests were performed by drawing anodes which had been placed between the uncoated anvil and the compression plate both made of aluminium. A relative velocity of 50 mm/min was chosen. The normal force was 29 N. The outcomes of the measuring are shown in Figure 42.

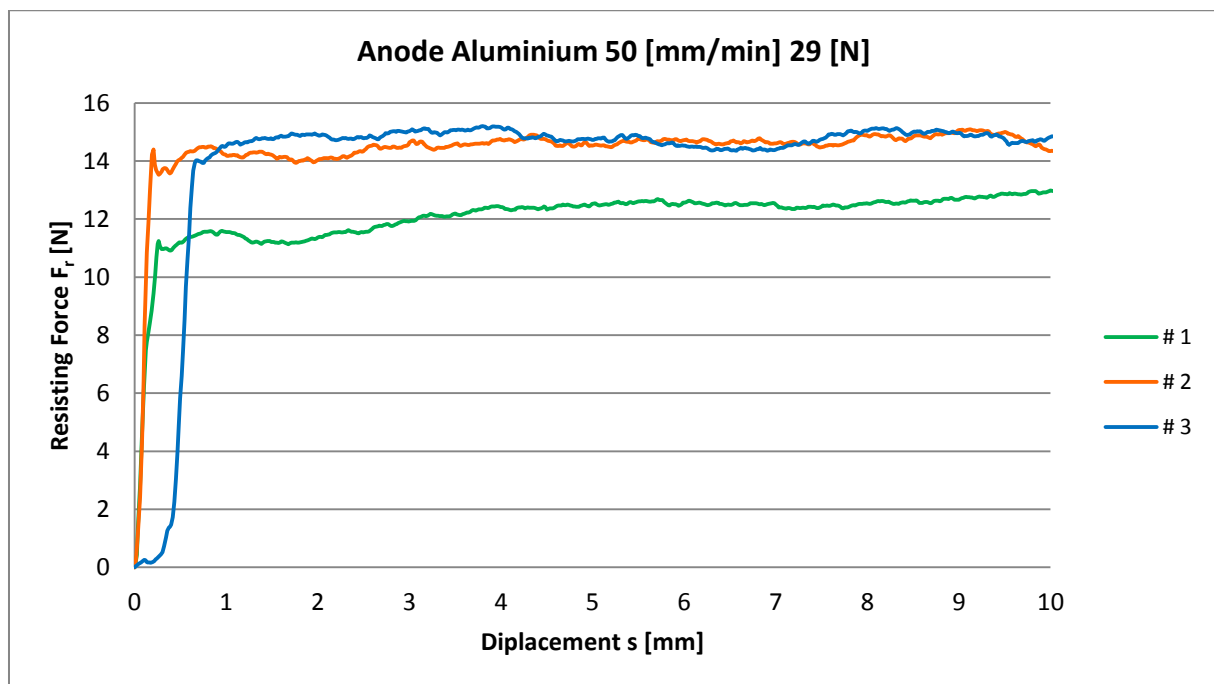


Figure 42: Anode Aluminium

The three graphs show a similar behaviour, although the green graph starts sliding at a lower force level but then the force climbs to almost the same level as examined in the other tests. In some tests small air bubbles were identified in the substitute electrolyte at the beginning of the test, which could have been inside the sliding gap and influence the resisting force. As soon as the relative movement started these bubbles were released. This would be a

possible reason for the green graph to show a different behaviour. A more or less constant force level can be identified during the whole test.

In the second series of pre-tests the cathodes was drawn. Figure 43 shows the outcomes.

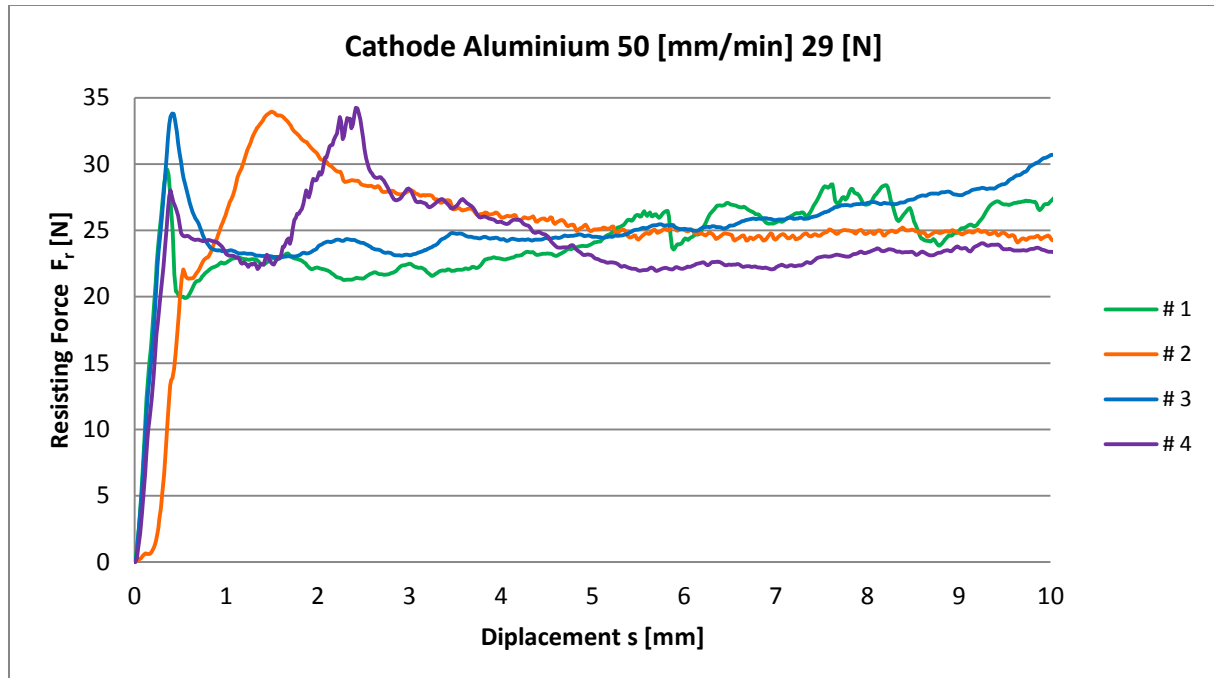


Figure 43: Cathode Aluminium

All three graphs show a peak in the first stage of the test with approximately the same maximum values. Then the force is declining to a lower level which is also almost the same. The differences where the peak occurs may depend on how tightly the anode is inserted as this was not particularly treated with care in this pre-test. A pre-drawing of the anode might have sufficiently tightened the electrode in the tests.

### 5.1.2 Pre-Tests electrodes combined with polyethylene

In order to see if there are differences because of the surface structure, tests with polyethylene plates were made. This was done to investigate if the special structure of the separator plays a role for the interactions.

Figure 44 shows the graphs resulting from the strip drawing of an anode which is clamped between polyethylene plates with a normal force of 29 N. The test was performed at a velocity of 50 mm/min. The different graphs show the results of three tests all of which were made using the same specimens. There is not only a difference in the dispersion of the test,

but also one caused by changes of the anode and the polyethylene resulting from the already performed tests.

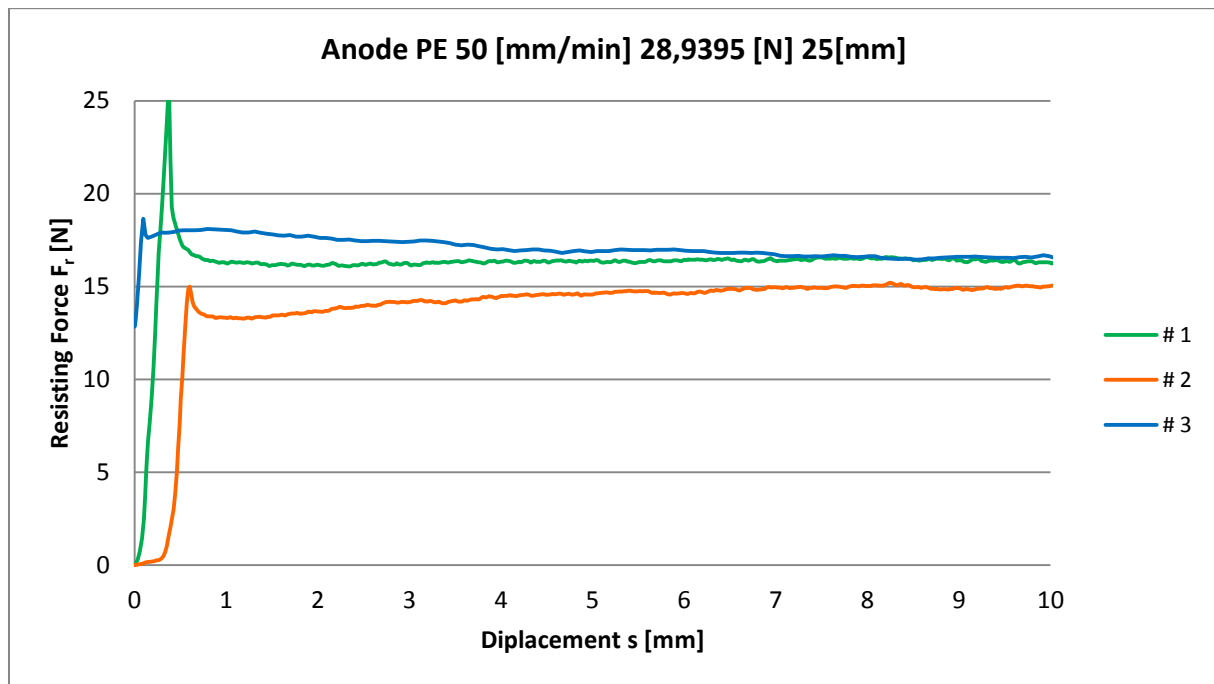


Figure 44: Anode PE

The first test with the new materials is represented by the green graph. Then tests represented by the orange and the blue graph were performed. There is a clearly visible difference between the first test and the following ones because of the significant peak. The following tests showed distinctly smaller peaks. The smaller peaks could be the cause of abrasion effects in the first test. All the tests show approximately the same level after a difference within the first millimetres.

The test with the polyethylene parts was also performed with the cathode and the results are presented in Figure 45.



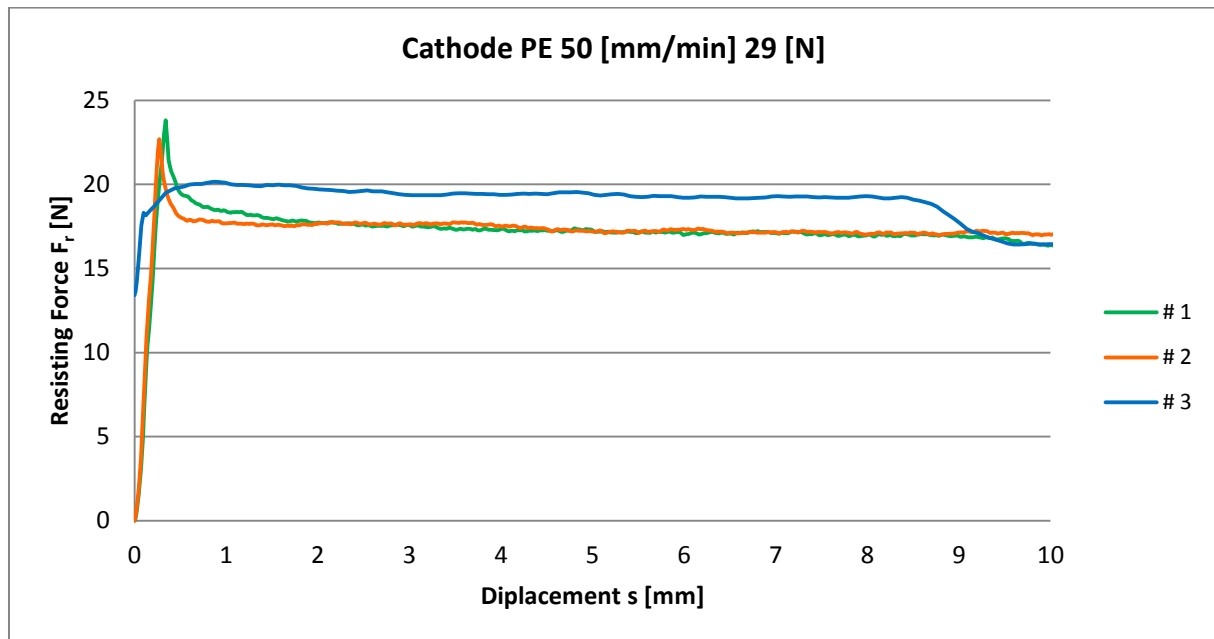


Figure 45: Cathode PE

These two tests, the green one and the orange one, were performed using new specimens. Only the blue one was made with the specimens that had already been used before. After the first tests damage of the active media of the cathodes was visible and the results of the #3 test, the second draw test of the same specimen, have to be considered carefully. A detailed peak was missing in this second test. The two levels of the measured force with a sudden drop of around 9 mm could be explained with the damage of the active media in the course of this displacement. When the damage of the active media was drawn out of the clamped gap just undamaged surfaces were interacting and the level of the force matched that of the other tests.

### 5.1.3 Recovery properties

The recovery tests were performed to investigate if the resistance force changes after a stop and if this change also depends on the duration of the stop.

The tests were performed by drawing always the same anode between separator specimens that were attached to the anvil and the compression plate by means of a double-sided adhesive tape. The velocity of the test was 50 mm/min and the normal force 15 N. The previous tests had indicated a considerable difference concerning the first drawing with a relatively high peak. To get rid of this influence, the electrode was pre-drawn in a pre-test with also 50 mm/min and 15 N in all subsequent tests (see Figure 46).

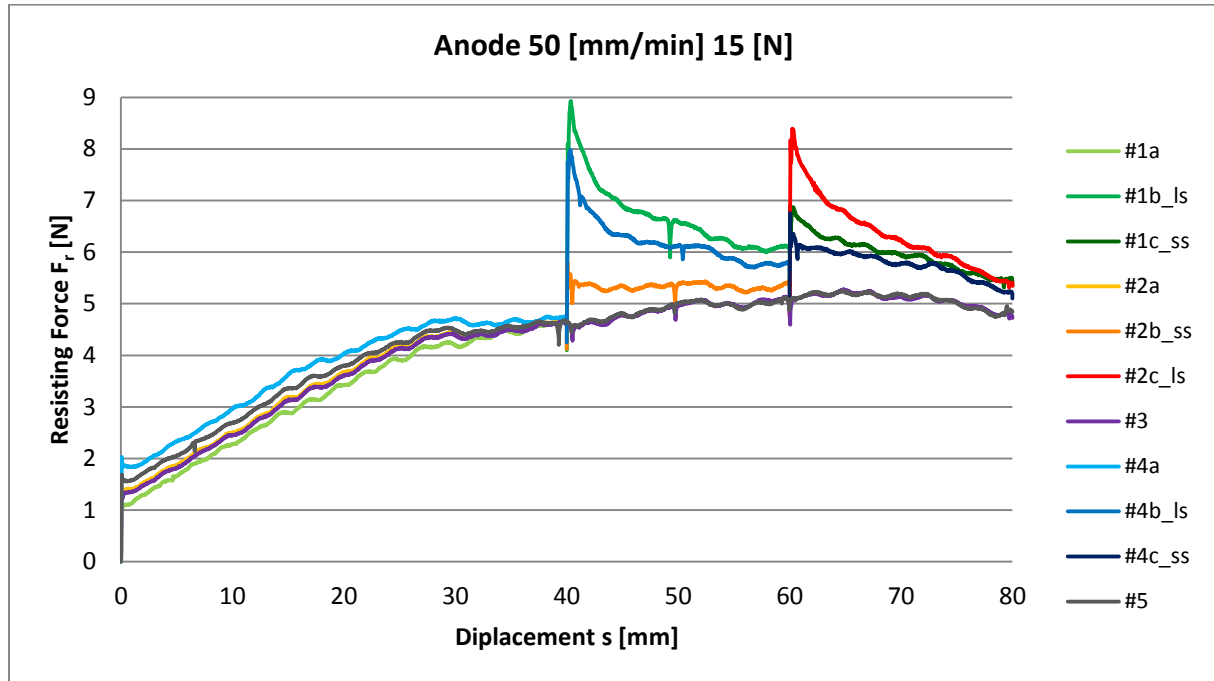


Figure 46: Anode – separator with stops

The graphs show a declining increase of the force level and are very similar to each other. After a stop a significant increase in the force was measurable. The short stop, which is marked with the abbreviation ss, lasted about 10 s, the long stop, which is marked with the abbreviation ls, lasted about 300 s. In following cycles the order of the stop-duration was changed. Results indicate that the longer the stop the bigger is the rise in draw-force. Further, the force level slightly decreases with every repetition, which could be caused by abrasion effects and the smoothening of the surface roughness.

The results of the tests were different from those of other tests, because no clear level of relative force which had occurred after a few millimetres in the tests before could be identified. Compared to previous testing, the separator specimens were fixed by double sided adhesive tape. So it very likely, that the adhesive tape is biasing results. Presumably, the substitute electrolyte dissolves the glue of the adhesive tape. Probably, the glue diffuses through the separator and biases test results.

The same test regime was applied to the cathode. As before, one pre-test with 50 mm/min and 15 N was performed. The results are shown in Figure 47.

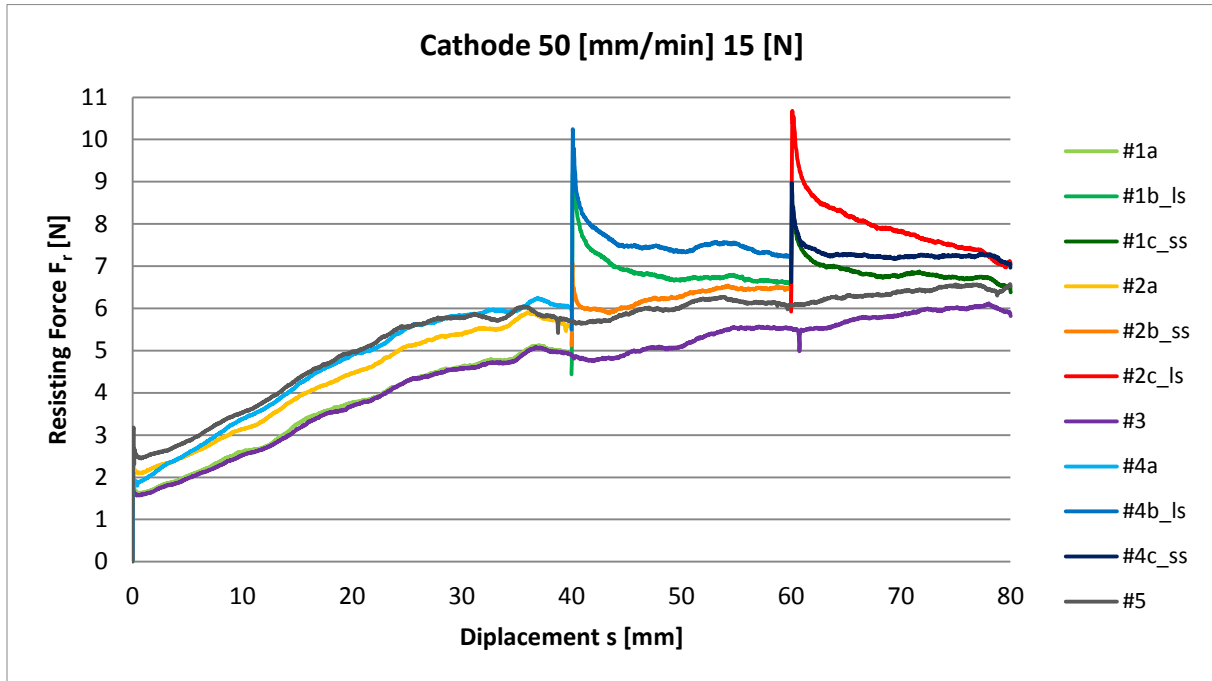


Figure 47: Cathode – separator with stops

Although the force level was different, the behaviour which was observed in the anode tests was also identified in the cathode tests. A declining and flattening increase of the force was observed. The duration of the stops also influenced the break-away force in a way that the longer the stops were, the bigger was the break-away force. Repeating the tests with the same specimens also led to a slight decrease of the force.

The influences which may occur because of the separator fixation when using the double-sided adhesive tape may also have occurred in this test set-up.

Having identified a possible impact of the double-sided tape the need for a different fixation technique for the final tests was revealed.

### 5.1.4 Final tests

Considering the lessons learnt from the pre-tests, a set of final tests was performed. These final tests were required to simulate the actual interfaces in the battery very accurately because these results should serve as a basis for implementing the interactions into a numerical model.

For the final tests of anode and cathode a colour code was used to illustrate the different tests distinctly. These colours can be seen in the test matrix table for the final tests.

Figure 48 shows the graphs of the final tests of the anode.

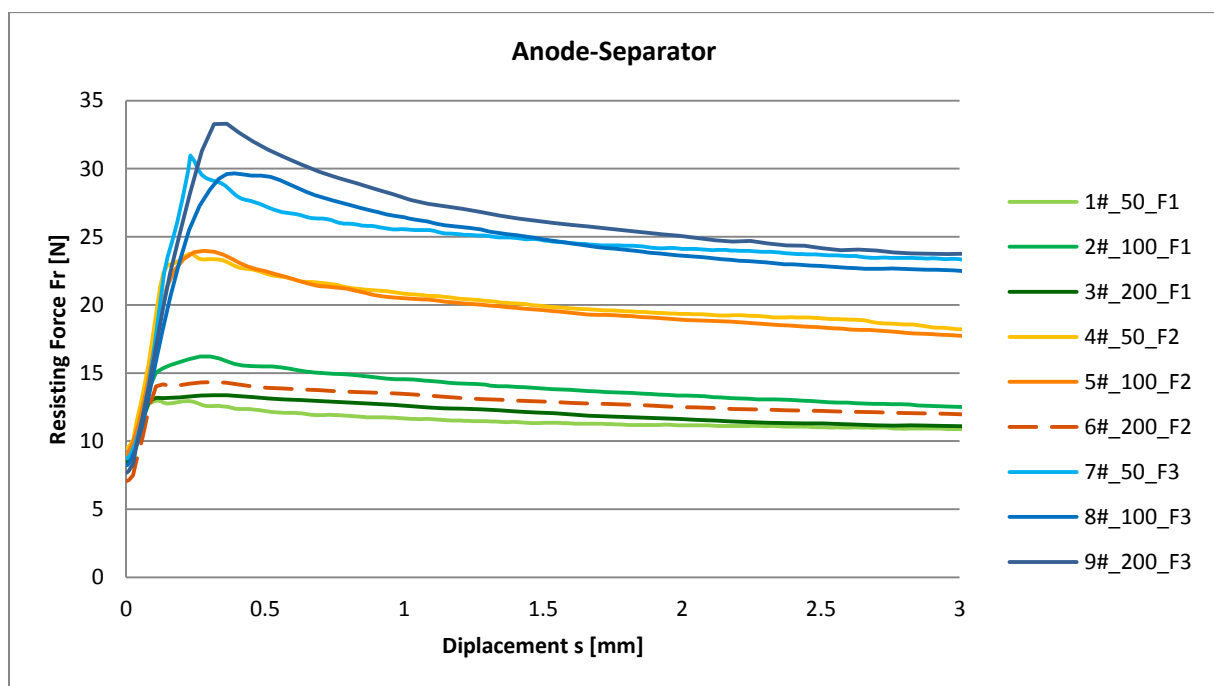


Figure 48: Anode-Separator velocity force

All graphs show an increase in the force until a more or less distinctive peak and then a decrease of the force which gradually becomes flatter. The green graphs have almost the same starting force and the 50 mm/min as well as the 200 mm/min have a similar behaviour, whereas the 100 mm/min shows a bigger increase. The graphs of the highest normal force, the blue ones, also have a similar starting force. The maximum force is within a similar range and all graphs show a nearly identical level after 2 mm of movement. When measuring the force shown by the light orange graph, there was a failure when zeroing the load cell. That is why the originally measured results of the resisting force were smaller. After testing when load had vanished, the test software which assessed the load cell still returned a value of minus five Newton. This curve was afterwards offset by that value. When performing the

test at medium force and highest velocity (dark orange dotted line) the compression plate was probably deadlocked when increasing force. Presumably, the total force was not applied to the specimen. This conclusion was drawn because this graph corresponds to the results obtained from tests with the smallest force (15 N). Hence, this test was not further considered.

The results of the final tests with the cathode are illustrated in Figure 49.

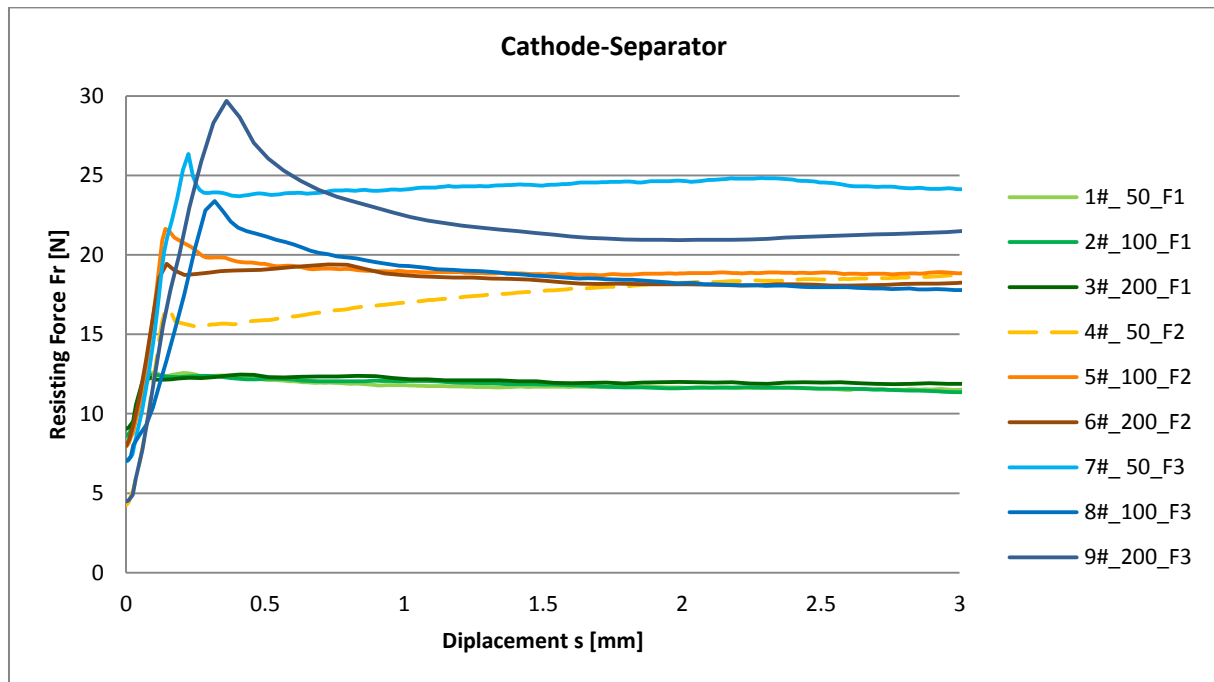


Figure 49: Cathode-Separator velocity force

The graphs of the 15 N normal force tests look very much alike. No clear peak can be identified and there is a similar force level. The orange graphs, which visualize the results of the 29 N normal force tests, all also approach the same force level. Only the test performed with 50 mm/min reaches the level later. So this test (4#\_50\_F2) showed an unusual behaviour and was therefore not considered for further calculations. Each blue graph shows a significant peak followed by a level. There is some variation in the height of the peaks and the levels.

One of the final investigations was the testing of the interactions between the pouch and the separator. The results are shown in Figure 50.

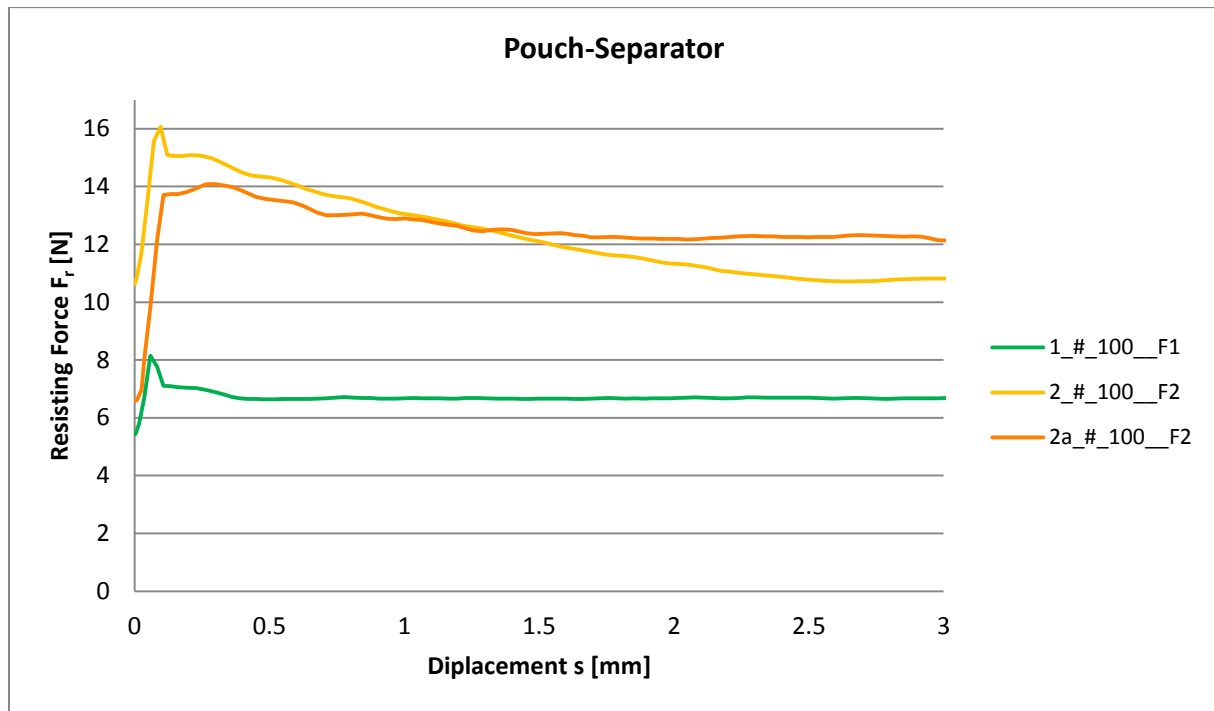


Figure 50: Pouch separator final

The resisting forces in the pouch tests show a peak followed by a more or less constant level. This was seen in both tests with different normal forces. The orange test was made with an already tested pouch to investigate also potential differences. It could be seen that when testing an already tested pouch the starting peak is reduced.

## 5.2 Microscopy results

Each of the following pages shows two microscopy figures of the same component, like anode, cathode or separator. The magnification of both figures on one page is always the same. The figure at the top is a specimen which was directly investigated, and is called 'undrawn specimen', and the figure at the bottom shows a specimen which was tested with the strip draw test before and is referred to as 'drawn specimen'.

### 5.2.1 Anode

Figure 51 shows an anode of the investigated battery cell without any performed test, whereas Figure 52 shows an anode which had been tested before.

The black rectangle indicates the position of the more detailed microscopy investigations.

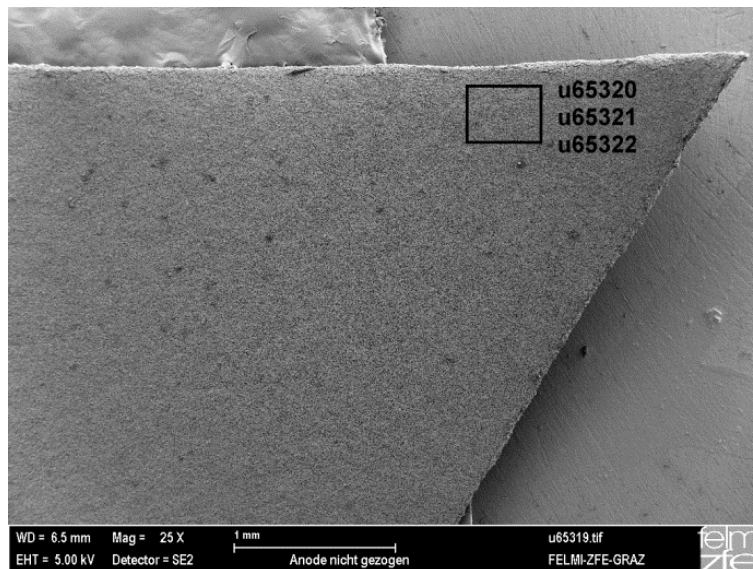


Figure 51: Anode Pre synoptic view

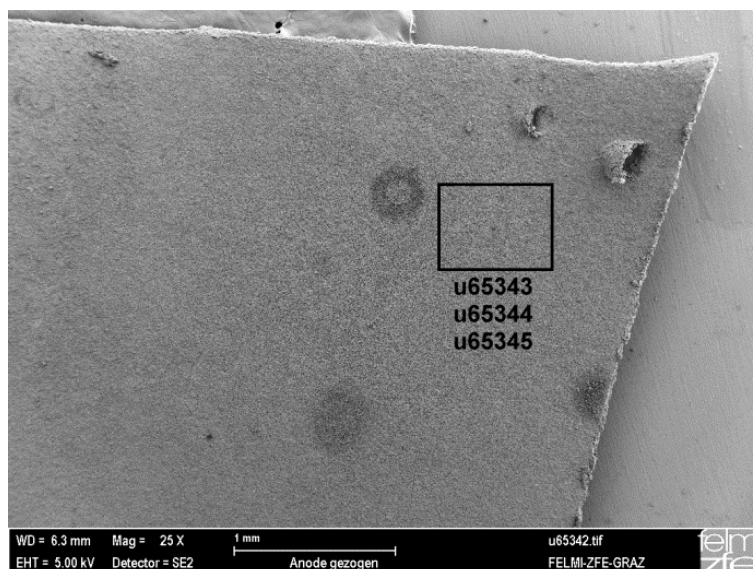


Figure 52: Anode Post synoptic view

In the synoptic views hardly any difference was seen. In the drawn specimen damage to the active media resulting from holding it with tweezers while cutting the specimen can be seen. Apart from this three darker spots could be identified.



A more detailed view of the surface of the anode is provided by Figure 53, which shows the undrawn specimen, and Figure 54, which shows the drawn specimen.

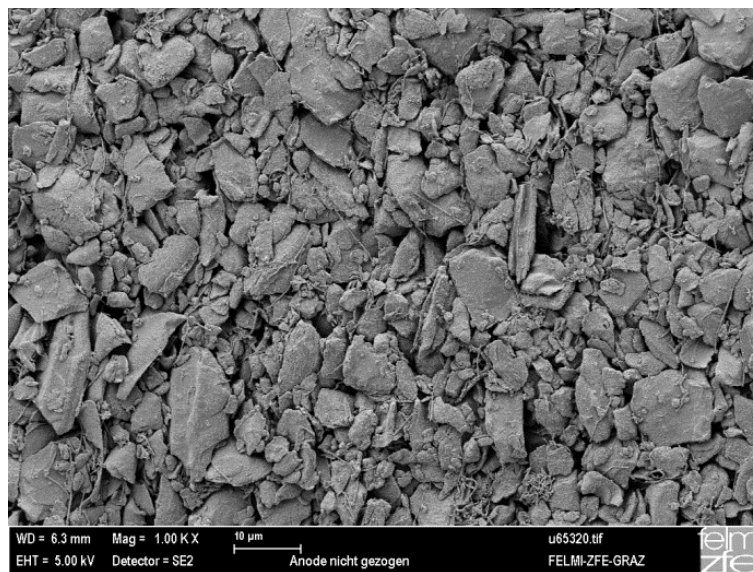


Figure 53: Anode Pre 10 μm

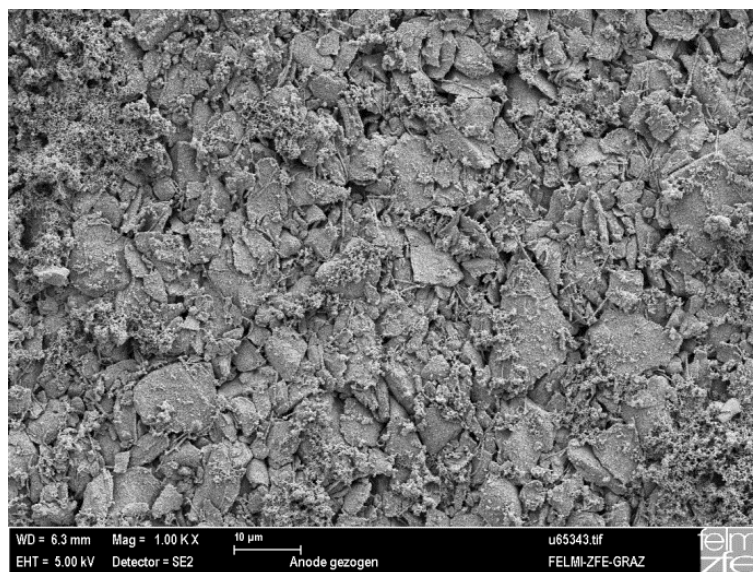


Figure 54: Anode Post 10 μm

The basic surface structures of the specimens look the same, but in the drawn figure some additional material, which could have been caused by abrasion, can be seen.

Figure 55 shows the undrawn, and Figure 56 the drawn anode, looked at with the largest magnification that was used in this investigation.

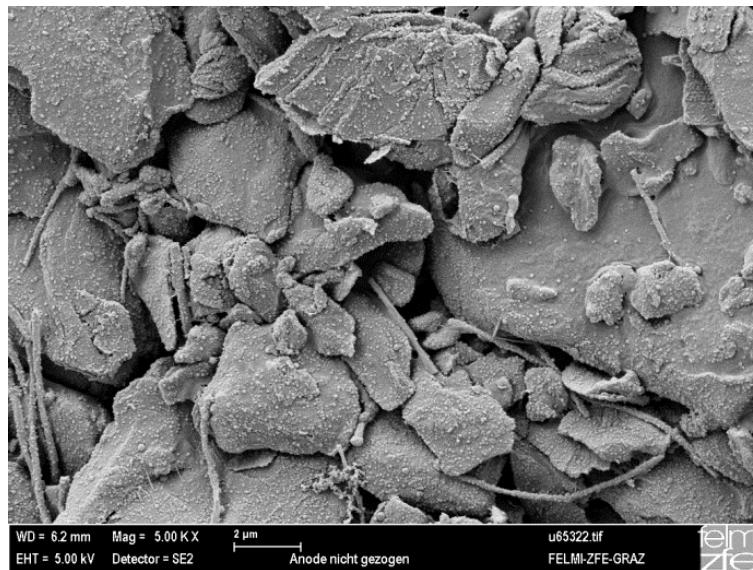


Figure 55: Anode Pre 2  $\mu\text{m}$

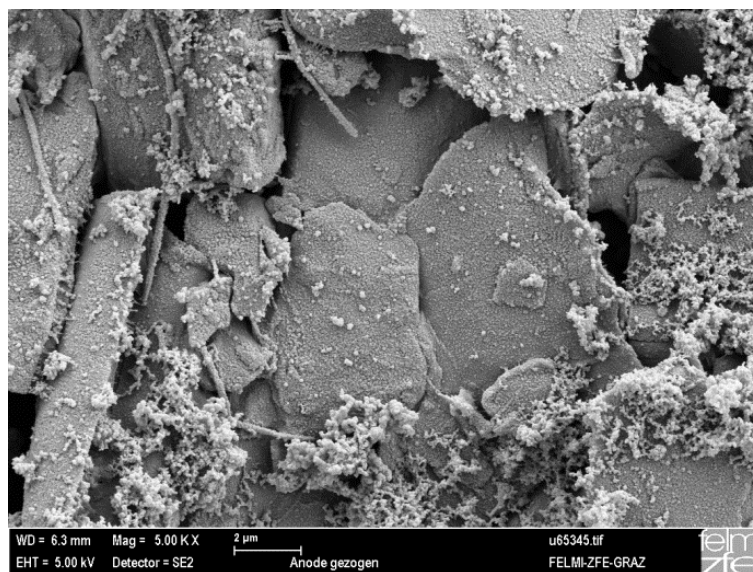


Figure 56: Anode Post 2  $\mu\text{m}$

In these figures it is even more visible that there is additional material on the surface of the anode.



## 5.2.2 Cathode

The microscopy investigation of the surface of the undrawn cathode is shown in Figure 57, and Figure 58 illustrates the surface of the drawn cathode.

The black rectangle marks where the detailed investigations were made.

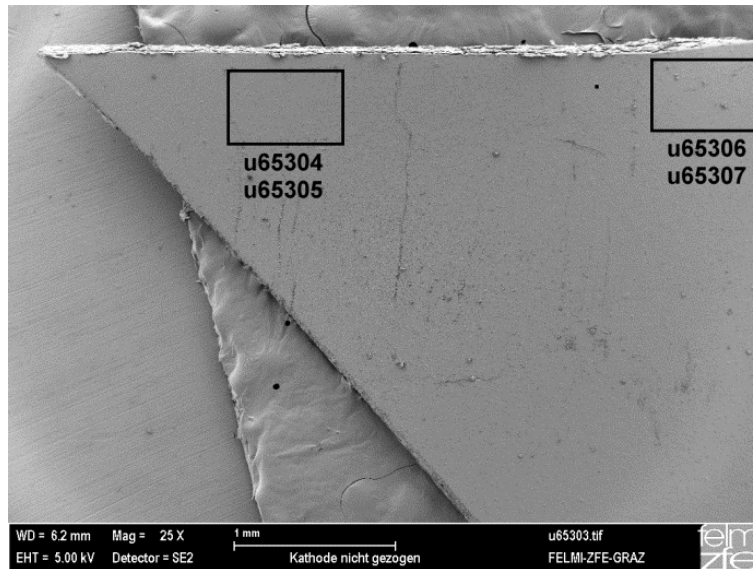


Figure 57: Cathode Pre synoptic view

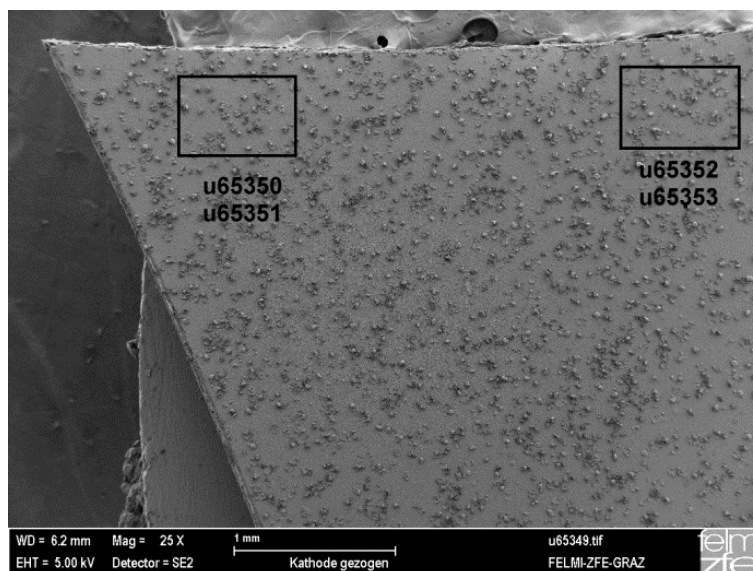


Figure 58: Cathode Post synoptic view

Even in the synoptic view a significant difference of the surfaces can be observed. The drawn specimen was studded with tiny protrusions.

Figure 59 shows a detail of the undrawn cathode. The drawn cathode with a magnified protrusion in detail is shown in Figure 60.

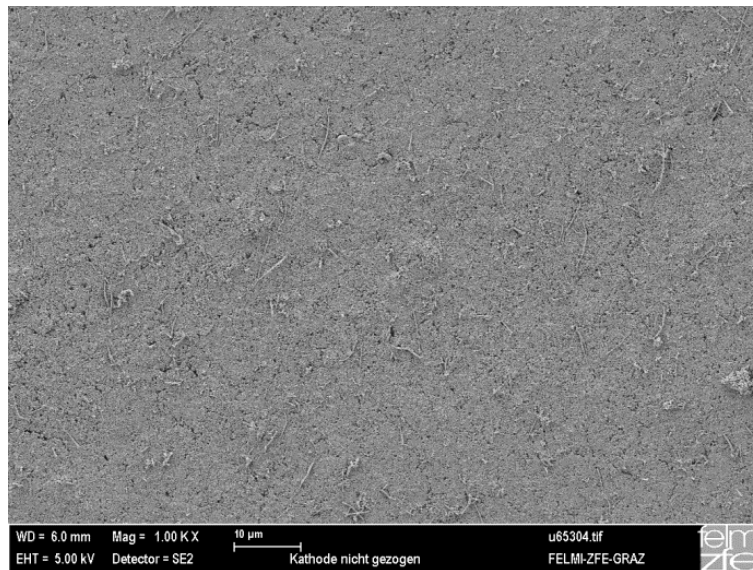


Figure 59: Cathode Pre 10 μm

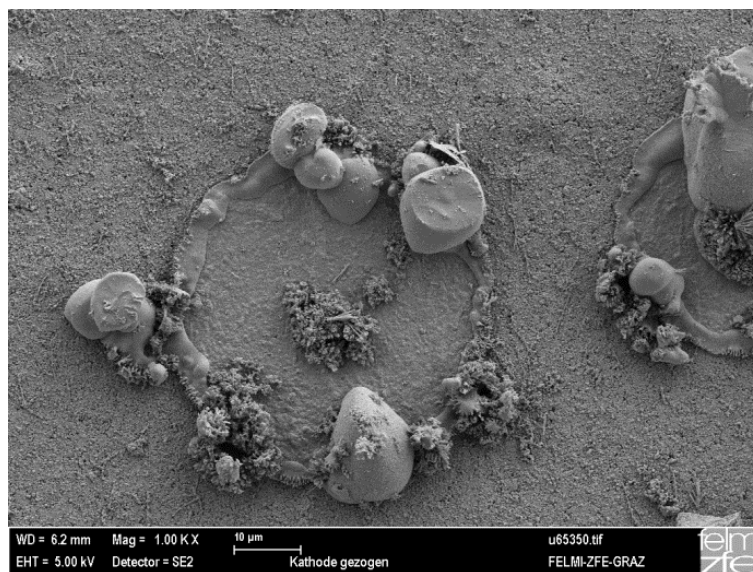


Figure 60: Cathode Post 10 μm

Protrusions can be identified at a drawn specimen. It is assumed that the protrusions did not result from the relative movement of the test, but from chemical effects. These chemical effects could have been caused by the longer time the specimen was exposed to conditions outside the battery. The exposure to humid air when taking the specimen to and from the test station could have led to this structural change.



A very detailed view of the cathode surface can be seen in Figure 61.

Figure 62 shows a segment of the same magnification of the cathode's surface, but of the drawn specimen and among the protrusions.

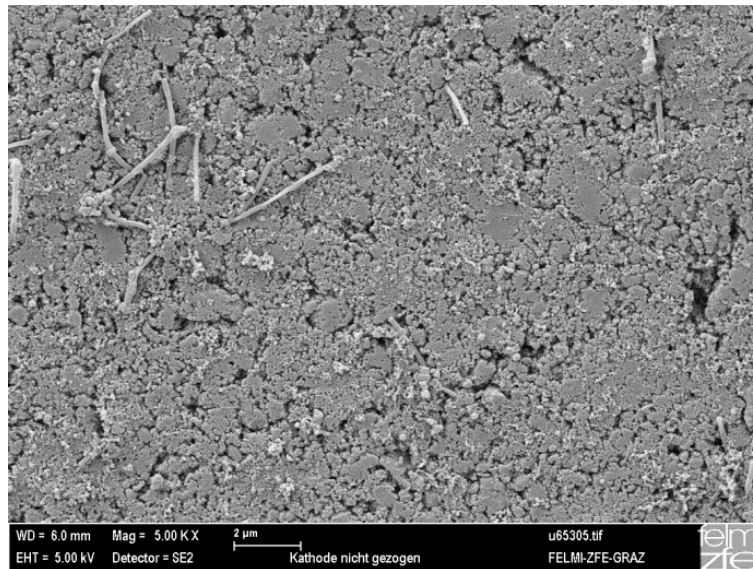


Figure 61: Cathode Pre 2 μm

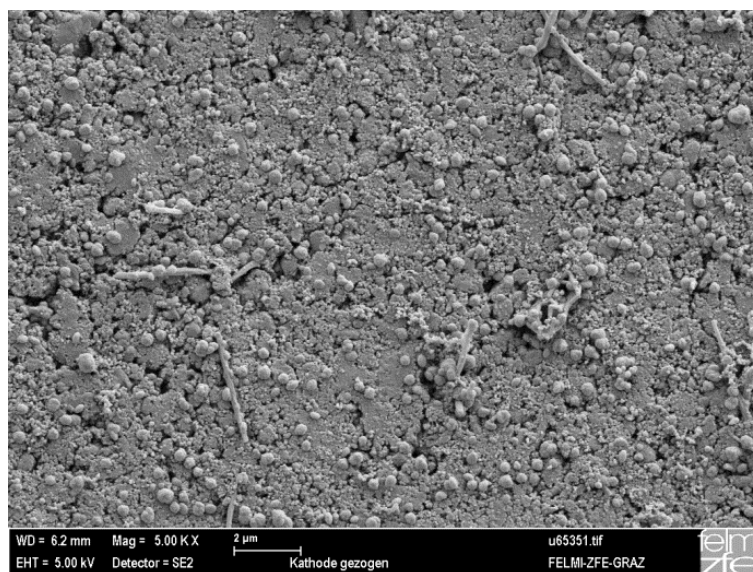


Figure 62: Cathode Post 2 μm

Here no protrusions can be seen because this figure shows the surface among them. By comparing these surfaces some differences can be identified. There were small particles on top of the surface, which may have been deposited there and likely stem from abrasion processes.

### 5.2.3 Separator

Specimens of the separator were also investigated by means of a microscope. The untested separator can be seen in Figure 63. The tested separator, which was also washed and dried before, is shown in Figure 64.

The black rectangles serve as markers of the position of more detailed figures again.

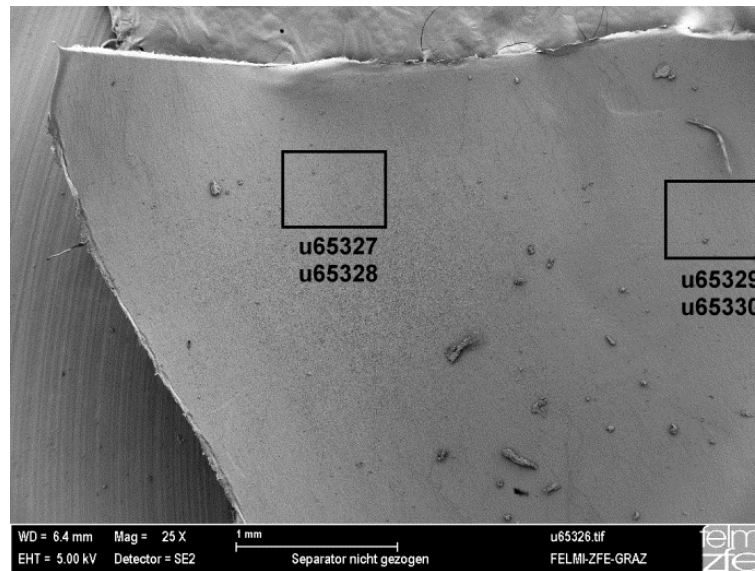


Figure 63: Separator Pre synoptic view

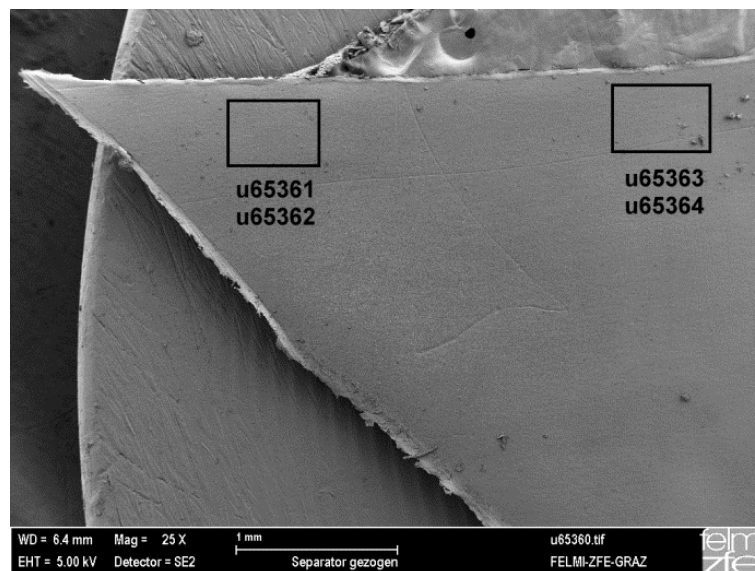


Figure 64: Separator Post synoptic view

The two specimens almost look alike. Scattered particles can be identified, but are probably not related to the separator.



A more detailed view of the undrawn separator is shown in Figure 65. The drawn separator with the same magnification is illustrated in Figure 66.

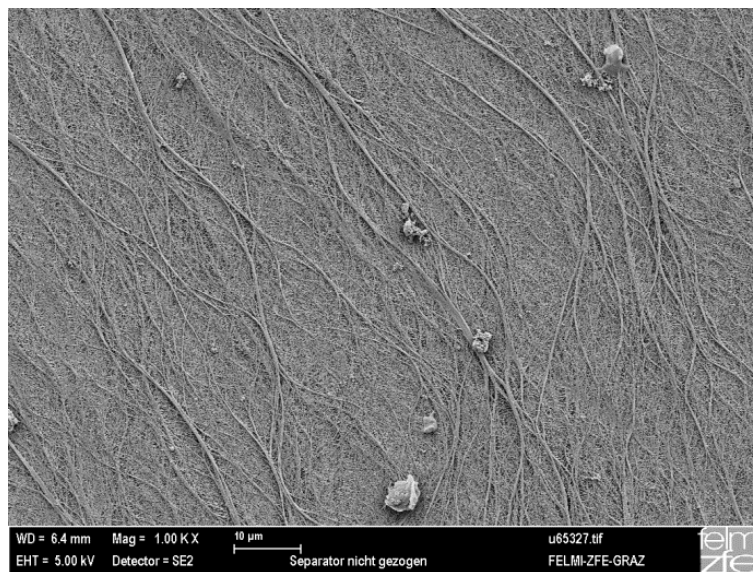


Figure 65: Separator Pre 10 μm

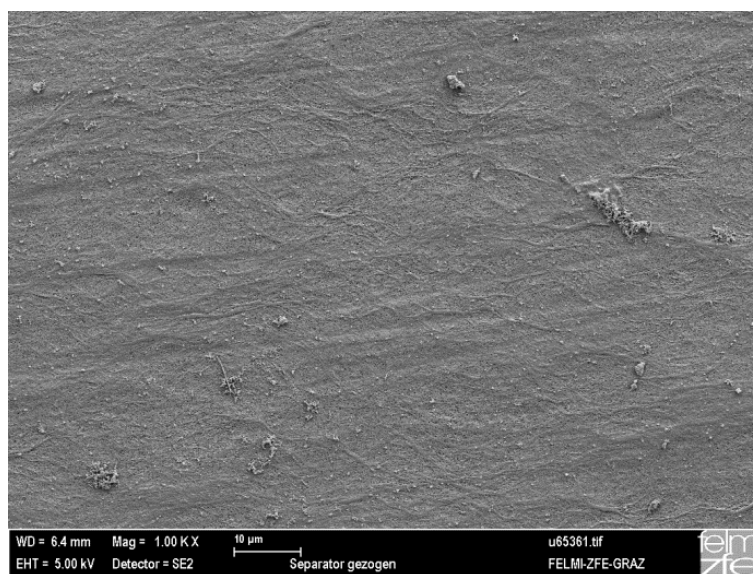


Figure 66: Separator Post 10 μm

A distinct difference can be seen between the drawn and the undrawn specimen. The structure of the separator, which looks like the branches of a tree, nearly disappeared at the drawn specimen. The surface of the separator changed distinctly in the course of the drawing process.

An even more detailed view of the surface of the undrawn separator is shown in Figure 67, the drawn specimen for comparison in Figure 68.

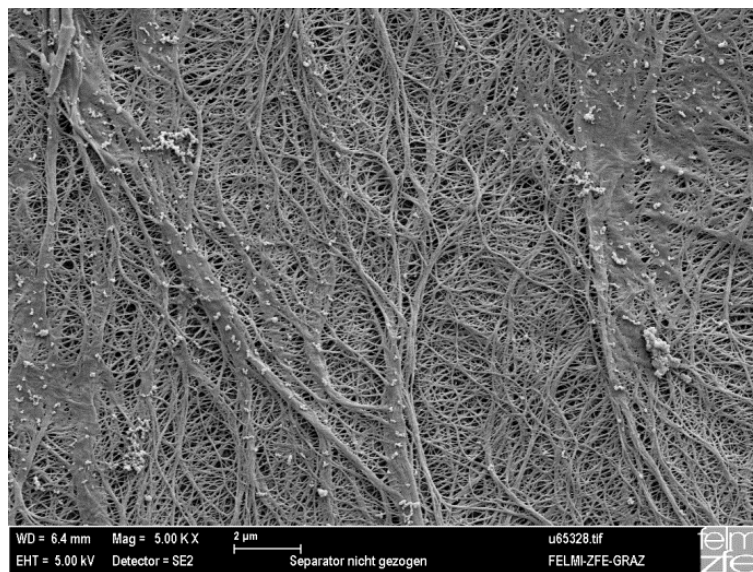


Figure 67: Separator Pre 2 μm

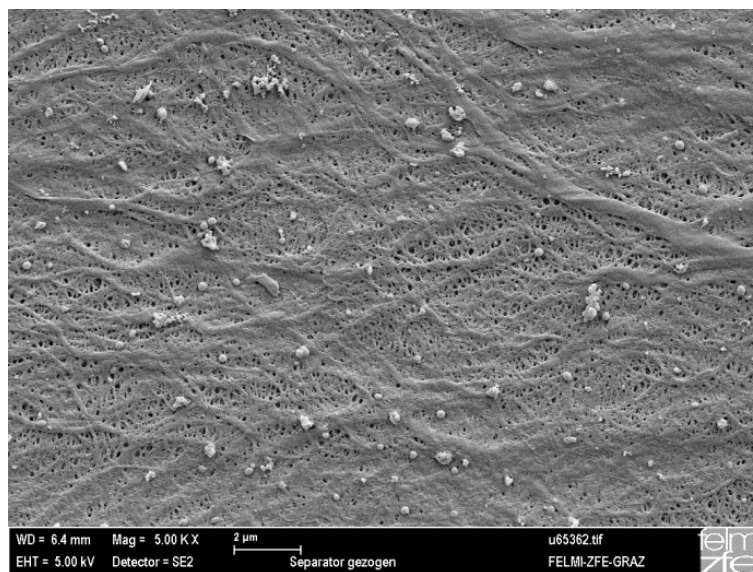


Figure 68: Separator Post 2 μm

The figures with different magnifications confirm the difference between the specimens and the flattening of the structure because of the drawing process. Remains of the structure can be identified in the drawn specimen. Some small particles can be identified in both figures.



## 6 Discussions

All the results were discussed in this chapter and relations to the objectives were dealt with. A brief discussion of specific topics relevant for the description of the results was done in the chapter on results.

### 6.1 Discussion of the test station development

As requested in the objectives a test stand was developed for measuring the resulting force in case of interlaminar shear. The test stand is suitable for use also under chemically aggressive conditions. The suitability of the test stand was evidenced with validation tests. By testing the sensitive components of the battery sometimes a distribution of the results could be identified, but in most cases a reason for bigger deviations like defects of the tested specimens which must have happened during the test, could be found.

The temperature control for the test stand was disregarded. This could be an important feature for further investigations because batteries of electric vehicles are exposed to a broad range of temperatures. Changes in temperature could change the behaviour of the whole battery and especially of the electrolyte, which is an important component in interlaminar shear movements.

The problem with the separator fixation led to the method to fix the separator with a double sided adhesive tape on both sides of the parts which serve as anvil and as compressing body. This was done by hand and so variations in the exact alignment of the orientation of the separator could have occurred. This is especially important because the separator has a main direction of its structure looking like the branches of a tree. To prevent wrinkles of the thin separator during the test the specimen had to be tightened while fixing it. This was also done by hand and variations might have influenced the results.

### 6.2 Discussions of the strip draw tests

It was shown that the results are strongly affected by a proper test setup. If the specimens are only slightly damaged, the results strongly vary from the results of proper specimens. By inserting the specimens into the test station sometimes little scratches, which can't be seen with the naked eye, which had happened before the test, but the results of the strip draw

test do not correlate with the results of normal tests and afterwards the former small damage can be seen.

One weakness of the investigation was that all the specimens came from uncharged battery cells. So strip draw results of charged electrodes may differ. The fact that the different layers have to be detached for investigations of the test stand will result in an impact of the results. The specimens cannot be reattached that well that there would be no difference to specimens which were not detached at all.

During the months of performing different tests the substitute electrolyte visually changed which could be identified as a change of the colour from clear to brownish. Also suspended particles could be seen. The substitute electrolyte was sucked out of the tub after each testing day and was stored in a glass container. To counteract the changes the substitute electrolyte was filtered each time before filling the tub of the test stand using filter paper. A reduction of suspended particles could be identified because of this measure, but very tiny particles could probably not be filtered out. A reduction of the amount of substitute electrolyte, most probably resulting from evaporation, was noticed. The difference to the needed volume was compensated by diethyl carbonate. This was done because this component of the substitute electrolyte is the more volatile. During the months of testing a volume of more than 1 litre had to be substituted in comparison to the total amount of substitute electrolyte of about 6 litres.

One difficulty was that the specimens had to be brought in always the same initial position. Particularly the tightening of the electrode was important. To achieve this, pre-tests were made for the final tests in order to tighten the electrode. The advantage of a defined initial position was achieved but the tightening also influenced the results. Especially for tests of the anode this tightening was very important. The flexibility of the anode is much higher than the flexibility of the cathode. So the anode had to be handled with specific care to prevent buckling when fixing the cathode and inserting it into the test stand. This flexible behaviour leads to the fact that the cathode always sags a little when there is no tension. So the necessary pre-tensioning was made by drawing the specimen a small displacement.

By analysing the results it has been found out that probably a dead lock occurred in a test. But as this was observed just once, it could also have been caused by a not proper test set-up.

Not depending on the different material combinations some general effects could be seen.

Also a waiting time had a big influence on the results. By stopping the test after a certain displacement and starting the measuring after some waiting time again, there was a significantly higher force level. Here the theory arose that the roughness of the electrode surface penetrates the surface of the separator. This penetration increases with an increasing stop duration and normal force.

### 6.3 Discussions of the microscopy results

Microscopy has presented interesting results which on the one hand may explain different effects but on the other hand raise some new questions. The specimens for the materials which had been tested with the strip draw test before could have been influenced not only by the strip draw test, but also by the handling when performing the test. In order to set up the strip draw test the specimens were shortly exposed to air where chemical reactions could have happened or started due to the contact with components of the air like oxygen or due to the contact with humidity. Also the specimens of the already drawn materials had an older age in terms of being outside the original battery cell because it took some time to perform the tests.

#### 6.3.1 Anode

The investigations showed additional material, which can be seen in the drawn specimen. Investigations of this material would allow conclusions where this material comes from. It is assumed that this stems from an abrasion of the separator.

#### 6.3.2 Cathode

Already in the synoptic view big differences were seen. While the surface of the initial specimen appeared smooth and regular, the surface of the drawn specimen is strewn with protrusions and not smooth at all.

The differences could have been caused by two different effects. At first the strip draw test could have affected the surfaces, but there is also the possibility that the significant changes of the surface were caused by the different treatment of the specimens. The specimen for the strip draw test was taken out of a battery cell which was disassembled some time before the microscopy. This specimen was also shortly exposed to air and humidity while taking the specimen to the test and back to the container. So also this could have contributed to the

changes of the surface. By considering the microscopy investigations of the specimens with the highest magnification also micro changes could be discovered.

### 6.3.3 Separator

The results of the microscopy of the separator clearly illustrate differences in the structure of the material. It seems that the separator is kind of smoothed and the structure is not that detailed anymore.

These significant changes may have wide ranging influences and consequences. The friction between the layers could have changed because of a deformation and then the deformation behaviour of an additional deformation could be different.

The structure of the separator is also very important for the ion conductivity. The surface changes due to a deformation could also change the properties of the separator.

## 7 Conclusion

The results have led to the conclusion that the resisting force which hinders a relative movement of the layers within the battery strongly depends on the normal force. Not only was the resisting friction force found to be sensitive to the normal force, but the coefficient of friction, too. The sensitivity to sliding velocity and relative displacement is comparatively small.

Up to now all the measurements, results and discussion have been based on force - displacement graphs as a function of normal forces and sliding velocity.

Referring to the model of dry friction, where a coefficient is used for calculations, a coefficient was developed to derive the resisting force from the normal force. Concerning friction there are two coefficients, referred to as the coefficient of static friction and the coefficient of dynamic friction, sometimes also referred to as coefficient of kinetic friction. The results revealed that nearly all force measurements show an abrupt increase up to a certain peak, referred to as break loose force. Then the force is decreasing and gradually approaching a certain constant force. Therefore a coefficient for the peak force  $\mu_p$  and a coefficient for the constant force  $\mu_c$  are introduced. In the velocity range the performed tests showed no distinct dependency on the shear velocity. As the measured graphs with higher velocities sometimes present values higher and sometimes lower than the other graphs no clear dependency on the shear velocity could be detected.

The development of the coefficients is based on the measured results and the range of validity is strongly influenced by the quantity of the normal force. Particular values which are used for the development of the coefficients are marked in the following charts. The marker on the left side is used to mark the peak values, whereas the marker on the right side highlights the coefficient of friction after a displacement of 3 mm. (See dotted and dashed lines in the charts for the anode, the cathode and the pouch) The peak value was determined by calculating an average of the maximum values of each normal force series. The constant value was calculated by taking the average of the values at 3 mm. The value of 3 mm displacement for the second coefficient was used because the graphs flatten after a displacement of about 0.5 mm and seem to remain constant afterwards. This value is used for describing kinetic friction.

The results of the anode-separator pairing are illustrated in Figure 69. For the green graphs, representing the measurements of the 15 N normal force, the peak force of 14.2 N and a constant force of 11.5 N was taken. Run 6#\_200\_F2, which was an outlier, was disregarded in the selection of the values. Only two orange graphs representing the 29 N measurements were taken for the determination of the peak value of 23.9 N and the constant value of 18 N. Run #6 was neglected, for reasons described in the chapter ‘Discussions’. In tests a normal force of 42 N, a peak value of 31.3 N and a constant value of 23.2 N were applied.

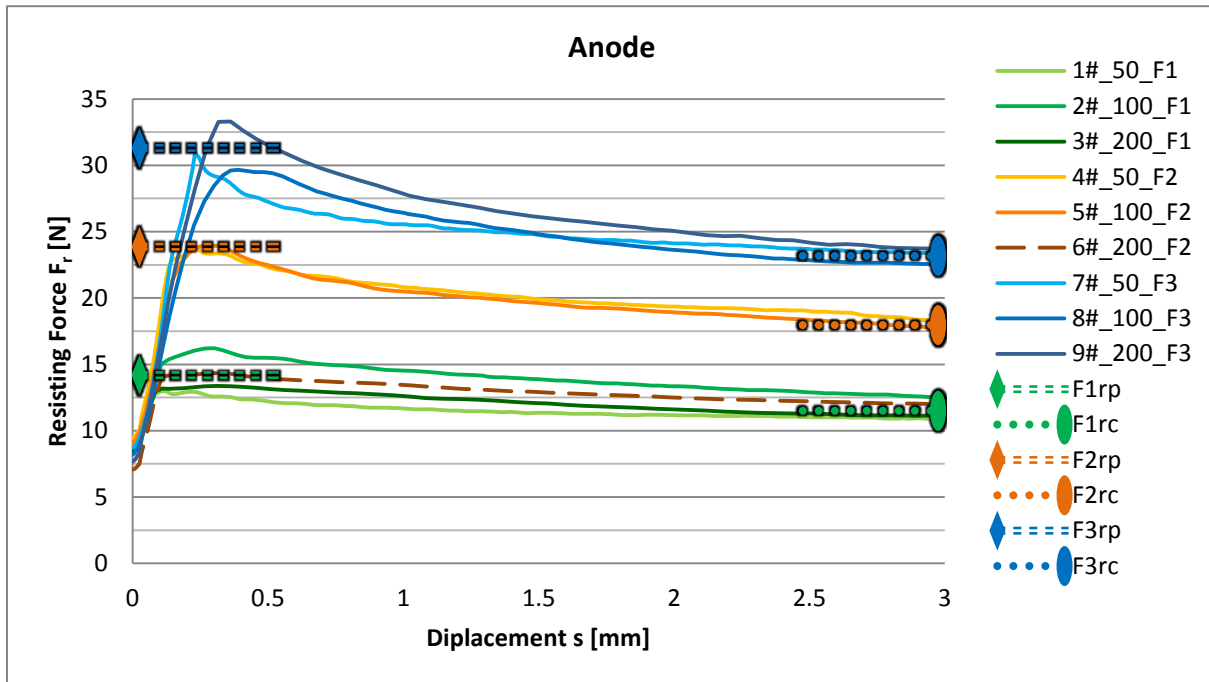


Figure 69: Anode - Determination of values

Figure 70 shows the determined values for the peak force and the constant force which are chosen with 12.5 N peak and 11.6 N for the green graphs, 20.5 N peak and 18.6 N for the orange graphs and 26.5 N peak and 21.2 N for the blue graphs.

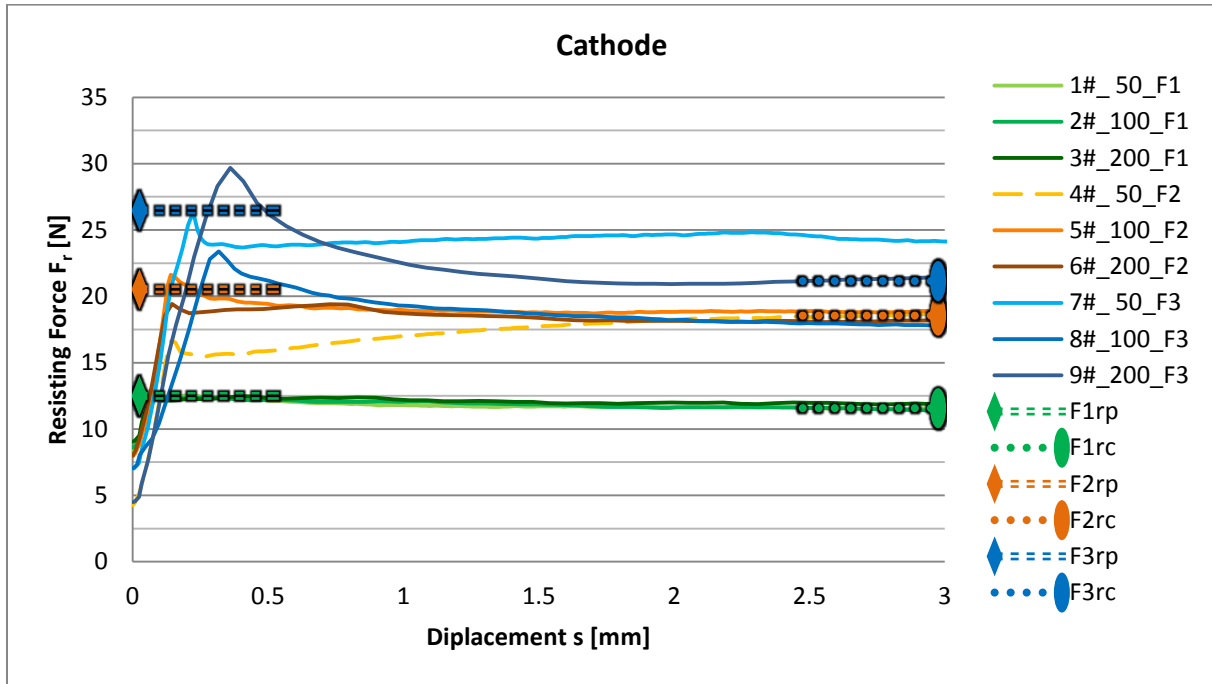


Figure 70: Cathode - Determination of values

The pouch measurements contain values of the medium normal force measurement with 29 N and of the small normal force measurement with 15 N. Together with the determined values of 8.2 N peak and 6.6 N for the 15 N test and the values of 16 N peak and 11.6 N for the 29 N test. These graphs are shown in Figure 71.

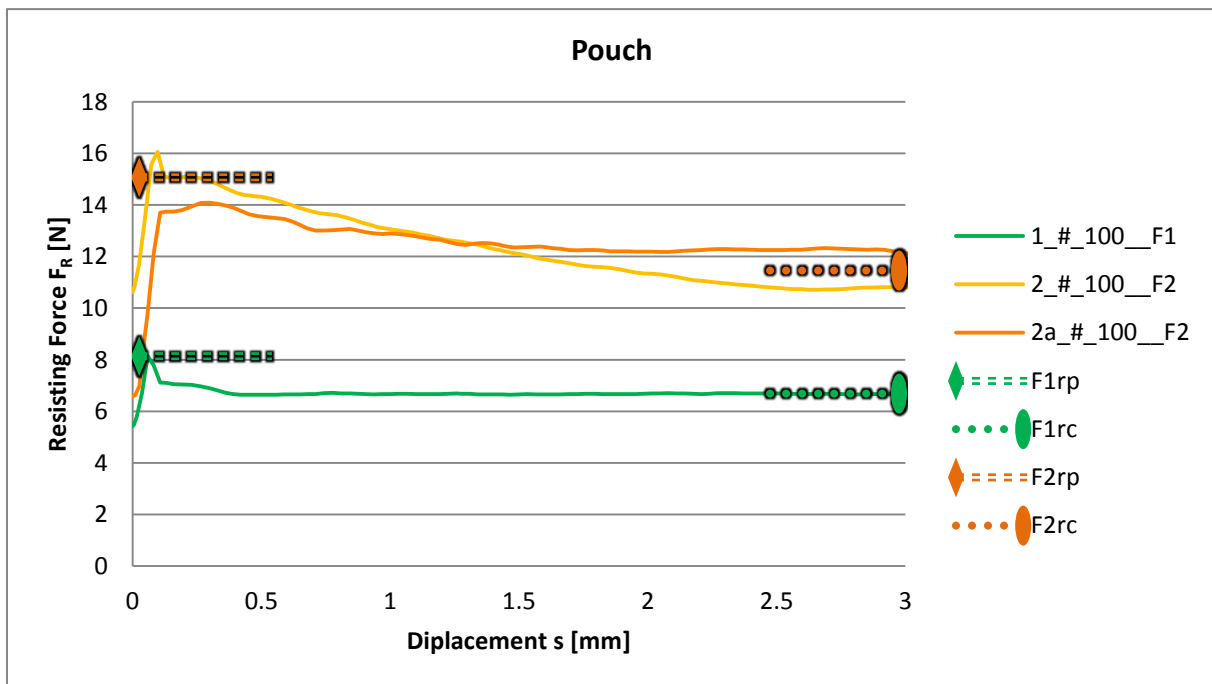


Figure 71: Pouch - Determination of values

Figure 72 shows the coefficients of the peak values as well as of the constant values for the anode, the cathode and the separator. The peak values for the different normal force tests are shown by means of triangles and the constant values are shown by means of dots. This chart serves as synoptic view of the different coefficient values. A distinct dependence on the shear velocity was not found and is therefore also not depicted in the charts.

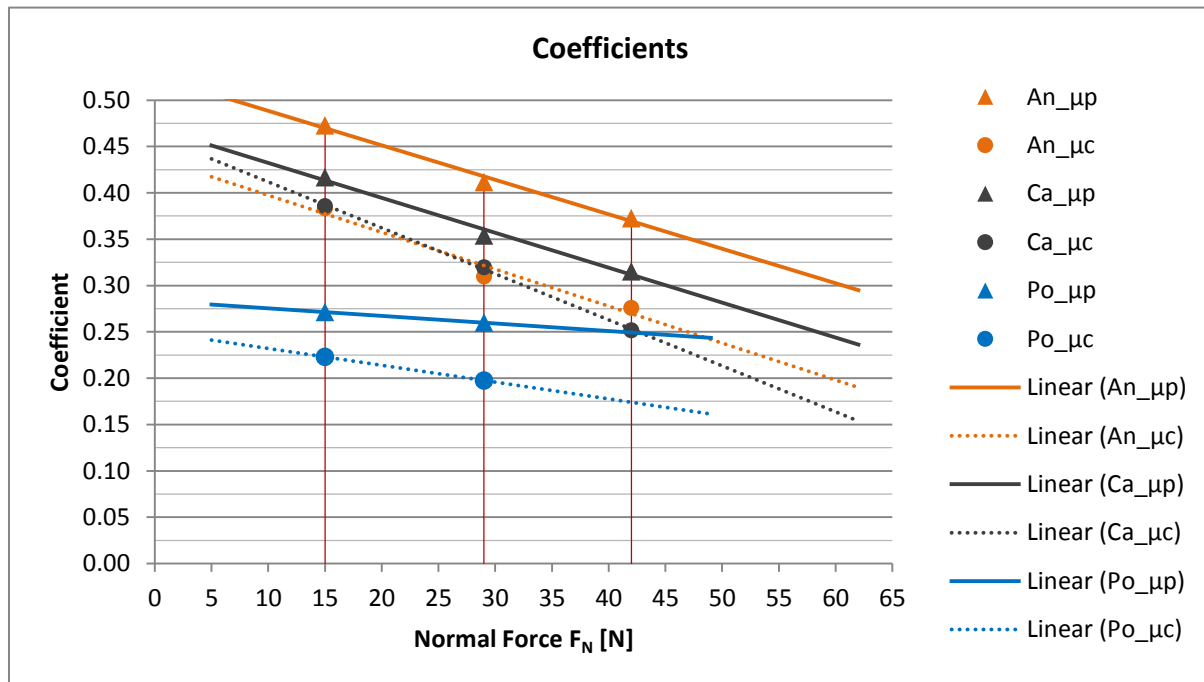


Figure 72: Coefficients synoptic view

A linear trend function is shown for the different materials to illustrate an approximate trend. These functions are created out of the final tests of each material combination. Especially for the pouch test the values have to be considered with caution because of the small number of performed tests.

It is remarkable that the electrodes values depend much more on the normal force than the pouch. For satisfying the requirements of the model for dry friction the trend function should be horizontal as there is just one coefficient for every normal force. The behaviour of the pouch and separator pairing is most similar to this model. Electrodes are much more dependent on the normal force. It can also be seen that the peak coefficients of all three drawn materials are less dependent on the normal force than the constant coefficients.

A more detailed view of the peak coefficients is shown in Figure 73.



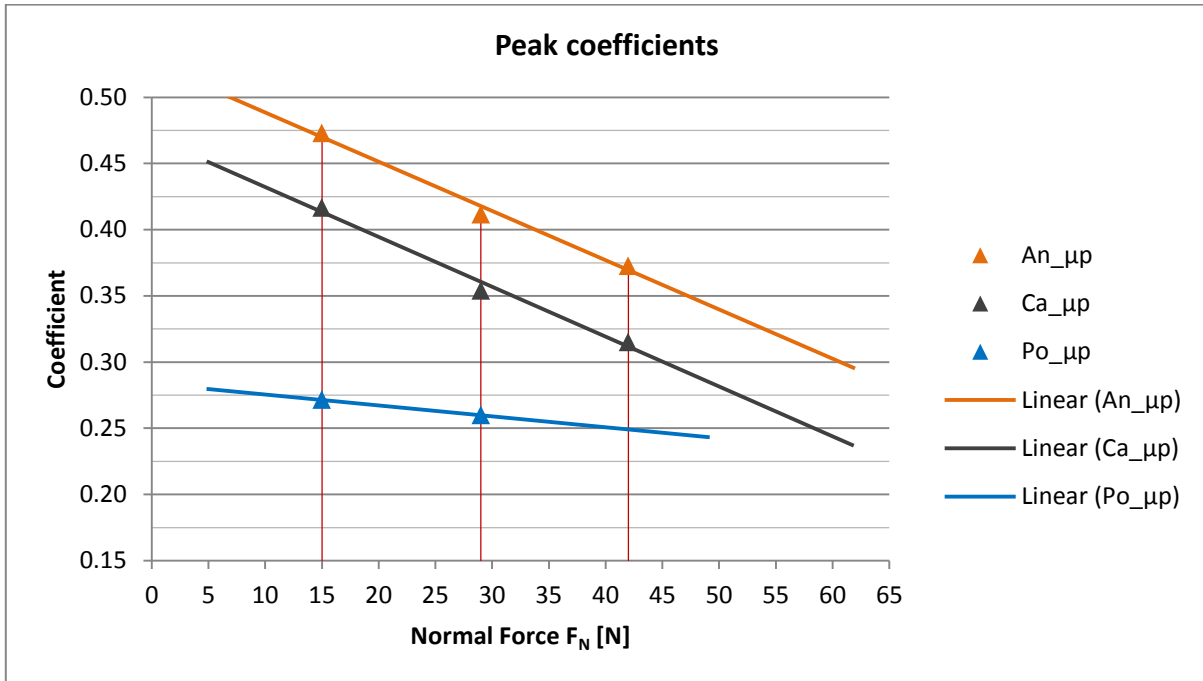


Figure 73: Peak coefficients

The results of the constant coefficients are illustrated in Figure 74.

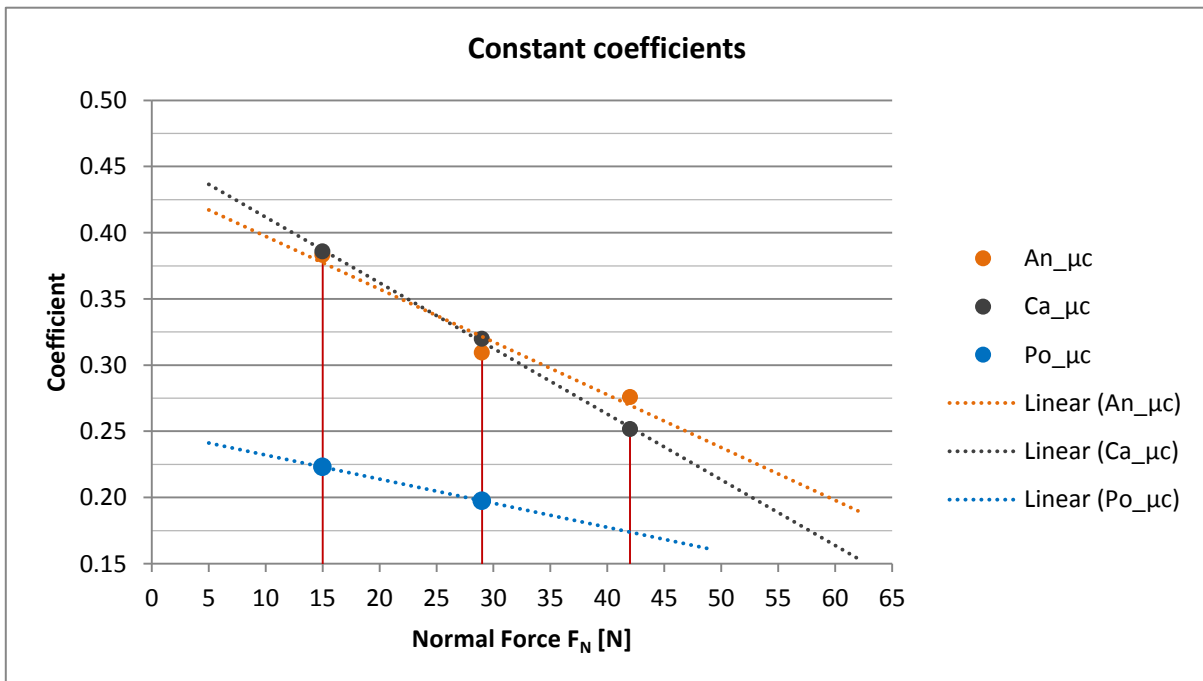


Figure 74: Constant coefficients

By considering the results for the description of these values formulas could be derived which can be seen in Table 12: Trend functions. The formulas were created with the help of the linear trend function in excel. To get the value of the coefficients the normal force has to

be inserted in kN. These formulas may only be valid for normal forces within the range of the tested forces. Because the coefficients are declining, they would become zero or even negative in case of a high normal force, which is very unlikely. At a certain point the normal force would be too high and the components would be damaged because of this high force. Therefore boundaries of the model have to be considered. The development of the coefficients is a first approach but has to be tested and further developed with a greater number of tests. Furthermore, a broader variety of tests with respect to normal force, relative velocity and temperature need to be carried out.

	Anode	Cathode	Pouch
$\mu_p$	$\mu_p = - 3.7 * F_N + 0.5257$	$\mu_p = - 3.8 * F_N + 0.47$	$\mu_p = - 0.8 * F_N + 0.2837$
$\mu_c$	$\mu_c = - 4 * F_N + 0.4372$	$\mu_c = - 5 * F_N + 0.4613$	$\mu_c = - 1.8 * F_N + 0.2503$

Table 12: Trend functions

This thesis has dealt with the new topic of interlaminar interactions in lithium ion battery cells. The test stand developments as well as the realisation of measurements of interlaminar interactions in shear were important steps for starting the research work. For developing models which reflect reality as far as possible, further investigations with regard to other influencing factors, like temperature or state-of-charge in particular, have to be made.

In order to be able to investigate interlaminar interactions more precisely, displacements on a smaller scale have to be analysed.

All the tests have been performed with new batteries. There could be a difference if batteries had been operating for years with a big number of alternating charging cycles and operation cycles. An effect which has not been completely investigated at the moment is the probable formation of dendrites inside the battery. Such dendrites can be considered as micro gearing and would also affect interlaminar interaction.

The fixation of the separator on the clamping plate and the anvil should be rethought. When performing tests with a normal force exceeding about 50 N the separator ripped. On the other hand, any kind of cohesive biased results.

The total draw force, which is the same as the resisting force, was introduced into the interface via the electrode. Combined with the separator which is fixed laterally, these boundary conditions may cause a slip in some areas of the interface and a stick in others.

Also the pre-drawing of the specimens for the final tests can be investigated in detail to find out if a tightening would be an alternative to a starting force.

Apart from the areas where specialised measures lead to an improvement, also measuring failures and inertia forces have to be further considered.

The battery cell has to be disassembled to perform the tests with the developed test stand and this caused problems with respect to testing processes. Environmental influences of the materials or the initial separation of the specimens for later tests could lead to changes which may also cause some impact on the interactions. To circumvent these influences tests with the whole battery cell could be made. This would be inconsistent to the 'microscopic' battery modelling approach, but as single components of the battery have already been investigated, conclusions in terms of the interactions of the interfaces could be drawn. This would be a reverse approach of investigation, but difficult because the interactions depend on the material combinations and are therefore not the same between all contacts. With the knowledge of the test stand investigations a ratio between the different interactions could be derived, which in turn could be used to determine values gained from the reverse approach. This approach would also make the investigation of charged cells possible as there is no need for disassembling and for this purpose, discharging before.

The capillary forces may be the reason for the outcome of two-point bending tests. Even when the pouch is removed an adhering force is present and leads to an increased shear strength.

## 8 Outlook

Interlaminar interactions play an important role for the structural behaviour of a battery, because of the make-up of many very thin layers, which can be considered as a laminate. This master thesis gives a first insight into this research topic and recommendations for further investigations. The topic is very complex as many different disciplines are related to the interlaminar interactions of batteries. Mechanical knowledge is essential for the understanding of structure and load considerations. Electric knowledge is important to comprehend the principle and possible hazards of batteries, especially when a short circuit happens. A chemical consideration of the research field is also essential as the principle of a battery is to store energy chemically, and materials which are used in batteries are often dangerous and react with a variety of other substances. The physical aspect also plays an important role as there are numerous effects which influence the interaction between layers.

In order to obtain a detailed research outcome an investigation carried out by of a team of specialists in the different fields of science is recommended.

Apart from all the research work also data resulting from accidents which happen in reality are needed for further investigations and development. Because of the fact that the number of battery driven vehicles is still small at the moment, sufficient data are not available yet.

In my opinion mobility will always be of great importance for people and vehicles powered by electric motors have tremendous advantages compared to vehicles driven by combustion engines. The challenge is to store electric energy properly and safely and to lose as little energy as possible. The way I see it, lithium ion batteries will not be the most suitable solution for storing electrical energy in the long run, but based on the current state of knowledge these batteries are of immense importance to serve as bridge technology for the traffic concepts in the near future.

Customer acceptance of battery driven vehicles may strongly depend on safety, price, performance and durability issues. Because of the step from vehicles with a combustion engine to electrically driven battery vehicles a lot of changes of the whole vehicle are both required and possible. All these changes may affect the overall safety or/and performance.

Therefore it is not sufficient to calculate risks and the impact of substitute components, but a new approach towards guaranteeing the best possible safety is of utmost importance.

## 9 Bibliography

1. **King, Paul W.** *Climbing Maslow's Pyramid*. Leicester: Matador, 2009. 978-1848761-124.
2. **World Health Organization.** who. [Online] 2013. [access date: 25. November 2013.]  
[http://www.who.int/violence\\_injury\\_prevention/road\\_safety\\_status/2013/en/index.html](http://www.who.int/violence_injury_prevention/road_safety_status/2013/en/index.html)
3. **eurostat.** eurostat. [Online] February 2013. [access date: 18. September 2013.]  
[http://epp.eurostat.ec.europa.eu/statistics\\_explained/index.php/Transport\\_statistics\\_at\\_regional\\_level/de](http://epp.eurostat.ec.europa.eu/statistics_explained/index.php/Transport_statistics_at_regional_level/de)
4. **Polk & Co.** statista. [Online] October 2013. [access date: 5. November 2013.]  
<http://de.statista.com/statistik/daten/studie/247129/umfrage/weltweite-neuzulassungen-von-pkw>
5. **Lienkamp, Markus.** *Elektromobilität: Hype Oder Revolution?* Garching: Springer-Verlag, 2012. 978-3-642-28548-6.
6. **Schmied, Martin und Knörr, Wolfram.** DSLV Deutscher Speditionen und Logistikverband e.V. *Berechnung von Treibhausgasemissionen in Spedition und Logistik gemäß DIN EN 16258*. [Online] March 2013. [access date: 14. November 2013.]  
[http://www.verkehrsrundschau.de/sixcms/media.php/4513/DSLV-Leitfaden\\_Berechnung\\_von\\_THG-Emissionen\\_Stand\\_03-2013.pdf](http://www.verkehrsrundschau.de/sixcms/media.php/4513/DSLV-Leitfaden_Berechnung_von_THG-Emissionen_Stand_03-2013.pdf)
7. **Daimler AG.** Fuelcell e-Mobility. [Online] Daimler AG. [access date: 15. November 2013.]  
<http://www.fuel-cell-e-mobility.info/h2-infrastruktur/Well-to-Wheel>
8. **Daimler.** [Online] Data after: Concawe, Eucar, JCR-WELL-to-WHEELS Report, Version 3c, October 2011. [access date: 16. November 2013.]  
<http://www2.daimler.com/sustainability/optiresource/index.html>
9. **Wallentowitz, Henning, Freialdenhoven, Arndt und Olschewski, Ingo.** *Strategien zur Elektrifizierung des Antriebsstranges*. Vieweg+Teubner, 2011. 978-3-8348-0847-9.
10. **Statistisches Bundesamt, Energie-Informationsdienst, MWV.** statista. [Online] November 2013. [access date: 17. November 2013.]  
<http://de.statista.com/statistik/daten/studie/779/umfrage/durchschnittspreis-fuer-dieselmotoren-seit-dem-jahr-1950>

11. **Hülsmann, Michael und Fornahl, Dirk.** *Evolutionary Paths Towards Mobility Patterns of the Future.* Berlin: Springer-Verlag, 2014. 978-3-642-37557-6.
12. **PRTM.** statista. [Online] 2010. [access date: 15. October 2013.]  
<http://de.statista.com/statistik/daten/studie/168350/umfrage/prognose-zur-bestandsentwicklung-von-hybrid---und-elektrofahrzeugen>
13. **Brokate, Jens, Özdemir, Enver Doruk und Ulrike, Kugler.** *Der Pkw-Markt bis 2040: Was das Auto von morgen antreibt.* Stuttgart: Deutsches Zentrum für Luft- und Raumfahrt, 2013.
14. **International Electrotechnical Commission.** Electrical Energy Storage. *White paper.* [Online] December 2011. [access date: 15. November 2013.]  
<http://www.iec.ch/whitepaper/pdf/iecWP-energystorage-LR-en.pdf>
15. **Kramer, Florian.** *Integrale Sicherheit von Kraftfahrzeugen: Biomechanik Simulation Sicherheit im Entwicklungsprozess.* Wiesbaden: Springer Vieweg, 2013. 978-3-8348-2607-7.
16. **Weber, Julian.** *Automotive Development Processes.* Berlin: Springer-Verlag, 2009. 978-3-642-01252-5.
17. **Justen, Rainer und Schöneburg, Rodolfo.** *Crash safety of hybrid- and battery electric vehicle.* Germany: Daimler AG, 2011. PaperNo 11-0096.
18. **Brodd, Ralph J.** *Batteries for Sustainability.* New York: Springer Science & Business, 2013. 978-1-4614-5790-9.
19. **Moseler, Michael.** Fraunhofer IWM. [Online] [access date: 12. November 2013.]  
[http://www.iwm.fraunhofer.de/fileadmin/media/kompetenzen/werkstoffmodellierung-und-simulation/pdf/JB10\\_G1-6.pdf](http://www.iwm.fraunhofer.de/fileadmin/media/kompetenzen/werkstoffmodellierung-und-simulation/pdf/JB10_G1-6.pdf)
20. **Crompton, Thomas P J.** *Battery Reference Book.* Butterworth Heinemann, 2000. 978-0750646253.
21. **Park, Jung-Ki.** *Principles and Applications of Lithium Secondary Batteries.* Weinheim: Wiley-VCH Verlag, 2012. 978-3-527-33151-2.
22. **Internal Energy Agency.** Energy Efficiency & Renewable Energy. *Vehicle Technologies Office.* [Online] Johnson Control - SAFT, 25. January 2010. [access date: 5. November 2013.]  
[https://www1.eere.energy.gov/vehiclesandfuels/facts/2010\\_fotw607.html](https://www1.eere.energy.gov/vehiclesandfuels/facts/2010_fotw607.html)

23. **A123**. A123-Systems. [Online] [access date: 8. October 2013.]  
<http://www.a123systems.com>
24. **van Schalkwijk, Walter A. und Scrosati, Bruno**. *Advances in Lithium-Ion Batteries*. New York: Kluwer Academic, 2002. 0-306-47356-9.
25. **Roth, Peter und Orendorff, Christopher**. How Electrolytes Influence Battery Safety. *The Electrochemical Society Interface*. [Online] 2012. [access date: 20. November 2013.]  
[http://www.electrochem.org/dl/interface/sum/sum12/sum12\\_p045\\_049.pdf](http://www.electrochem.org/dl/interface/sum/sum12/sum12_p045_049.pdf)
26. **Schlögl, Robert**. *Chemical Energy Storage*. Berlin: Walter de Gruyter GmbH, 2013. 978-3-11-026407-4.
27. **Lipp, Silke**. *Erstellung eines mechanischen Simulationsmodells einer Batteriezelle mit dem expliziten FE-Code PAM-Crash*. Graz: s.n., 2013.
28. **Daniel, Claus und Besenhard, Jürgen O**. *Handbook of Battery Materials, 2 Vols*. Wiley VCH, 2011. 978-3-527-29469-5.
29. **Pistoia, Gianfranco**. *Electric and Hybrid Vehicles*. Amsterdam: Elsevier, 2010. 978-0-444-53565-8.
30. **Cunningham, Brian**. U.S. department of energy. *Energy Efficiency & Renewable Energy*. [Online] 15. May 2012. [access date: 20. November 2013.]  
[http://www1.eere.energy.gov/vehiclesandfuels/pdfs/merit\\_review\\_2012/energy\\_storage/es116\\_cunningham\\_2012\\_o.pdf](http://www1.eere.energy.gov/vehiclesandfuels/pdfs/merit_review_2012/energy_storage/es116_cunningham_2012_o.pdf)
31. **Doughty, Daniel H. und Crafts, Chris C**. *FreedomCAR Electrical Energy Storage System Abuse Test Manual for Electric and Hybrid Electric Vehicle Applications*. Sandia National Laboratories, 2006. SAND2005-3123.
32. *Concepts for Mechanical Abuse Testing of High-Voltage Batteries*. **Sinz, Wolfgang, et al**. SAE 2012 World Congress & Exhibition, 2012. DOI:10.4271/2012-01-0124.
33. **Mikolajczak, Celina, et al**. *Lithium-Ion Batteries Hazard and Use Assessment*. Springer-Fire Protection Research Foundation, 2011. 978-1-4614-3485-6.
34. *EV HEV Rechargeable Energy Storage Systems (RESS) Safety and Abuse Testing Procedure*. **Doughty, Daniel H**. SAE, 2010. SAE J2464.

35. **Parc Technologique Alata** . Certification scheme for battery cells and packs for rechargeable electric and hybride vehicles. [Online] October 2012. [access date: 12. November 2013.] <http://www.ineris.fr/centredoc/referentiel-certification-elllicert-version-e-octobre2012-anglais--1364288373.pdf>
36. **Butt, Hans-Jürgen, Graf, Karlheinz und Kappl, Michael**. *Physics and Chemistry of Interfaces*. Weinheim: Wiley-VCH Verlag GmbH & Co. KGaA; Auflage: 2. überarb. u. erw. Auflage (20. Januar 2006), 2003. 978-3527406296.
37. **Mota Soares, Carlos A., Mota Soares, Cristóvão M. und Freitas, Manuel J. M.** *Mechanicsof Composite Materials and Structures*. Springer. 978-0792358718.
38. **Butt, Hans-Jürgen and Kappl, Michael**. *Surface and Interfacial Forces*. Darmstadt: WILEY-VCH Verlag GmbH&Co.KGaA, 2012. 978-3-527-40849-8.
39. **Popov, Valentin**. *Kontaktmechanik und Reibung*. Heidelberg: Springer-Verlag, 2009. 978-3-642-13301-5.
40. **Astarmathsandphysics**. The Force Between Two Sheets of Glass Separated by a Thin Film of Water. [Online] [access date: 5. December 2013.] [http://www.astarmathsandphysics.com/a\\_level\\_physics\\_notes/fluid\\_mechanics/a\\_level\\_physics\\_notes\\_the\\_force\\_between\\_two\\_sheets\\_of\\_glass\\_separated\\_by\\_a\\_thin\\_film\\_of\\_water.html](http://www.astarmathsandphysics.com/a_level_physics_notes/fluid_mechanics/a_level_physics_notes_the_force_between_two_sheets_of_glass_separated_by_a_thin_film_of_water.html)
41. **Fh-Muenchen**. Oberflächenspannung von Flüssigkeiten und Festkörpern. [Online] [access date: 5. December 2013.] [http://dodo.fb06.fh-muenchen.de/herberg/texte/mikronanotechnik/vass/kap4\\_5.pdf](http://dodo.fb06.fh-muenchen.de/herberg/texte/mikronanotechnik/vass/kap4_5.pdf)
42. **Bhushan, Bharat**. *Intrudoction to Tribology*. John Wiley & Sons. 0-471-15893-3.
43. **Kondo, Yuriko, Tahahiro, Koyama und Sasaki, Shinya**. Tribological Properties of Ionic Liquids. [Online] 23. January 2013. [access date: 5. September 2013.] <http://www.intechopen.com/books/ionic-liquids-new-aspects-for-the-future/tribological-properties-of-ionic-liquids> DOI: 10.5772/52595.
44. **Kopeliovich, Dmitri**. SubSTech. *Substances and Technologies*. [Online] 1. June 2012. [access date: 12. October 2013.] [http://www.substech.com/dokuwiki/doku.php?id=lubrication\\_regimes](http://www.substech.com/dokuwiki/doku.php?id=lubrication_regimes)



45. **Bartel, Dirk.** *Simulation Von Tribosystemen: Grundlagen und Anwendung.* Wiesbaden: Vieweg + Teubner, 2010. 978-3-8348-1241-4.
46. A 'Microscopic' Structural Mechanics FE Model of a Lithium-Ion Pouch Cell for Quasi-Static Load Cases. **Breitfuss, Christoph, et al.** Detroit: SAE Int. J. Passeng.Cars -Mech. Syst., 2013. DOI: 10.4271/2013-01-1519.
47. **Knauder, Christoph.** *Entwicklung einer Prüfumgebung zur Untersuchung der mechanischen Eigenschaften von lithiumbasierenden Batterien.* Graz: 2012.
48. **Lichtenegger, Bernhard.** *Entwicklung eines Finite Elemente Modells zur Untersuchung der mechanischen Eigenschaften von lithiumbasierenden Batterien.* Graz: 2012.
49. **Riewoldt.** Riewoldt. [Online] [access date: 12. October 2013.]  
<http://www.riewoldt.de/wissenscenter/grundlagen-der-klebeteknik>
50. **Moosbauer, Dominik Johann.** *Die Lithium-Ionen-Batterie - Energiespeicher der Zukunft.* Suedwestdeutscher Verlag fuer Hochschulschriften, 2011. 978-3838124551.
51. **Testmatic.** Testmatic. [Online] [access date: 12. October 2013.] <http://www.testmatic.de>
52. **Nordic Transducer.** Datasheet S Beam Model TCTN-9110. [Online] [access date: 2013. October 12.] [http://www.ntt.dk/TCTN-9110\\_280505.pdf](http://www.ntt.dk/TCTN-9110_280505.pdf)
53. —. Load cells & Transducers. [Online] [access date: 12. October 2013.] <http://www.ntt.dk/tension.htm>
54. **Kellermann, R. und Klein, H.-Ch.** Untersuchung über den Einfluss der Reibung. [Online] [access date: 5. september 2013.] [http://www.kamax.com/fileadmin/user\\_upload/dokumente/veroeffentlichungen/einfluss\\_reibung.pdf](http://www.kamax.com/fileadmin/user_upload/dokumente/veroeffentlichungen/einfluss_reibung.pdf)
55. **Fischer, Alfons und Bobzin, Kirsten.** *Friction, Wear and Wear Protection.* Weinheim: Wiley-VCH Verlag GmbH & co KGaA, 2009. 978-3-527-32366-1.
56. **Peters, George A. und Peters, Babara J.** *Automotive Vehicle Safety.* London: Taylor & Francis, 2002. 0-415-26333-6.
57. **Matzer, Claus Uwe.** *Untersuchung zur Darstellung interner Kurzschlüsse von HV-Batteriezellen.* Graz: 2013.

58. **Israelachvili, Jacob N.** *Intermolecular and Surface Forces, Second Edition*. Amsterdam: Elsevier Ltd., 1991. 978-0-12-375181-2.

59. **Reddy, Thomas B. und Linden, David.** *Handbook of Batteries*. McGraw-Hill Professional, 2011. 978-0071359788.

## 10 List of Figures

The numbers in brackets refer to the sources as listed in the bibliography.

Figure 1: Maslow's Hierarchy (1).....	1
Figure 2: New registrations of passenger cars worldwide (4).....	2
Figure 3: Life cycle assessment (7) .....	4
Figure 4: Energy and CO <sub>2</sub> scenarios (8) .....	4
Figure 5: Average price of diesel fuel in Germany (10).....	5
Figure 6: Estimation of the worldwide quantity of hybrid cars and electro cars (12) .....	6
Figure 7: Fleet estimation Germany (13) .....	7
Figure 8: Classification of EESS according to the energy form (14) .....	8
Figure 9: Accident deformations (17) .....	9
Figure 10: Battery concepts (21) .....	11
Figure 11: Battery types (22).....	11
Figure 12: Battery principle (based upon) (9) .....	12
Figure 13: A123 AMP20 (23) .....	14
Figure 14: Schematic makeup of the pouch cell .....	14
Figure 15: Drop test impact (31) .....	20
Figure 16: Interlaminar shear .....	22
Figure 17: Schematic separation round plates (based upon) (40).....	24
Figure 18: Schematic separation electrodes .....	24
Figure 19: Capillary force.....	25

Figure 20: Stribeck curve (43) .....	27
Figure 21: Boundary lubrication (44) .....	28
Figure 22: Mixed lubrication (44) .....	28
Figure 23: Hydrodynamic lubrication (44) .....	29
Figure 24: Two-point bending tests .....	30
Figure 25: Current battery model (27) .....	31
Figure 26: Types of interfacial loads (49) .....	33
Figure 27: Schematic strip draw principle .....	38
Figure 28: Conventional friction model .....	38
Figure 29: Test stand friction model .....	39
Figure 30: Z3-X500 (51) .....	40
Figure 31: Load-cell (53) .....	40
Figure 32: Bound with wrinkles .....	41
Figure 33: Separator fixation methods .....	42
Figure 34: Glass beads and plates .....	42
Figure 35: Test stand 3D .....	43
Figure 36: Test stand .....	43
Figure 37: Principle inclined plane .....	45
Figure 38: Inclined plane .....	45
Figure 39: Inclined plane aluminium PTFE .....	46
Figure 40: Microscopy .....	50
Figure 41: Microscopic specimen orientation .....	51

Figure 42: Anode Aluminium.....	52
Figure 43: Cathode Aluminium .....	53
Figure 44: Anode PE .....	54
Figure 45: Cathode PE .....	55
Figure 46: Anode – separator with stops .....	56
Figure 47: Cathode – separator with stops .....	57
Figure 48: Anode-Separator velocity force .....	58
Figure 49: Cathode-Separator velocity force .....	59
Figure 50: Pouch separator final .....	60
Figure 51: Anode Pre synoptic view .....	62
Figure 52: Anode Post synoptic view .....	62
Figure 53: Anode Pre 10 $\mu\text{m}$ .....	63
Figure 54: Anode Post 10 $\mu\text{m}$ .....	63
Figure 55: Anode Pre 2 $\mu\text{m}$ .....	64
Figure 56: Anode Post 2 $\mu\text{m}$ .....	64
Figure 57: Cathode Pre synoptic view .....	65
Figure 58: Cathode Post synoptic view .....	65
Figure 59: Cathode Pre 10 $\mu\text{m}$ .....	66
Figure 60: Cathode Post 10 $\mu\text{m}$ .....	66
Figure 61: Cathode Pre 2 $\mu\text{m}$ .....	67
Figure 62: Cathode Post 2 $\mu\text{m}$ .....	67
Figure 63: Separator Pre synoptic view .....	68

Figure 64: Separator Post synoptic view .....	68
Figure 65: Separator Pre 10 $\mu\text{m}$ .....	69
Figure 66: Separator Post 10 $\mu\text{m}$ .....	69
Figure 67: Separator Pre 2 $\mu\text{m}$ .....	70
Figure 68: Separator Post 2 $\mu\text{m}$ .....	70
Figure 69: Anode - Determination of values .....	76
Figure 70: Cathode - Determination of values .....	77
Figure 71: Pouch - Determination of values.....	77
Figure 72: Coefficients synoptic view.....	78
Figure 73: Peak coefficients .....	79
Figure 74: Constant coefficients.....	79

## 11 List of Tables

The numbers in brackets refer to the sources as listed in the bibliography.

Table 1: Test recommendations (32) .....	18
Table 2: EUCAR hazard levels (31).....	19
Table 3: Test principles.....	35
Table 4: Friction as provided in specialist literature (54).....	44
Table 5: Validation results.....	44
Table 6: Tests: electrodes - aluminium .....	47
Table 7: Tests: electrodes - PE.....	48
Table 8: Tests: electrodes – separator with stops .....	48
Table 9: Final tests anode.....	49
Table 10: Final tests cathode.....	49
Table 11: Final tests pouch.....	50
Table 12: Trend functions.....	80

## 12 List of Equations

The numbers in brackets refer to the sources as listed in the bibliography.

Equation 1: Anode reaction during discharge (26) .....	13
Equation 2: Cathode reaction during discharge (26) .....	13
Equation 3: Characteristic length scale .....	21
Equation 4: Adhesion force (38).....	23
Equation 5: Capacitor force (based upon) (38) .....	23
Equation 6: Force relating to pressure .....	23
Equation 7: Separation force round plates (40).....	24
Equation 8: Separation force electrodes.....	24
Equation 9: Dry friction .....	26
Equation 10: Hydrodynamic force (38) .....	29
Equation 11: Relative force test stand .....	39
Equation 12: Coefficient calculation .....	39
Equation 13: Buoyancy force .....	39
Equation 14: Static friction coefficient inclined plane .....	45



## 13 List of symbols

### 13.1 SI base units

Unit Symbol	Unit name	Quantity name	Dimension symbol
A	ampere	electric current	I
cd	candela	luminous intensity	J
K	kelvin	thermodynamic temperature	$\theta$
kg	kilogram	mass	M
m	metre	length	L
mol	mole	amount of substance	N
s	second	time	T

### 13.2 Units

Unit Symbol	Unit name	Conversion of units
°C	degree centigrade	$^{\circ}\text{C} = \text{K} - 273.15$
bar	bar	$\text{bar} = \text{Pa} / 10^5$
C	coulomb	$\text{C} = \text{A} \cdot \text{s}$
h	hour	$\text{h} = \text{s} / 3600$
J	joule	$\text{J} = (\text{kg} \cdot \text{m}^2) / \text{s}^2$
l	litre	$\text{l} = \text{m}^3 / 10^{-3}$
min	minute	$\text{min} = \text{s} / 60$
N	newton	$\text{N} = (\text{kg} \cdot \text{m}) / \text{s}^2$
Pa	pascal	$\text{Pa} = \text{kg} / (\text{m} \cdot \text{s}^2)$
rad	radian	-
V	volt	$\text{V} = (\text{kg} \cdot \text{m}^2) / (\text{A} \cdot \text{s}^3)$
W	watt	$\text{W} = (\text{kg} \cdot \text{m}^2) / \text{s}^3$

### 13.3 Constants

Constant Symbol	Constant name	Value
e	elementary charge	$1.60218 \cdot 10^{-19} \text{ C}$
g	gravity acceleration	$9.80665 \text{ m/s}^2$
$\epsilon_0$	vacuum permittivity	$8.85419 \cdot 10^{-12} \text{ As/(Vm)}$
$\pi$	circle constant	$\sim 3.14159$

### 13.4 Used Symbols

Symbol	Description	Unit
$\mu$	coefficient of friction	-
$\mu_c$	constant coefficient	-
$\mu_p$	peak coefficient	-
A	area	$\text{m}^2$
a	acceleration	$\text{m/s}^2$
d	distance	m
F	force	N
$F_{adh}$	adhesion force	N
$F_{cap}$	capillary force	N
$F_{chem}$	chemical bounding f.	N
$F_{el}$	electrostatic force	N
$F_F$	friction force	N
$F_{Fb}$	bottom friction force	N
$F_{Ft}$	top friction force	N
$F_H$	hydrogen bounding f.	N
$F_N$	normal force	N
$F_{Nb}$	bottom normal force	N

Symbol	Description	Unit
$F_{Nt}$	top normal force	N
$F_R$	resisting force	N
$F_{vdW}$	van der Waals force	N
$h$	height	m
$L$	length	m
$m$	mass	kg
$M$	mass	kg
$P$	pressure	Pa
$p$	pressure	Pa
$R$	radius	m
$r$	radius	m
$r_m$	middle radius	m
$s$	displacement	m
$U$	voltage	V
$V$	volume	$m^3$
$v$	velocity	m/s
$W$	width	m
$\alpha$	angle	rad
$\gamma$	specific surface energy	N/m
$\Delta v$	delta velocity	m/s
$\Delta z$	delta height	m
$\epsilon_r$	relative permittivity	-
$\eta$	viscosity	Pa*s
$\lambda_c$	characteristic length scale	m
$\rho$	density	$kg/m^3$

## 14 List of Abbreviations

Abbreviation	Meaning
%	percentage
3D	three dimensional
A123	battery producing company
A123 AMP20	battery pouch cell from A123 with 20 Ah
A-CAES	adiabatic compressed air energy storage
Anode	donating electrode during cell discharge process (Negative electrode)
ANSI	American National Standard Institute
BEV	battery electric vehicle
C	carbon
CAES	compressed air electric storage
Cathode	electron accepting electrode during cell discharge (Positive electrode)
CO <sub>2</sub>	carbon dioxide
cos	cosine
DEC	diethyl carbonate
deg	degree
DLC	double layer capacitor
e-	electron (negative charged)
EC	ethylene carbonate
EESS	electric energy storage system
E-Mobility	electro mobility
et al.	'et alii / et aliae / et alia' and others
EU27	states of the European Union up to and including June 2013
EUCAR	European Council for Automotive Research & Development
EV	electric vehicle
excel	table calculation program
FELMI-ZFE	Institute for Electron Microscopy and Nanoanalysis- Graz Centre for Electron Microscopy

Abbreviation	Meaning
FES	flywheel electric storage
FreedomCAR	United States national office of energy efficiency and renewable energy
h	height
HEV	hybrid electric vehicle
i.e.	'id est' namely
IEC	International Electro technical Commission
IEEE	Institute of Electrical and Electronics Engineers
kph	kilometres per hour
LCA	life cycle assessment
Li	lithium
Li+	lithium ion (positive charged)
LiFePO <sub>4</sub>	lithium iron phosphate
LiPF <sub>6</sub>	lithiumhexafluorophosphate (conducting salt)
LPG	liquefied petroleum gas
ls	long stop (300 s)
max	maximum
MDB	moving deformable barriers
min	Minimum
NaS	sodium sulphur
NiCd	nickel cadmium
NiMh	nickel metal hydride
p.a.	per anno
PE	polyethylene
PHEV	plug-In hybrid electric vehicle
PHS	pumped hydro storage
PMMA	polymethylmethacrylate
post	prefix after
PP	polypropylene
pre	prefix before
PTFE	polytetrafluoroethylene

Abbreviation	Meaning
PVC	polyvinylchloride
R&D	research and development
SAE	Society of Automotive Engineers
SEI	solid electrolyte interface
sin	sinus
SMES	superconducting magnetic energy storage
SNG	synthetic natural gas
SOC	state of charge
ss	short stop (10 s)
TCTN-9110-100N	load cell 100 N
TtW	tank to wheel
UL	Underwriters Laboratories
UN	United Nations
VSI	Vehicle Safety Institute
w	with
WHO	World Health Organisation
WtT	well to tank
WtW	well to wheel
Z3-X500	tensile test station
Zn x	zinc coated, x representing the coating thickness
$\alpha$	Alpha (angle °)
$\Delta$ mass	difference in the mass

This page intentionally left blank

## 15 Appendix

### 15.1 Curriculum Vitae

The Curriculum Vitae can be found on the following pages.



# Reinhard Schmid, BSc

Name **Reinhard Schmid, BSc**  
Address Höf 81  
3300 Amstetten  
AUSTRIA  
E-Mail reinhard\_schmid@gmx.at  
Mobile (+43) / 0676 / 68 58 051



Date of birth 08.05.1987, Amstetten  
Nationality Austria  
Family status unmarried

## Education and Training

since **Master programme Production Science and Management**  
03/2011 University of Technology Graz (F066483)

Faculty of Mechanical Engineering and Economics  
English master program  
Three pillars of PSM: technical, economic and social competences

**Master thesis** at the Vehicle Safety Institute since 11/2012

*'Investigation of the interlaminar interfaces in a lithium ion pouch cell'*

Supervision: DI Dr. techn. Florian Feist

Assessment/ grading: Univ.-Prof DI Dr. techn. Hermann Steffan



[www.tugraz.at](http://www.tugraz.at)



[www.psm.tugraz.at](http://www.psm.tugraz.at)



[www.vsi.tugraz.at](http://www.vsi.tugraz.at)

10/2007 **Bachelor programme Mechanical Engineering and Business Economics**  
to University of Technology Graz (F033282)  
03/2011

Faculty of Mechanical Engineering and Economics

**Bachelor thesis** at the Vehicle Safety Institute

*'Sensorintegration eines Laserscanners in ein automatisiert fahrendes Modellauto'*

Supervision: DI Dr. techn. Wolfgang Sinz, DI Dr. techn. Nikolai Schretter

Assessment/ grading of the bachelor thesis (1) top grade



[www.tugraz.at](http://www.tugraz.at)



[www.vsi.tugraz.at](http://www.vsi.tugraz.at)

09/2001 **College of Mechanical Engineering**  
to Waidhofen an der Ybbs  
06/2006

Specialization: **Automation Technology**

Class representative for five years

Overall result in final year of tuition (5<sup>th</sup> class): Passed with distinction

Graduation 2006 – Result of VET diploma exams: Passed with distinction

Diploma project in English: (1) top grade

*'Automatic Fruitprocessing System'*

The diploma project won prizes and was top-ranked in several competitions:



Jugend Innovativ  
[www.jugendinnovativ.at](http://www.jugendinnovativ.at)



RIZ Jugendpreis  
[www.riz.at](http://www.riz.at)



Hypo Umweltpreis  
[www.noehypo.at](http://www.noehypo.at)







[www.htlwy.ac.at](http://www.htlwy.ac.at)





## Work experience

07/2012 to 08/2012	<b>MASSIV Automated Systems, Toronto Canada</b>  Internship in the departments: Program Management, Sales Management, Robotics, Controls, Welding, Shop floor Operations, Toolmaker and Robot-Simulation	 <a href="http://www.massiv.com">www.massiv.com</a> 
10/2011 to 06/2012	<b>TU Graz – Vehicle Safety Institute, Graz</b> Student Assistant Assistance for student laboratory courses / DGPS-System / Laser scanner	 <a href="http://www.vsi.tugraz.at">www.vsi.tugraz.at</a>
07/2011 to 08/2011	<b>MAGNA Steyr, Graz</b> Practical training in the department: Safety Technology construction of a testing system / assistance in safety tests	 <a href="http://www.magna.com">www.magna.com</a>
10/2010 to 06/2011	<b>TU Graz – Vehicle Safety Institute, Graz</b> Student Assistant Assistance for student laboratory courses / NI-cRIO	 <a href="http://www.vsi.tugraz.at">www.vsi.tugraz.at</a>
07/2008 to 08/2008	<b>ENGEL AUSTRIA, Schwertberg</b> Practical training in the department: Innovation programming data bases / 3D-CAD	 be the first. <a href="http://www.engelglobal.com">www.engelglobal.com</a>
07/2007 to 09/2007	<b>Rotes Kreuz, Amstetten</b> Practical work for the Austrian Red Cross emergency medical technician / driver of ambulance cars	 ÖSTERREICHISCHES ROTES KREUZ <a href="http://www.rotekreuz.at">www.rotekreuz.at</a>
08/2005	<b>Böhler Uddeholm, Munkfors Schweden</b>  Practical training in the department: Quality Assurance analyses in the laboratory for material technology	 <a href="http://www.boehler-uddeholm.com">www.boehler-uddeholm.com</a>
07/2004	<b>INOVA-LiSEC Technologiezentrum, Seitenstetten</b> Practical training in the department: Innovation electronic administration / stock lists administration	 <a href="http://www.lisec.com">www.lisec.com</a>
08/2003	<b>INOVA-LiSEC Technologiezentrum, Seitenstetten</b> Practical training in the department: Design Engineering construction design and techniques / 2D-/3D-CAD	 <a href="http://www.lisec.com">www.lisec.com</a>
07/2002 to 08/2002	<b>Wagner Gewölbekonstruktion, Neuhofen</b> Practical work in the construction sector work experience in construction of vaulted cellars	 <a href="http://www.gewoelbekonstruktion-aw.at">www.gewoelbekonstruktion-aw.at</a>

## Scholarships and Awards

2013	<b>Circle of Excellence - University Graz</b> Career-network for high potentials with practical experience	 <a href="http://www.coe-graz.at">www.coe-graz.at</a>
2013	<b>Scholarship of the Frank-Stronach-Institute of the TU Graz</b> For a promising master thesis and study-performance	 <a href="http://www.tugraz.at">www.tugraz.at</a>
2013	<b>Students 4 Excellence</b> Student network for high potentials	 <a href="http://www.students4excellence.com">www.students4excellence.com</a>
2012	<b>Performance Scholarship of the TU Graz</b> For outstanding study-performance	 <a href="http://www.tugraz.at">www.tugraz.at</a>

## Voluntary Work and Community Service

10/2006 to 06/2007	<b>Community Service at the Austrian Red Cross</b> (Zivildienst Rotes Kreuz – Amstetten) medical technician and driver of ambulance cars	 <a href="http://www.rotekreuz.at">www.rotekreuz.at</a>
since 10/2007	<b>Austrian Red Cross</b> Emergency medical technician and driver of ambulance cars regular voluntary service at the red cross	 ÖSTERREICHISCHES ROTES KREUZ <a href="http://www.rotekreuz.at">www.rotekreuz.at</a>
since 04/2010	<b>Austrian Mountain Rescue Team</b> Member of the rescue team (Bergrettung Amstetten) regular voluntary service and operation service	 <a href="http://www.bergrettung.at">www.bergrettung.at</a>
since 01/2001	<b>Austrian Alpinist Association</b> (Alpenverein Amstetten) Coach in skiing courses	 <a href="http://www.alpenverein.at">www.alpenverein.at</a>

## Qualifications

Languages	English – business fluent <ul style="list-style-type: none"><li>▪ Master program PSM in English</li><li>▪ Language courses in England und Malta</li><li>▪ Internships in Sweden and Canada</li></ul>
Computer-Skills	<ul style="list-style-type: none"><li>▪ MS Office: Word, Excel, PowerPoint</li><li>▪ PTC Creo (ProEngineer)</li><li>▪ Mathcad</li><li>▪ Adobe: Photoshop, Premiere</li><li>▪ National Instruments LabView</li><li>▪ SAP, Catia, C# Grundkenntnisse</li></ul>
Driving License	Class B

## Free time

Hobbies	<ul style="list-style-type: none"><li>▪ Sports: climbing, skiing, kayak, swimming</li><li>▪ Individual travelling</li><li>▪ Red Cross, Mountain Rescue, Alpine Association (see 'Voluntary Work')</li></ul>
---------	---

Graz, 15 December 2013

Reinhard Schmid

This page intentionally left blank